Università degli Studi di Firenze

European laboratory for non-linear spectroscopy

INTERNATIONAL PhD IN
"*Molecular and Atomic Spectroscopy*"
FIS/07
Cycle XXV

COORDINATOR Professor Pavone Francesco Saverio

"COMBINING SINGLE-MOLECULE LOCALIZATION, OPTICAL TRAPPING AND MICROFLUIDICS FOR THE STUDY OF PROTEIN-DNA INTERACTION"

PhD Student
Dott. Belcastro Gionata

Supervisor
Professor Pavone Francesco Saverio

2010/2012

Contents

1. Overview of the thesis

Protein binding to DNA is an important event that unravels and modulates the information contained in the genome. DNA replication, transcription, regulation of gene expression, site-specific recombination, transposition, restriction and modification of DNA by sequence specific endonucleases and methyltransferases are all processes that rely on binding of proteins with DNA. Also structural features of DNA, such as compaction in nucleosomes in eukaryotes, for example, are due to proteins that bind DNA (DNA Binding Proteins). We can thus distinguish two big groups of DBP: sequence-specific DBP and non-specific DBP according if their biological function depends on specific binding to a DNA sequence called target or cognate site or if it is independent from sequence. Transcription Factors (TFs) are a class of DNA binding proteins that regulate gene expression, that is activate or repress expression of specific genes when bound to their target sequence. These proteins, as all sequence-specific DBP, have a high affinity for their cognate sequence and a low affinity for non-specific DNA while non-specific proteins as, for example, histones or proteins involved in DNA repair have a high affinity for DNA independently on sequence. I focused my work on the first group, more precisely on the study of *lac* repressor (LacI). LacI is representative of a large family of bacterial transcription factors that has largely served as a model for transcriptional regulation and protein–DNA interactions. As the name suggests, this protein when specifically bound to its target sequence on DNA, represses expression of genes involved in the metabolism of lactose. The mechanism by which TFs find their targets among all combinations present in a genome with millions of base pairs is a long-standing question. In the 70's Riggs and coworkers (Riggs et al., 1970) measured the association rate of LacI and found it 100 times faster than the value expected from a 3D-random collision in the cytoplasm. From this moment, the most accredited model to explain such finding is the facilitated-diffusion, according to which proteins alternate between 3D diffusion and 1D diffusion along non-specific DNA. Nevertheless, the complete characterization of this model (and also the finding of Riggs), including its experimental observation still remains object of debate.

It is intuitive that to study such process, that is to track a single protein while searching for its target, it is necessary to use a single molecule approach. In particular, it is possible to detect the position of a fluorescently labeled protein using a microscope suitable for single molecule fluorescence detection. In this thesis a novel experimental set-up that combine single molecule high precision localization with a dual optical traps system, developed in our laboratories, is presented together with a microfluidic system used to assemble all components of the experiment. This apparatus allows to tether DNA between two optically trapped beads thus controlling and/or applying precise forces to the molecule which is, at the same time, kept far from the cover slip. A single fluorescently labeled *lac* repressor is imaged, when bound to DNA, through a wide-field illumination. I will discuss results obtained with this FIAT (Fluorescence Imaging And Trapping) apparatus. In particular, methodologies for protein labeling will be first introduced because, for fluorescence assays, it is a crucial step in that it could alter the native conformation of the protein thus leading, in case, to artifacts. Labeling a *lac* repressor mutant LacIQ231C with an organic fluorophore, ATTO532, did not alter the activity of the protein as shown by the measurement of characteristic times of association and dissociation through the FIAT set-up.

It will be discussed the impact of exposure time and DNA tension on the accuracy of localization and compared the commonly used 2D-Gaussian fit with a novel rapid and accurate algorithm for calculation of the Radial Symmetry Centre (RCS) for localization measurements. The last method has some advantages as rapidity that makes it more suitable for analyzing data of 1D-diffusion.

From trajectories obtained with the RSC calculation, 1D-diffusion coefficients have been measured of LacI diffusing on a DNA at different DNA tensions, thus exploiting the advantages of the FIAT apparatus for studying the target search mechanism.

2. Biology *In singulo*

At their most elementary stage, all biological reactions are carried out by single molecules. These processes have been largely explored by conventional biochemical and structural biology methods. However, these so-called "bulk measurements" describe the biological behaviour of a large ensemble of molecules by averaging the measured properties over the whole molecular population, leading to various limitations: can the different conformations, properties or even the dynamics of individual molecules be revealed by these methods? Generally, the answer is no. In order to be able to follow the dynamic changes on a molecular ensemble, the activities and the "biochemical state" of all molecules must be synchronized over their time trajectories, which would be impossible due to their intrinsic stochastic nature. Some techniques start a biochemical reaction from a population synchronized in a specific state, thus enabling the measurement of reaction kinetics or conformational dynamics of some biochemical transitions. However, even if initially synchronized in the same microscopic state, the population rapidly loses its initial "coherence" because the molecules are subjected to random fluctuations from the interaction with the thermal bath and, thus, exhibit stochastic dynamics (Bustamente et al., 2008). *Single-molecule* methodologies instead avoid the ensemble averaging of bulk experiments, since the dynamics of individual biomolecules are followed in real-time as they undergo their reactions (Finkelstein et al., 2010; Tafvizi et al., 2010; Bustamante et al., 2008; Kapanidis et al., 2009; Walter NG et al., 2008;, Huang CY et al., 2008; Zlatanova J. et al. 2006; Bustamante C. et al., 2005; Lu HP et al., 1998). In fact, this is one of the major and unique features of single-molecule approaches. Following the real-time trajectories of individual biomolecules undergoing their biochemical transitions affords the observation of entire multi-step reactions pathways and also reports on the kinetics and, possibly, the conformations of the intermediate steps. Rare and transient phenomena (that would be lost in averaging) can also be detected. In single-molecule approaches, there is no requirement for synchronization, since just one molecule is tracked at the time. Among other striking

features of single-molecule techniques is the possibility to localize biomolecules and their assemblies with nanometer accuracy and to directly measure the biophysical and mechanical properties while they undergo the biological process.

On the other hand, the development of single molecule methods, from its beginning applied to Physiology (with single-channel recordings and patch-clamp in 1976 (Neher et al., 1976)) to the present boom of applications in biosciences like Structural Biology, Nanotechnology, Enzymology and Systems Biology, has encountered a wide range of problems. Single-molecule techniques pose some challenges on the technical ground mainly due to the weakness of the signal: the order of magnitude of the experimental signal raised from an ensemble of molecules is very different from the one deriving from one molecule (Bustamante et al, 2008). Moreover, in order to accurately determine kinetics and draw statistically meaningful conclusions, a large dataset of individual single-molecule measurements must be acquired. Other drawbacks deal with the spatial and temporal resolutions, accessible measurement accuracies and instrument sensitivity.

Two general single-molecule methodological approaches have been developed: single-molecule *detection* and *manipulation* methods. The former allows the observation of individual molecules both in thermodynamic equilibrium or non-equillibrium conditions. Manipulation techniques instead, rely on the application of an external perturbation to the system, being the behaviour of the molecule studied under an external applied force. Both types of methods are described separately in more detail in the next chapters.

This revolution in Biology and Biochemistry and the establishment of single-molecule methodologies can be easily witnessed by the exponential growth of the number of publications with single-molecule words in the title by a simple search in PubMed (Moerner et al., 2007) and by the proliferation on their application in a broad range of biological systems as protein/RNA folding (Wang et al., 2012; kellermayer et al., 2007; Woodside et al., 2008), molecular motor (Capitanio et al., 2012; Yildiz et al., 2003; Yildiz et al., 2005; Svoboda et al., 2004), nanobiomachines (Noji et al., 1997; Xiao et al., 2008), nucleic acid-binding proteins (Finkelstein et al., 2010; Tafvizi et al., 2010; Lee et al., 2006; Abbondanzieri et al., 2008), DNA and RNA direct sequencing (Braslavsky et. al., 2003; Ozsolak et al., 2009) , translation (Blanchard et al., 2009; Vanzi et al., 2003), viral biology (Brandenburg et al., 2007), among others.

3. Molecular basis of protein-DNA interaction

The classic view of the Central Dogma in Molecular Biology was first formulated by Francis Crick, one of the co-discoverers of the structure of the DNA (Deoxyribonucleic acid), in 1958 (Crick et al., 1958; Watson et al., 1953) and later on popularized in a *Nature* paper published in 1970 (Crick et al., 1970). DNA is a polymer made up of two polynucleotide chains wrapped on each other to form a double helix (figure 3.1 a). The backbone of each strand is composed by sugars alternated with phosphate groups while base pairs are projected in the inside but are accessible through major and minor groove (figure 3.1 b)

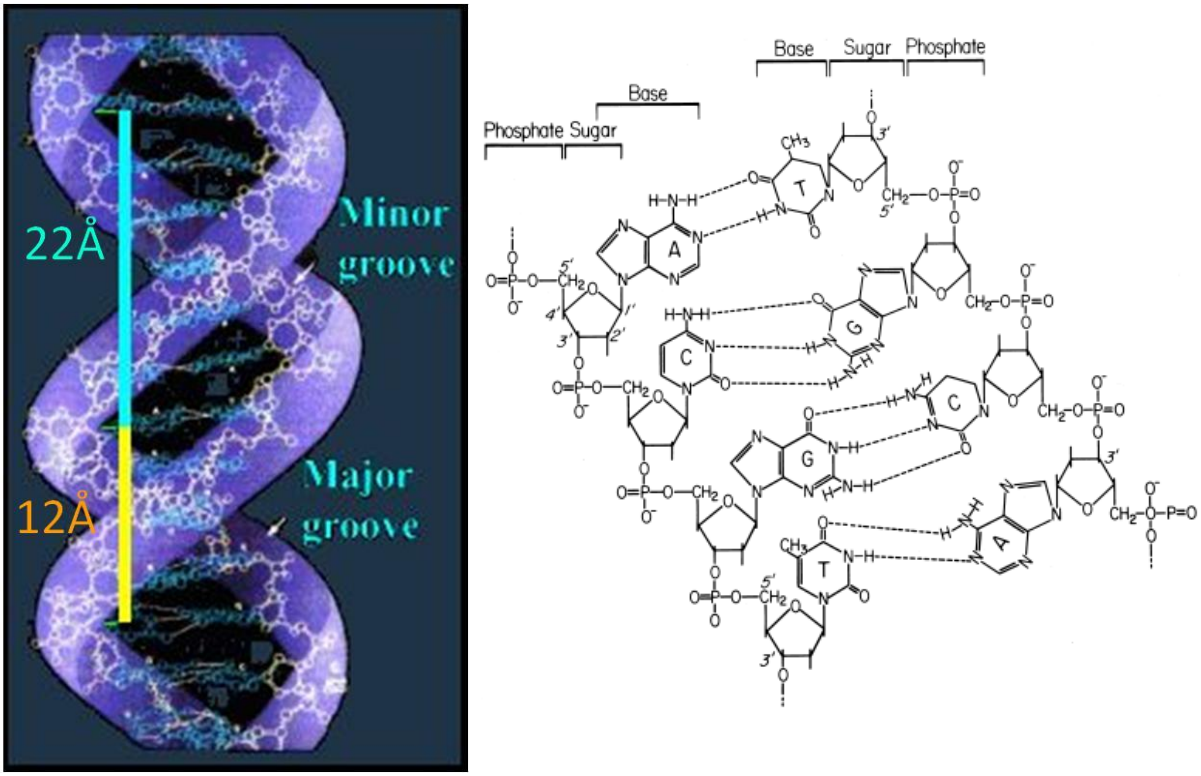

Figure 3.1: (a) Structural model of the DNA double helix. One helix turn (3.4 nm) contains about 10.5 base pairs. Base pairs are only available from the minor and major grooves. Adapted from http://www.phiengineering.com/what_is_phi.htm. (b)Chemical structure of the double-stranded DNA. A nucleotide (which is the elementary unit of the polymer) is composed by a phosphate moiety (P), linked to the 5' hydroxyl of a pentose sugar, whose 1' carbon is linked to an organic base. The pentose sugar is a ribose in the case of RNA and a deoxyribose in DNA. There are five different nitrogenous bases: the purines Adenine and Guanine (containing a pair of fused rings) and the pyrimidines Cytosine, Thymine. The first three bases are present in both nucleic acids (RNA and DNA), but Thymine is present just in DNA (by convention, the bases are often abbreviated A, G, C, T). Due to the chemistry of the sugar structure, the ends of the two chains are referred as either 5' or 3'. The bases can interact via hydrogen bonds and the standard Watson-Crick base pairs are G•C (which make three hydrogen bonds) and A•T (two hydrogen bonds) in DNA. Base pairing and hydrophobic interactions between adjacent bases in the same strand stabilize its native structure. Image reproduced from http://www.gene-quantification.de/mrna.ht

As shown in figure 3.1, minor and major grooves alternate each other due to the helical structure of the strands. Base pairs atoms are accessible for DBP from both grooves, but the major groove provides more chemical information. Basically, from the major groove there are more possible contacts available and for DBP is easier to recognize the right base pairs. In fact proteins usually bind at this groove (Pabo et al., 1984) (figure 3.2).

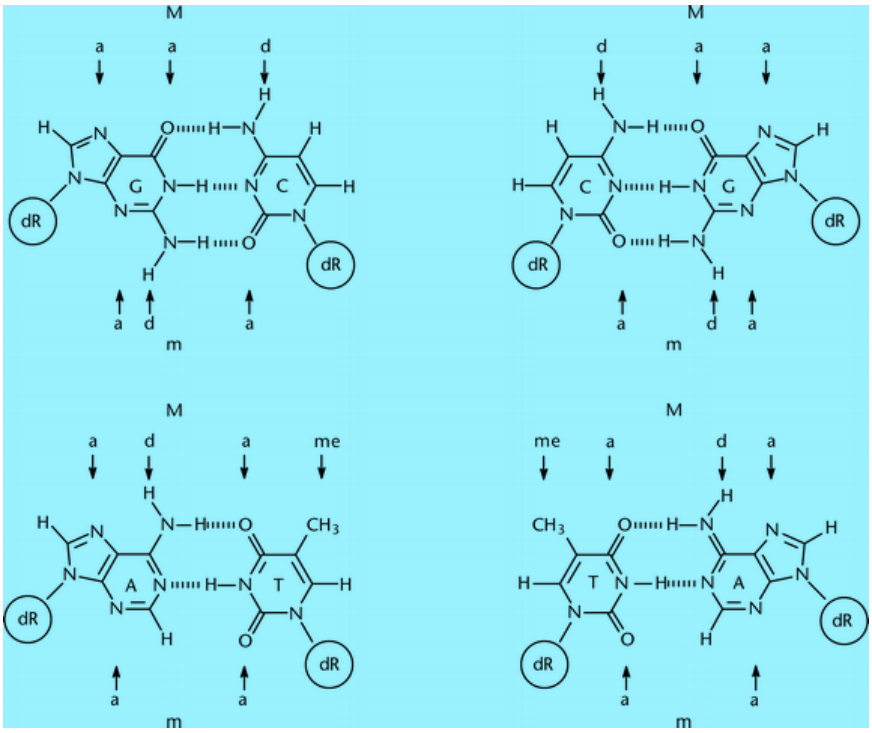

Figure 3.2. Points of recognition in the major (M) and minor (m) grooves of DNA for each of the four base pairs. a, electron acceptor; d, electron donor; me, methyl group. Hydrogen bonding in base pairs is indicated by dashed lines. dR in circles denotes the deoxyribose-phosphate backbone of DNA. Strauch, Mark A(Apr 2001) Protein–DNA Complexes: Specific. In: eLS. John Wiley & Sons Ltd, Chichester. http://www.els.net [doi: 10.1038/npg.els.0001357]

On the other hand, the structure adopted by proteins for DNA binding and recognition is the alpha helix which perfectly fits with the major groove (figure 3.3).

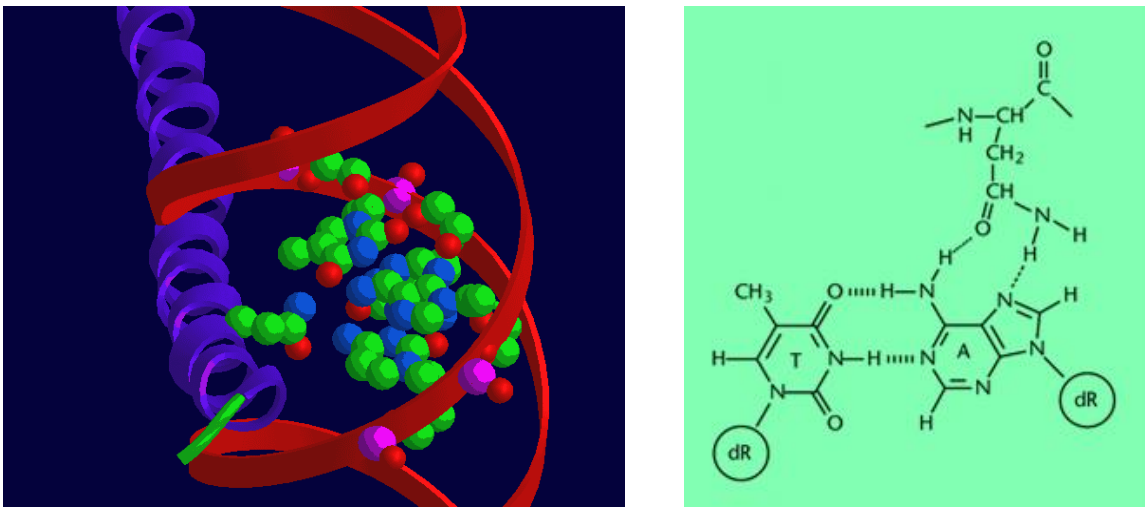

Figure 3.3.(a). Bondings between an asparagine of an alpha helix (violet ribbon) and base pairs (cartoon) in the major groove. Blue is nitrogen while red is oxygen and green sphere is carbon. Adapted from http://www.biosino.org/mirror/swift.embl-heidelberg.de/course/DNAold/chap1.html. (b). Atomic details of an asparagine bonding to adenine from the major groove. Hydrogen bonds are denoted by dashed lines. T= timine, A=Adenine, dR= deoxyribose. Strauch, Mark A(Apr 2001) Protein–DNA Complexes: Specific. In: eLS. John Wiley & Sons Ltd, Chichester. http://www.els.net [doi: 10.1038/npg.els.0001357]

The interactions and recognition between biomolecules is the basis of the central dogma of biology which states that each gene in the DNA molecule carries the information coding for one protein, the primary molecules that make up cell structures and carry out cellular processes. In this one-way flow of genetic information from DNA to proteins, a third molecule is required: the messenger RNA (Ribonucleic acid) (mRNA), that serves as the proxy and carries the information specifying the correct order of amino acids to be assembled into a protein, during protein synthesis or *Translation* (figure 3.4).

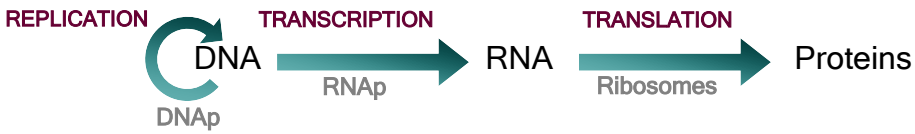

Figure 3.4: Schematic representation of the central dogma in molecular biology.

This critical trio of macromolecules – *DNA*, *RNA* and *proteins* – is present in all living cells and sits at the core of the pathways controlling cellular processes and fate. The properties of these *molecules of life* and their innumerable variations present in different organisms have been broadly studied by modern researchers, which have employed concepts and experimental procedures drawn from biochemistry, genetics, molecular and cellular biology to also biophysics.

Regarding the goal of this thesis, from the biophysical point of view, DNA is described as a *semi-flexible polymer* that bends locally as a result of thermal fluctuations. The binding of proteins to DNA (required for numerous biological processes, such as DNA replication, transcription, packaging, restriction, DNA repair, among others) can also deform its helical structure, causing local bending, twisting, looping or unwinding of the molecule.

4. The *lac* Operon

The *lac* repressor (LacI) is a bacterial protein involved in gene expression regulation in *Escherichia Coli*, where it represses the expression of genes involved in the metabolism of the disaccharide lactose. Like gene expression, all biological processes, are finely regulated by organisms. This is because living organisms have to adapt themselves to a fluctuating environment to survive while keeping energy expense minimal. In other words, to minimize energy expense, the same biological process can be activated or not according to the external conditions. In the case of lactose metabolism regulation, the fluctuation arises from the type of carbon and energy source available: glucose or lactose. Gene expression represents a huge energy expense for the cell because many biomolecules (RNA and proteins) have to be synthesized. If there is no lactose in the external environment,

expression of genes involved in its metabolism, would be definitively a waste of energy for the cell.

At the molecular level,this waste is minimized in several ways. An operon is a group of genes transcribed as a single unit. In the case of Lac operon, there arethree genes: *LacZ*, *LacY* and *LacA* encoding respectively for β-galactosidase (which hydrolyses lactose into glucose and galactose), β-galactoside-permease (responsible for the up-take of lactose) and for β-glactoside transacetylase (which links an acetyl group to β-galactosides). When the operon is transcribed, RNA polymerase synthesizes a unique mRNA containing the information for all three genes and that will be eventually translated by ribosomes into the three proteins (Jacob & Monod 1961). It is intuitive that all the genes constituting the operon are under the same regulation. The first step of transcription requires the binding of the RNA polymerase at the promoter which is located up-stream the genes to be transcribed. As we can see in figure 4.1, there is another sequence superimposed to promoter: the Operator. This is the sequence by which *LacI* has high affinity for ($Kd=5x10^{-11}$ M) (Hsieh et al., 1987). This superimposition suggests that there is a competition between *LacI* and RNApol for binding at that region of DNA. When *LacI* is bound to operator, RNA polymerase is physically hindered to transcribe for sterical hindrance. This is the situation when lactose metabolism proteins are not required, i.e. when lactose is not present in the medium. The presence of lactose is sensed by the repressor itself; lactose binds to its lactose binding region which in turn makes the protein lose its affinity for operator. Since for expressing lac operon genes glucose has also to be absent, there is a molecular sensing for glucose too. In absence of glucose, cyclic Adenosin Mono Phosphate (cAMP) is produced and binds to its receptor, catabolite activator protein (CAP). This binding enhances CAP affinity for its target on DNA.

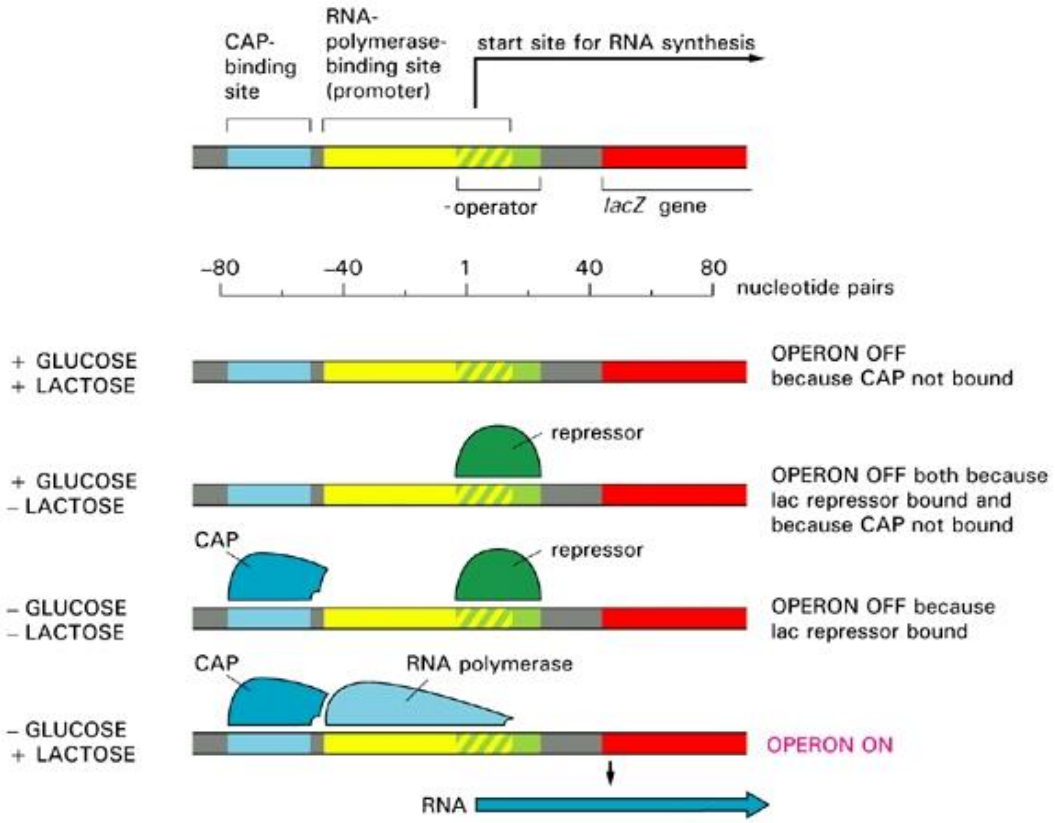

Figure 4.1. The figure represents the four combinations of external conditions, varying from the presence of both sugars to the situation when just one sugar is present, or when there are no sugars available. Lac repressor is bound to operator and physically prevent genes transcription just when lactose is absent; on the other hand, CAP protein is bound to its site and enhances transcription when glucose is absent. Image reproduced from http://www.thetruthaboutgenetics.com/2011/07/lac-operon.html

When bound to DNA, CAP directly interacts with RNA polymerase which facilitates its binding to the promoter and thus transcription. In summary:

- When lactose is absent there is very little Lac enzymes production (LacI is bound to the operator).
- When lactose is present but a preferred carbon source (like glucose) is also present, a small amount of enzymes is produced (Lac repressor is not bound to the operator).
- When only glucose is absent, CAP-cAMP binds to a specific DNA-site (situated upstream to the promoter) and makes a direct protein-protein interaction with RNA polymerase which leads to an enhanced binding of RNA polymerase to the promoter

4.1 *Lac* Repressor

The *lac* repressor was isolated in 1966 by Walter Gilber and Benno Müller-Hill (Gilbert et al., 1966).The purified protein may exist in a monomeric, dimeric or tetrameric form. The last consists of four identical subunits, each one composed by 360 amino acids. When assembled into its tetrameric form, the repressor has a molecular weight of 154.52 KDa. Figure 4.2 shows the monomeric structure of *LacI* (4.2a) and its tetrameric structure in association with DNA (4.2b). Each monomeric subunit is composed by three domains: N-terminal domain (residues 1-62), the core protein domain (residues 63-340), and the C-terminal domain (residues 341-357). The N-terminal domain is involved in DNA binding and can be subdivided into two further subdomains: the DNA-binding region (residues 1-45) and hinge region (residues 46-62). DNA binding region, also known as the repressor head-piece, contains a helix-turn-helix (HTH) motif and the hinge region links DNA-binding region to the core of the protein. This flexible region of the LacI allows the DNA-binding region and the core of the protein to move independently of each other. (Friedman et al., 1995).

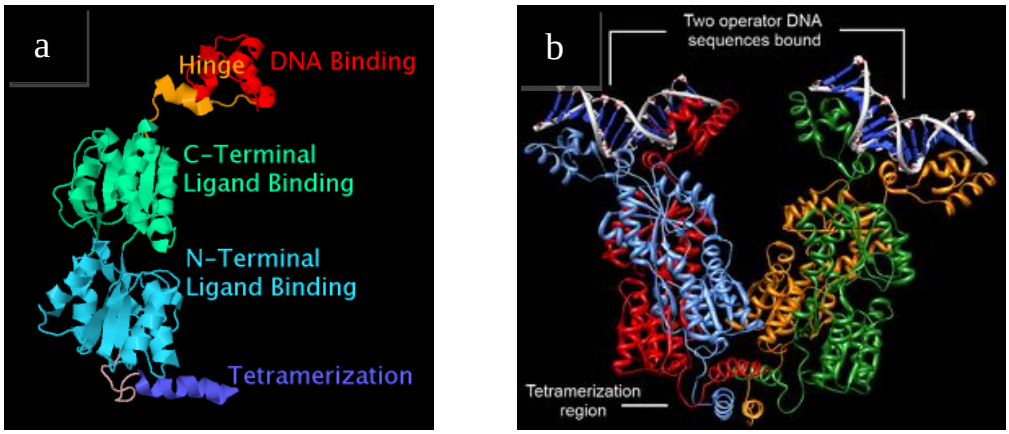

Figure 4.2. (a) Structure of the *lac* repressor monomer. Reproduced from http://proteopedia.org/wiki/index.php/Help:Snapshots (b) structure of the complex formed between the tetrameric lacIand the DNA operators. Reproduced from http://en.wikipedia.org/wiki/Lac_repressor (Lewis et al., 1996)

It has been shown (Lamerichs et al., 1989) that the hinge region makes specific interactions with *lac* operator, orienting the head piece for DNA-binding. The hinge region is capable of doing so through a conformational switch of residues 50-58 from an unstructured coil to a defined helix in presence of operator DNA. In the absence of the operator these

residues are relaxed, allowing repressor head piece to freely dangle. The core repressor protein is also known as the inducer binding domain. The protein C-terminus is responsible for the molecule being a tetramer, formed when the alpha helixes of the four monomers associate in an antiparallel fashion (Friedman et al., 1995). Although the molecule is a homo-tetramer, it makes sense to think about it as a dimer of dimers; though all monomers are oriented to the same point in the space, dimers are oriented in different planes giving rise to the skewed, V shape of the molecule, with the two DNA-binding regions at the upper points of the V (figure 4.2b) (Friedman et al., 1995).

4.2 DNA looping

As described before, LacI contains two DNA binding domains so that two DNA target sequences can be bound simultaneously. In fact, wild type lac operon contains multiple operators: the “principal” operator O1 and two auxiliary operators designed O2 and O3 (table 1), (W.S. Reznikoff et. Al., 1974). LacI can thus bind to two out of the three operators inducing a loop in the intervening DNA as illustrated in figure 4.3 to fully repress the transcription of the operon lac, according to cell needs.

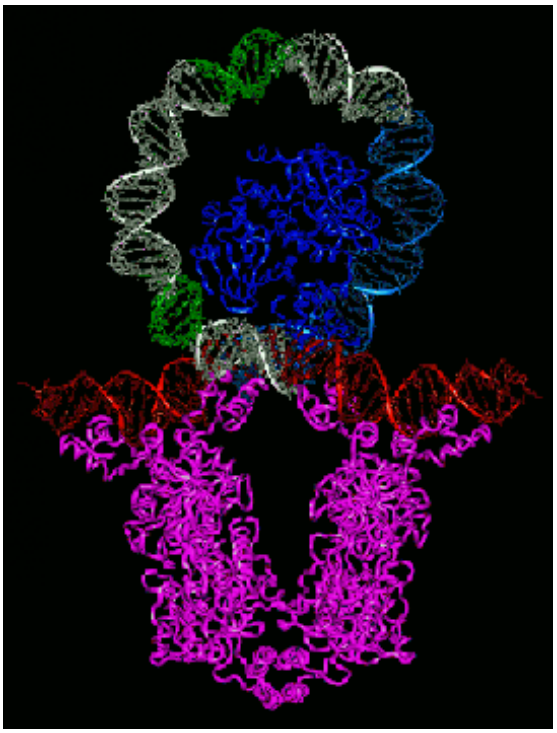

Figure 4.3. In 1996, the crystal structure of the LacI-DNA complex was reported (M. Lewis et al., 1996) and a model for the 93bp repression loop (corresponding to the lac operon -81 to +11) was proposed: the ends of the loop contain operators (red sequences) to which the bound LacI tetramer (violet) is shown . Inserted in the loop is the CAP protein and 30bp DNA complex (blue). Grey DNA was created by applying a smooth curvature to B-DNA. The curvature of the modeled portion of the loop is about 40 Å; highlighted in green are the sites of the lac promoter. Image reproduced from (M. Lewis et al., 1996).

operator	sequence	Affinity for LacI (Kd)
O1	AATTGTGAGCGGATA ACAATT	0.05nM
O2	AAATGTGAGCGAGTA ACAACC	0.1nM
O3	GGCAGTGAGCGCAAC GCAATT	100nM

Table 1. List of the three operators present in lac Operon with respective sequences and affinities for LacI.

The different sequences of operators lead to different affinities for *LacI* which in turn determine, together with the operators positions, different repression efficiencies. O2 was found 401 bp downstream of O1, whereas O3 was found 92bp upstream of O1. Since deletion of either O2 or O3 decreased repression two- or three fold, but the deletion of both leads to a 70-fold decrease in repression,O2 and O3 were termed auxiliary (Oehler et al., 1994). The increase in repression by auxiliary operators due to loop formation (i.e. simultaneous binding to O1 and O2 or O1 and O3) was first proposed in 1977 (Kania et al., 1997) and it is currently the most reliable hypothesis. An *E. Coli* cell contain ~10 copies of LacI molecules, so the limiting step of the repression is the search of the operator sequences among millions of base-pairs of non-specific DNA. This process occurs by diffusion and the binding probability depends on LacI concentration. If *LacI* stays in the proximity of the primary operator O1, the probability of binding to this site is much higher than a freely diffusing molecule in the cytoplasm. On the other hand, when the repressor is bound to one of the three operators, the protein remains close in space to the operon (i.e. it is physically confined to that area leading to an increase of the local concentrationof LacI), and correspondingly the repression increases.

5. Mechanism of Target search on DNA

Once discussed the mechanism through which Lac repressor regulates genes expression when associated to its target sequence on DNA, let us consider now the kinetics aspects of the association to the operator which represents the limiting step of the repression process. How fast the cell represses lactose metabolism genes in response to fluctuation of external source of carbon corresponds definitely to the association rate of lactose repressor to operator. This consideration is valid for all Transcription Factors (TFs) who must find their target on DNA among an extremely high number of base pairs. For lactose repressor we have to think that there are only 5-10 copies of the molecule per cell (Gilbert et al., 1966) and operator is 24 base pairs sequence (M. Lewis, 1996) in a genome which contains 4.6 million base pairs (F.R. Blattner, 1997) and genome is also in a coiled conformation (figure 5.1). What one would expect from this numbers is that the target search is effectively limiting. Nevertheless, once *lac* repressor occupies the operator for the first time, it will stay tightly bound for a long time (Kd=0.05nM), whereas it remains unbound only a short fraction of time. In this fraction of time, another molecule of repressor will bind because, even if there are few molecules in the cell, their concentration (10 molecules in $1\mu m^3$ corresponding to 10^{-8}M) and this value is three order of magnitude higher than the Kd meaning that there should be always a lactose repressor bound to the operator. This consideration implies that the limiting step is actually only the first event of operator occupancy by a *lac* repressor molecule.

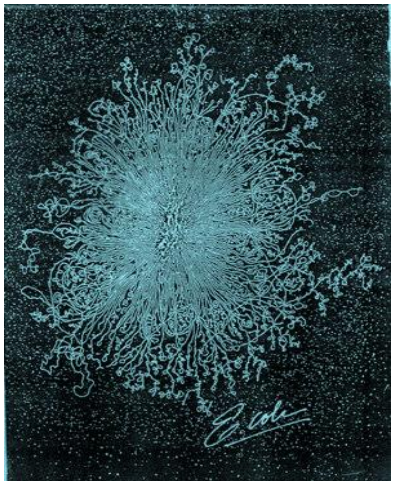

Figure 5.1. This picture shows an E. coli bacterium with its genomic DNA extruded onto an electron microscope slide. E. coli is about 1-2 microns long. Its circular genome is about 1000 times longer than the bacterium itself. When extruded from the cell, it looks like this. The mass in the center is what's left of the E. coli bacterium after lysis. Image from http://www.pitt.edu/~mcs2/ecoli.html.

At the beginning of 70s, Riggs and coworkers measured the association rate of lactose repressor to a 50 kbp long DNA containing the operator (Riggs et al., 1970) and found it surprisingly fast, following second-order kinetics with a rate constant for protein association to DNA, ka=7x10^{9} M^{-1}s^{-1}. The interest for the target search mechanism which is still active today, arises from the mismatch of the measured value from a theoretical value obtained considering (as one would expect) protein finding a DNA target sequence of length l_{seq} stochastically by random 3D diffusion. This theoretical value is obtained using Smoluchowski's equation (M. von Smoluchowski 1917, R.A. Alberty etal., 1958) for the association rate by 3D- diffusion:

$$K_{a(3D)} = 4\pi D_3 l_{seq} \qquad (1)$$

Where $D_3=K_BT/3\pi\eta a=9x10^{-7}$ cm^2/s is the 3D diffusion coefficient of the protein in solution, where K_B is the Boltzmann constant, T the temperature, η the viscosity of the solvent and $a\approx5$nm is the typical diameter of the protein. According to equation 1, the association rate of a protein to a DNA sequence length, l_{seq} , of 3 base pairs (1nm) should be theoretically equal to 10^8M^{-1}s^{-1}, two orders of magnitude slower than that found by Riggs and coworkers.

In 1981, in order to explain the measured association rate that appeared 100 fold faster than the diffusion limit, Berg, Winter and von Hippel introduced the facilitated diffusion model (Berg et al., 1981). The major feature of the facilitated diffusion model is

that two different kinds of exploration alternate during target search (Halford et al., 2004, L. Mirny et al., 2009). The fist way of exploration is three-dimensional free diffusion in the cytoplasm, unbound from DNA. The second kind of exploration is given by a non-specific DNA-bound state where proteins are assumed to non-specifically bind and slide along DNA, in the so-called 1D-diffusion. Sliding events can be seen as a scans of the base pairs composition by DNA proteins to find the right base pair sequence, i.e. their target cognate DNA. Such a mechanism is also defined "intermitted search" (figure 5.3a) and, for 1D search limited to few tens of base pairs and with appropriate 3D-1D transition kinetics, it is supposed to act increasing the effective protein concentration near the DNA and thus accelerating the target localization rate (Berg et al., 1981). This facilitated-diffusion modified protein-target association rate k_a per protein concentration has been derived by Halford and Marko (Halford et al., 2004):

$$\boldsymbol{k_a = \left(\frac{1}{D_3 l_d} + \frac{L l_d c}{D_1}\right)^{-1} = k_{a,3D}\left(\frac{l_{seq}}{l_d} + \frac{D_3}{D_1} l_{seq} L l_d c\right)^{-1}} \qquad (2)$$

Where D1 is the 1D diffusion coefficient of the nonspecifically bound protein along the DNA, L is the total length of the DNA molecule, l_d is the maximum contour distance covered by the protein before dissociation, c is the concentration of the target, and $\left(\frac{l_{seq}}{l_d} + \frac{D_3}{D_1} l_{seq} L l_d c\right)^{-1}$ is the acceleration factor to $k_{a3D}=4\pi D_3 l_{seq}$. Wang and coworkers (Wang et al., 2006) tried to measure the accelerator factor by measuring D_1 and l_d of lac repressor. They used a GFP fusion of *lac* repressor (which could not tetramerize and thus being only in the dimeric or monomeric aggregation state) and the DNA was anchored to the cover slip stretched to few pN; single molecule imaging was achieved using a TIRF (Total Internal Reflection Fluorescence) microscope with a mean exposure time of 10ms (figure 5.2).

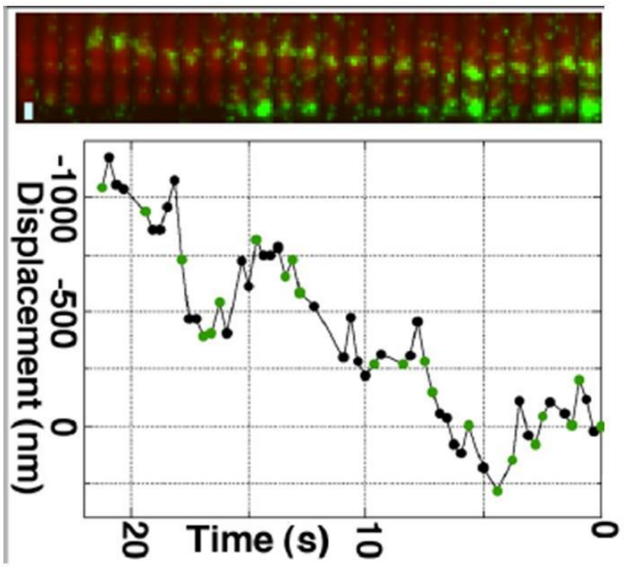

Figure 5.2. A kymogram of a diffusing protein (top) with its relative position during time before photobleaching (bottom) Adapted from Wang et al., 2006.

Figure 5.2 shows the kymogram of a protein trajectory and the relative displacement of the protein vs time curve. Kymograms are obtained by a 90° rotation of all frames (and, if desired, the cropping of the region of interest) followed by juxtaposition of all frames. In the resulting montage, the *x* axis, parallel to DNA, will be oriented vertically while the horizontal axis will be the time. The 1D diffusion coefficient was obtained from the Mean Square Displacemt (MSD) of all trajectories (Wang et al., 2006)

$$\boldsymbol{MSD}_{(n,N)} = \frac{\sum_{i=1}^{N-n}(x_{i+n}-x_i)^2}{N-n} = \boldsymbol{2D_1 n\Delta t + 2\sigma_s^2} \quad (3)$$

where N is the total number of positions measured, n is the measurements index going from 1 to N, Δt is the time interval between two consecutive position measurements, and σs is the localization uncertainty associated with each x_i. In this way they obtained a mean diffusion length l_d of 500nm (probably a lower bound of the true value due to photobleaching) and a mean 1D- diffusion coefficient D_1 of 2.1x10-10 cm^2s^{-1} . Using these values, with L=15.5µm and D_3=4x10^{-7} cm^2s^{-1} , they calculated the accelerator factor in equation 2, which corresponded to 93±20 which seems to solve the discrepancy between theoretical and experimental data for the association rate.

According to the facilitated diffusion model, proteins can slide along DNA keeping a continuous contact with DNA until they detach and undergo a 3D diffusion (figure 5.3a) or through very fast (with respect to the experimental temporal resolution) sequence of

unbinding and binding events. This behavior is thus called “hopping”. When, after unbinding, a protein binds far from the previous location, this is called “jumping”. Proteins with two DNA binding domains (like *lac* repressor) can bind to two sites on DNA (even not adjacent) inducing a loop; if the protein first binds on a site A, then binds to a site B with the other DNA binding domain making the loop and then unbinds from site A staying bound with only one binding domain to site B, the result is a transfer from a segment to another of DNA. This is in fact called “intersegmental transfer” (Figure 5.3b)[1].

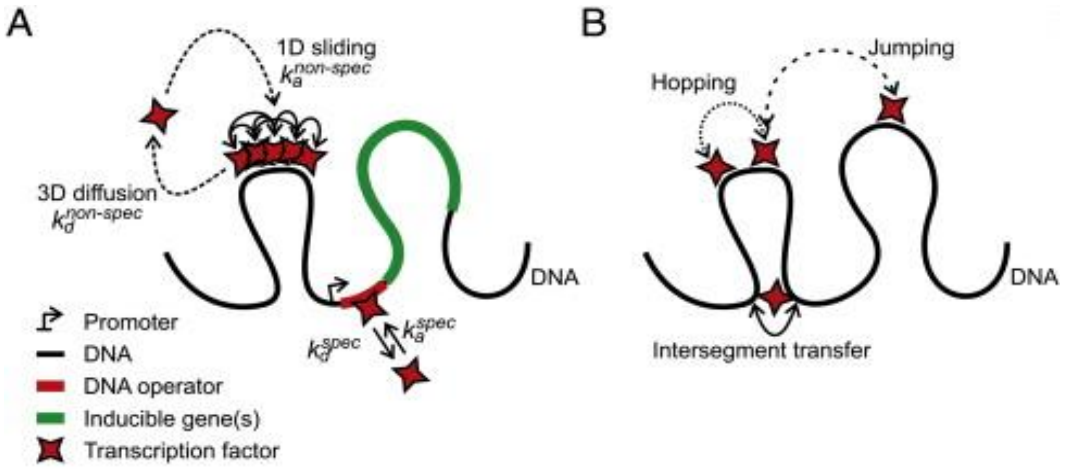

Figure 5.3. A a schematic representation of facilitated diffusion mechanism which implies an alternation between 3D-diffusion in the cytoplasm an 1D-diffusion bound to DNA. B Different modalities of target search. Image adapted from (Normanno et al., 2012)

[1] This is also the same mechanism monkeys use (brachiation) to move in a very fast fashion from a tree to another without passing from the soil. If monkeys should descend from one tree and then climb to another the speed of the food search would be definitively lower. Also for proteins, staying always bound to DNA, that is increasing their local concentration is the way to accelerate the target search.

6. Search vs recognition: the two-state model

For understanding why it is possible for a protein to move along DNA, one has to consider the energetics of the system. If the affinity of the protein for non-cognate DNA is high the protein would stay bound nonspecifically for long time. It has been estimated that a binding energy barrier landscape ≥ $2K_BT$ would extremely slow down diffusion, with the protein unable to diffuse more than a few base pairs. Experimentally observed and biologically relevant rates of search can be reached only when one-dimensional sliding proceeds through a fairly smooth landscape with a roughness of the order of K_BT. On the other hand, the stability of the protein-DNA complex at the target site requires a roughness of the binding energy landscape considerably larger than K_BT and diffusion at such a roughness is impossible. Slutcky and Mirny in 2004 (Slutcky et al., 2004) proposed a two-state model to resolve this apparently contradictory energetic considerations. The paradox can be resolved if the DNA-binding protein has two distinct (conformational) states in which it exhibits two modes of binding.

In the first mode which has weaker binding and smoother landscape, protein searches for the cognate site. In the second (recognition) mode, which has larger roughness of the binding landscape, the protein tightly binds DNA. They also suggested that this transition is a conformational transition or at least a partial folding. The standard deviation σ of the energy profile is used to quantify the roughness of the landscape and is about 1.0-2.0 K_BT for the search mode and greater than 5.0 K_BT for the recognition mode. A protein in nonspecific binding mode is “unaware” of the DNA sequence it is bound to. Thus, it should permanently alternate between the binding modes, probing the underlying sites for specificity. If the TF is to probe every site for specificity in this fashion, it would take hours to locate the cognate site resulting in a waste of time. The proposed model suggests that only sites whose binding energy is correlated with the actual specific binding energy (σ~5-6 K_BT) are probed. These sites, which represent sites similar in sequence and thus also in the relative binding energies, constitute a very small fraction of the total number of sites implying that transitions between modes are rare and so not limiting the target search rate.

The coupling between the conformational change and association at a site with low energy (“trap”) is likely to take place through time conditioning. This means that the

transition occurs if the protein spends some minimal amount of time bound to a certain site. This statement is basically equivalent to saying that the free energy barrier that the protein must overcome to transform to the final state must be comparable to the characteristic energy difference that controls hopping to the neighboring sites. Once the transition is occurred, the new structure offers additional contact points for new protein-DNA interactions. At the cognate site, these interactions further stabilize the recognition mode and the protein stays specifically bound for a very long time. If these new interactions are unfavorable, the search conformation is restored and diffusion proceeds as before. The folding of partially disordered protein loops of helices can provide the required free energy difference between the two modes.

Alternatively, the cognate site can lower the barrier by stabilizing the transition state, whereby it acts as a catalyst of partial folding (Abkevich et al., 1994, Mirny and Shakhnovich, 2001).

7. Fluorescence Microscopy

To study the dynamics of biomolecules at the single molecule level, the first step is to visualize them. Due to their nanometric dimensions, individual biomolecules must be tagged with probes to be detected, like organic fluorophores (as cyanine and rhodamine families) or alternatively with fluorescent protein probes, as Green Fluorescent Protein[2] (GFP) (Tsien et al., 1998) or its variants. Fluorescent molecules are characterized by emitting light at longer wavelengths than the excitation light; this phenomenon of *fluorescence* was first observed by the Irish Sir George Gabriel Stokes (Figure 7.1).

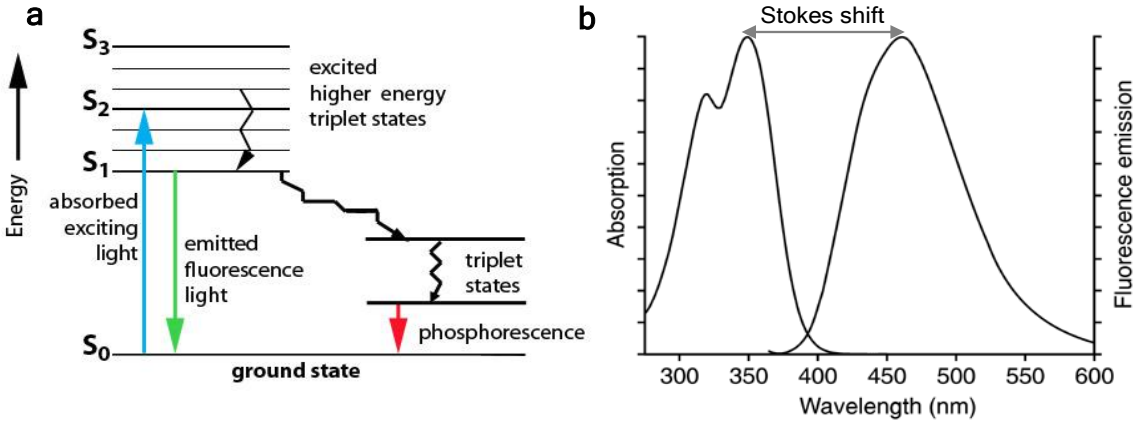

Figure 7.1: (a) A Jablonski diagram shows a number of possible routes for the relaxation mechanism of excited molecules. An incoming photon causes an electron to move from a stable singlet ground state (S_0) to a higher vibrational energy, unstable excited level (either S_1, S_2 or S_3). The excited electron can decay to the ground state, emitting a photon of light (fluorescence). There is always some energy lost to heat in the process, so the emitted photon has less energy than the original photon. Molecules in the S_1 state can also undergo a spin conversion to the first triplet state, in a process called intersystem crossing. Emission from T_1 is termed phosphorescence and is generally shifted to longer wavelengths. **(b)** Absorption and fluorescence emission spectra of quinine sulphate. In the case of quinine, the emission spectrum is not perfectly a "mirror image" of the absorption spectrum, as generally occurs with fluorophores. That is because the shorter wavelength absorption peak comes from the excitation to the second excited state (S_2), which relaxes immediately to the lowest singlet state S_1, so emission from S_2 energy level is not observed on emission spectrum of quinine. Note the stokes shift between the two spectra.

As depicted on the Jablonski diagram in Figure 7.1a, the spin of an electron on the excited singlet state of the fluorophore can invert producing a triplet. The triplet state is relatively long-lived with respect to the singlet, allowing thus excited molecules a much longer timeframe to undergo chemical reactions with components in the environment.

[2] GFP is a naturally fluorescent protein present in the specie of jellyfish *Aequorea Victoria* , discovered in 1961 by Shimomura and coworkers. He was awarded together with M. Chalfie and R. Y. Tsien the 2008 Nobel prize in Chemistry for the discovery and experimental development of GFP.

When such interactions produce irreversible covalent modifications, the fluorophore permanently loses the ability to fluoresce. This phenomenon is called *photobleaching* and it's due to photon-induced chemical damage and covalent modification.

In conventional *epifluorescence* microscopy the specimen is illuminated in wide-field by a collimated beam of light (figure 7.2.a); the fluorescence image is the sum of sharp image details from the in-focus-region combined with blurry signal from all the out-of-focus regions, leading to a decrease in the contrast of the in-focus image. *Confocal* microscopy overcomes this problem by spatial filtering (i.e. introducing a pinhole in front of the light source and/or in front of the detector) (figure 7.2.b) to eliminate out-of-focus contributions in specimens that are thicker than the focal plane. This feature allows a significant reduction of the background noise. To obtain an image with the confocal microscope, the focused spot of light is scanned across the specimen, producing optical sections of the specimen that can be reconstructed into a three-dimensional image. Another illumination geometry that allows a significant reduction of the background noise is *Total internal reflection* fluorescence (TIRF) microscopy (figure 7.2.a). TIRFM uses an induced evanescent wave to excite fluorophores in a limited region of the specimen, immediately adjacent to the interface between two media having different refractive indices (figure 7.2.c). The excitation laser hits the slide with an angle higher than the total internal reflection critical angle. The evanescent wave generated on the slide decays within typically 100 nm in the sample. This plays the role of spatial selection (comparable with the pinhole used for confocal microscopy, but with much higher background rejection) because only the molecules located in near proximity of the interface can be excited.

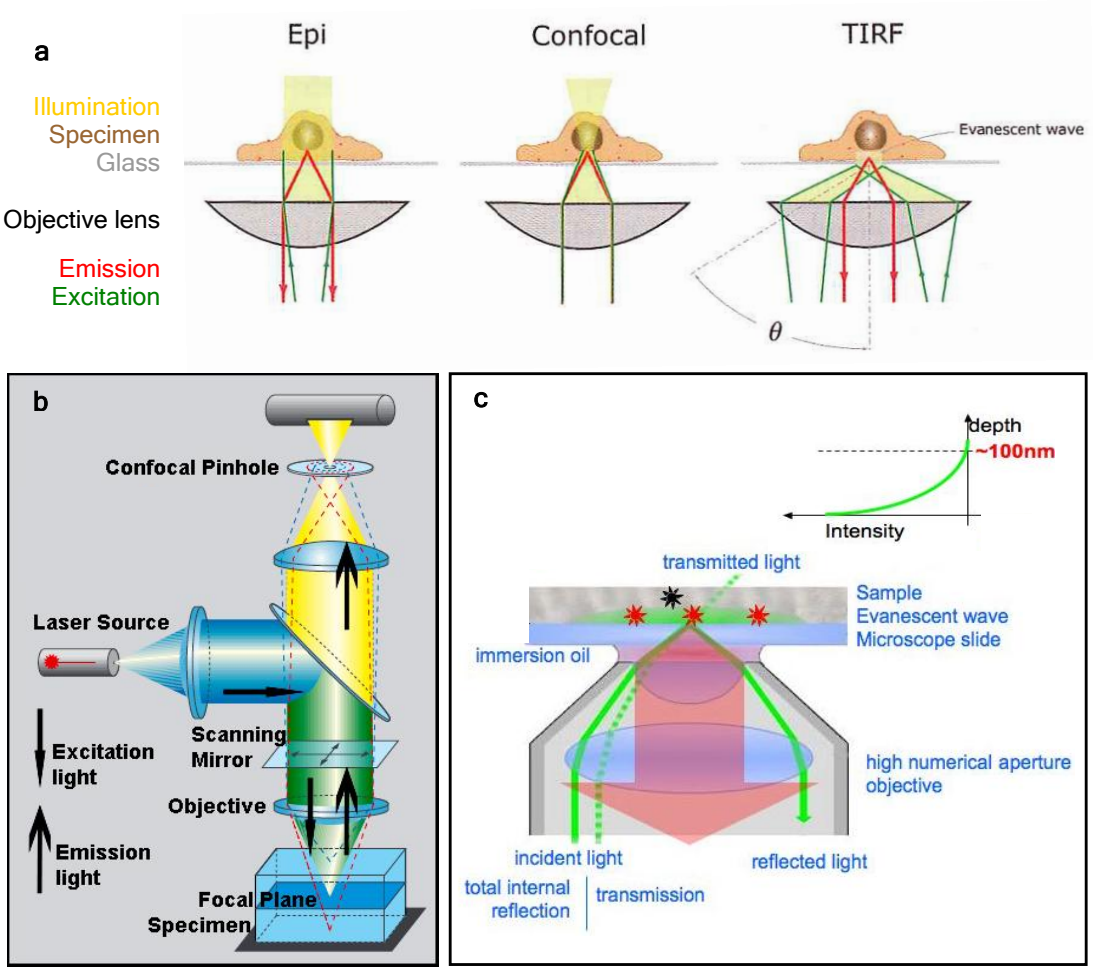

Figure 7.2: (a) Schematic drawing of three different fluorescence imaging geometries [32]. See text for further details. **(b)** Confocal microscopy. Due to the presence of a pinhole aperture, only the light from the focal plane of the objective (yellow) reaches the detector. Blue and red rays represent the contributions from above and below the focal plane, respectively. Adapted from http://www.rudbeck.uu.se/en/node48. **(c)** TIRF microscopy uses the evanescent wave from light that is totally internally reflected at an interface to selectively excite fluorophores that are in very close proximity to that interface. Figure adapted from http://atomoptic.iota.u-psud.fr/research/biophysics/biophysics.html

7.1 High Precision Single Molecule Detection

A point light source, like a single fluorophore or nanocrystal, appears as a diffraction limited image (Point Spread Function) whose width is ≈ ʎ/2 N.A. where ʎ is the wavelength of the excitation light and N.A. the numerical aperture of the collecting lens ("*Abbe's law*" or "*Rayleigh's resolution limit*"). Considering that for a microscope the practical maximum N.A. is < 1.65, this width, which represents the resolution limit, is ≈250nm for visible light. In these conditions, two point sources can be resolved as two separate entities, only if their distance is larger than 250 nm in the focal (x-y) plane.

Nevertheless, the centre of the PSF, which under proper conditions corresponds to the position of the light source, can be localized with an arbitrary high precision if a sufficiently high number of photons are collected. In order to determine the centre of the image, Cheezum and co-workers published in 2001 (Cheezum et. El., 2001) a work where they demonstrated that the best function to fit the intensity distribution of point image (also called Point Spread Function, PSF) is a 2D Gaussian curve:

$$G(x_0, y_0, \sigma_x, \sigma_y, b, A) = b + Ae^{\left\{-\frac{1}{2}\left[\left(\frac{x-x_0}{\sigma_x}\right)^2 + \left(\frac{y-y_0}{\sigma_y}\right)^2\right]\right\}} \quad (4)$$

where x_0 and y_0 are the coordinates of the centre, A is the amplitude, σ_x and σ_y are the widths along the two axes and b the background. From this fit is thus possible to obtain the coordinates of the centre of the distribution. Fit is performed in MATLAB using χ^2 minimization.

Any image acquired by a camera is affected by different contributions of noise (shot noise for photons collection statistics, fluorescence background, camera readout and pixelization effects). Thompson et al derived a theoretical expression for the error of localization in an article in 2002 (Thompson et. Al., 2002) considering all these contributions along one direction:

$$\sigma_{\mu i} = \sqrt{\frac{\sigma_i^2}{N} + \frac{a^2/12}{N} + \frac{8\pi\sigma_i^4 b^2}{a^2 N^2}} \quad (5)$$

Where the index *i* refers to the direction *x* or *y*. N is the number of detected photons, *a* pixel dimension in nanometers and *b* the standard deviation of background photons. The first term represents the uncertainty due to diffraction limit; the second represents the contribution due to the finite pixel size of the camera and the last term represents the contribution of background. When the pixel size is properly chosen and the fluorescence background can be reduced, the most influent contribution is the first, the diffraction limit. Nevertheless, each of the three terms decreases with an increasing number of collected photons. In principle, a localization measurement is thus obtained with an arbitrary high precision if a high number of photons are collected.

But there are also some external factors that could further decrease the localization precision, such as thermal fluctuations or mechanical vibrations. These factors are not taken into account in the Thompson's analysis.

8. Single-molecule Force Spectroscopy

8.1 Forces at the Single-molecule level

Force has a fundamental role in a wide array of biological processes. For example, it modulates enzymatic activity, induces structural changes in proteins and nucleic acids, alters kinetics of molecular bonds (Cecconi et al., 2005; Marshall et al., 2003), regulates motion of molecular motors (Rief et l., 2000; Reconditi et al., 2004) and has a role in mechanical transduction and sensory functions (Laakso et al., 2008). At the molecular level, these processes are ultimately related to the capacity of force to modulate lifetimes of molecular interactions and transition rates in biochemical reaction cycles that involve motion (Howard et al., 2001). Single molecule force spectroscopy approaches, such as *Optical* and *Magnetic tweezers* and *Atomic Force Microscopy* (AFM), which allow to apply and to measure forces at the molecular level, are crucial to study these mechanisms.

The application of forces to probe motion of single molecules perturbs the natural energy landscapes owing to the mechanical work required to move against the load. Consequently an external force changes the heights of energy minima and maxima and so the kinetics of motion, as illustrated on figure 8.1.

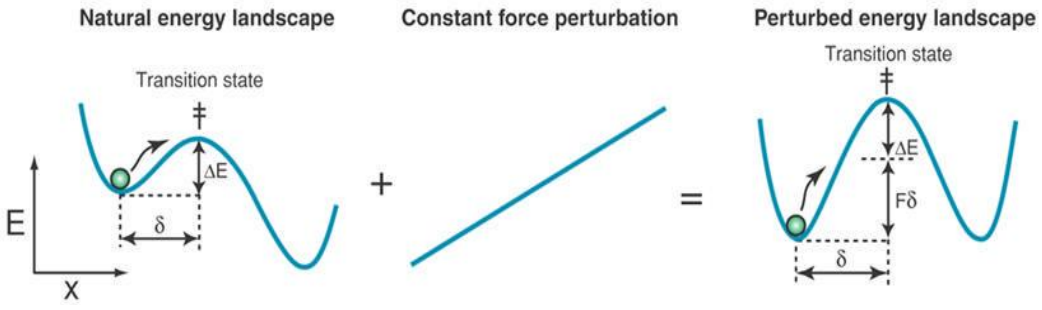

Figure 8.1: The application of a constant external force to single biomolecules perturbs their natural energy landscape. This perturbation alters the height of the energy barrier ΔE, by Fδ (Greenleaf et al., 2007).

The maximum practical force that can be applied to a single molecule is dictated by the force at which the molecule breaks, i. e. the rupture force of a covalent bond that is about 1.6 nN (Grandbois et al., 1999). This value is obtained by dividing the energy of a covalent bound (1 eV) by its length (typically 1Å). Below 1.6 nN, the chemical bonds in the molecule are extended, and the molecule behaves, in a first approximation, as a spring (enthalpic elasticity regime). In the low force regime, the elastic properties of the molecule are dominated by entropy. Regarding the lower limit of a measurable force, it is set by the thermal motion of the force probe: the force that arises from the collisions between an object and the solvent molecules. This force is usually called Thermal or Langevin force and it is the origin of Brownian motion. Since the time scale of molecules collisions is very short, in a first approximation, the spectrum of the Langevin force is flat as in the case of white noise (Neuman et al., 2007). Therefore, the amplitude of the Langevin force depends on the measurement bandwidth (B) according to:

$$F_L = (4\gamma k_B T B)^{1/2} \quad (6)$$

where F_L is the Langevin force, γ the drag coefficient (which depends on the size and shape of the object, its proximity to the walls or surfaces and the viscosity of the fluid) and $k_B T$ the thermal energy. Considering a measurement bandwidth of 1 Hz, a sphere of 1 μm in water at room temperature experiences a force of ~10^{-14} N.

Beyond revealing the forces that impel biological motion, single-molecule force experiments have been also used to assess the folding kinetics of nucleic acids and proteins, by disrupting molecular bonds, or to measure the elasticity (through force-extension relationships) of individual polymers, as described in the next chapters.

Just as the attachment of fluorophores to the molecule of interest allows its detection by fluorescence microscopy, so also the molecules under study need to be attached to a probe through which force is applied by single-molecule manipulation techniques. The kind of probe used depends on the technique: an optically trapped bead, a magnetic bead or an AFM tip. Ideally, the probe should be attached strongly enough to support the applied loads and, at the same time, it should not affect the mechanical or biological properties of the molecule under investigation. The attachment can be obtained by specific covalent bonds (based on amine, thiol or carboxyl chemistries), by specific non-

covalent bonds (for example biotin-avidin, antigenes and antibodies or even metals and chelators) or through nonspecific interactions (as charge-mediated adsorption). The last allows strong loads, but usually involves an unknown orientation of the molecule and of the mechanism of attachment, limiting in some cases its use in force experiments. Covalent attachments can support large forces (on the order of 1 nN), but frequently imply harsh chemical treatments that alter the properties of the biological sample. Covalent attachments by ligand-receptor pairs are commonly used because they afford specific and relatively tight binding to the probe (from ~10 to 300 pN). Other precautions regard the prevention of nonspecific interactions with surfaces like the experimental chamber, since it can introduce artifacts and uncertainty in the collected data; these nonspecific interactions can be prevented for example with inert proteins as casein or bovine serum albumin. In the next subsections Optical tweezers are briefly described.

8.2 Optical tweezers

Single-beam optical traps, known as *optical tweezers*, were introduced by Arthur Ashkin, Steven Chu and their co-workers (Ashkin et al., 1986) at AT&T Bell Laboratories. Optical tweezers exploit the fact that light carries both linear and angular momentum and hence exert forces and torques on matter. Optical tweezers are formed by tightly focusing a laser beam to a diffraction-limited spot with a high numerical aperture lens, such as a microscope objective. Dielectric particles, for example uniform beads or bacterial cells, can thus be stably trapped in the focal region due to the intense light gradient and the transfer of momentum from the scattering of incident photons. In the geometry of a tight focus of a laser beam, the high light intensity gradient leads to a three-dimensional “potential well”, keeping the trapped bead in place. The resulting optical force can be divided in two components: *scattering forces*, proportional to light intensity, pushing the object along the direction of propagation of the light beam, and *gradient forces* pulling the object in the direction of the spatial gradient of light intensity (i.e. towards the focal region) (figure 8.2). For stable three dimensional trapping, axial gradient forces must overcome the radiation pressure or scattering forces, thus the requirement for tightly focusing the laser beam. This

condition of axial equilibrium position of a trapped particle is located slightly beyond the focal point (Neuman et al., 2004).

The application of an external force disturbs the position equilibrium of the trapped bead by displacing it away from the trap center, with a linear dependence of displacement on force. An optical trap acts on a microsphere effectively placing it in a potential well (as depicted in figure 8.3). As a first approximation and within a certain range of displacements of the bead from the center of the trap (Δx), the potential can be regarded as parabolic and the optical trap behaves as a Hookean spring, with the restoring force F exerted by the trap on the bead determined by $F = -k\Delta x$. The trap stiffness *k* depends linearly on the polarizability of the trapped particle (and therefore, on its index of refraction) and the intensity of the trapping laser beam.

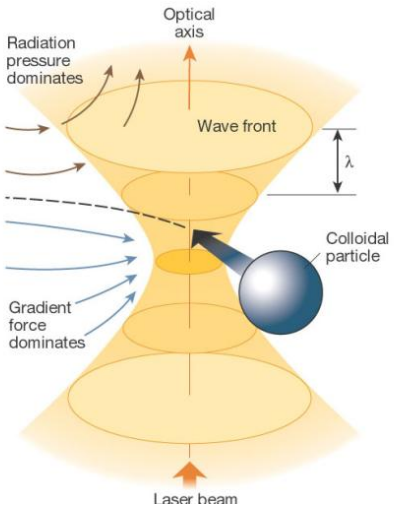

Figure 8.2: A strongly focused beam of light or optical tweezers can trap objects, such as a colloidal particle. Intensity gradients in the converging beam draw the particle towards the focus, though radiation pressure of the beam tends to push it away from that region. The particle is stable trapped in all three dimensions under conditions in which the gradient axial force dominates. Adapted from (Grier et al., 2003).

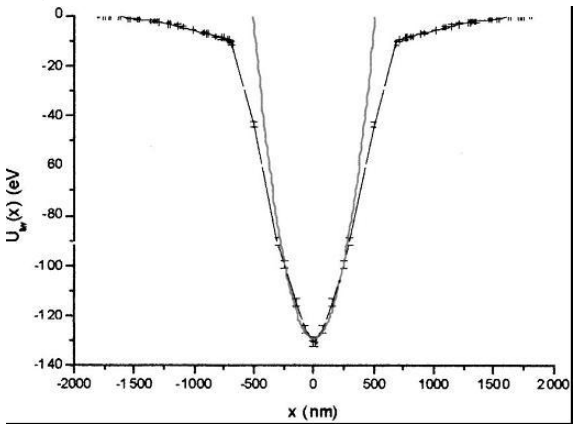

Figure 8.3: Potential well of the focused laser beam and parabolic fit of experimental data. Figure adapted from (Capitanio et al., 2002).

The displacements of the trapped bead from the trap center can be detected by Back-focal-plane interferometry (Gittes et al., 1998). This model describes the intensity shifts in the back focal plane of the condenser lens that is collimating the outgoing laser light. The image in the back focal plane is an interference pattern between the trapping laser light and scattered light from the trapped bead. This light distribution can be imaged onto a sensitive position detector, as Quadrant Photodiodes (QPD: a light sensitive diode which is divided into four equal segments) (figure 8.4). For small displacements of the trapped bead, the response of the detector is linear and the displacements of the trapped bead can be measured (see figure 11.3).

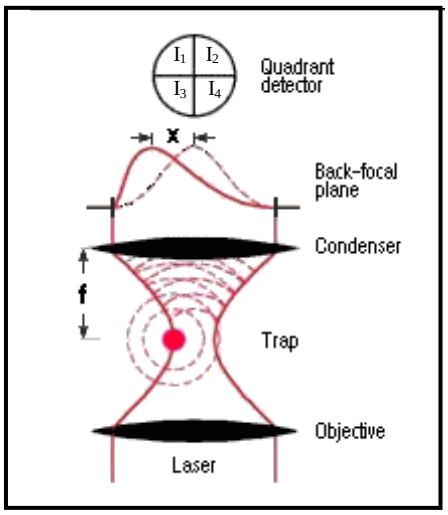

Figure 8.4: Back-focal-plane interferometry. The back focal plane of the condenser (of focal length **f**) is imaged onto a quadrant photodiode. Reading out the differential signals $(I_2+I_4)-(I_1+I_3)$ and $(I_1+I_2)-(I_3+I_4)$ (both normalized by the total intensity), displacement signal for both *x* and *y* directions are obtained, respectively.

To minimize sample damage from the intense light of the optical traps, usually the wavelengths used for trapping are chosen to be in the near infrared, in the region of near-transparency for most biological materials.

Optical tweezers can trap objects ranging in size from 5nm (Svoboda et al., 1994) to several micrometers. These include single cells (Neuman et al., 1999), organelles inside cells (Sacconi et al., 2007) or even lipid vesicles (Cherney et al., 2004). Nevertheless, most part of macromolecules and macromolecular assemblies are insufficiently refractive to be trapped

alone. This drawback is overcome by attaching them specifically to refractive spheres or "beads" and using these as handles (for example silica or polystyrene beads).

Typically, the stiffness of optical traps is in the range of 0.01-1pN.nm^{-1} and, consequently, the forces that can be applied are in the picoNewton and sub-picoNewton range (0.1-100pN) (Ghislain et al., 1994), making this technique being now best suited for the measurements of events occurring at the molecular scale (nm) and with energies of biological systems (k_BT = 4.11 pN•nm). In fact, optical tweezers are routinely applied to the study of classical molecular motors at single molecule level as kinesin (Svoboda et al., 1994), myosin (Finer et al., 1994) and dynein (Toba et al., 2006), as well as processive nucleic acid enzymes and macromolecular assemblies as helicases and exonucleases (Dumont et al., 2006; Dumont et al., 2003), DNA and RNA polymerases (Wuite et al., 2000; Galburt et al., 2009; Abbondanzieri et al., 2005) , viral DNA packaging motor (Smith et al., 2001), ribosome (Wen et al., 2008; Vanzi et al., 2003) among others. Due to the forces (~15pN) and displacements (~nm) associated with nucleic acid folding, optical tweezers are well suited to measure the kinetics of unfolding and refolding of single DNA (Wang et al., 1997; Bustamante et al., 2003) and RNA molecules (Liphardt et al., 2001), whereas larger forces are required in the case of proteins, giving way to AFM-based force spectroscopy. Besides their applicability in biological systems, optical traps have been also applied to the study of the physics of colloids and mesoscopic systems (Grier et al., 2003; Hough et al., 2002).

Figure 8.5 highlights different geometries commonly used for optical tweezers pulling assays.

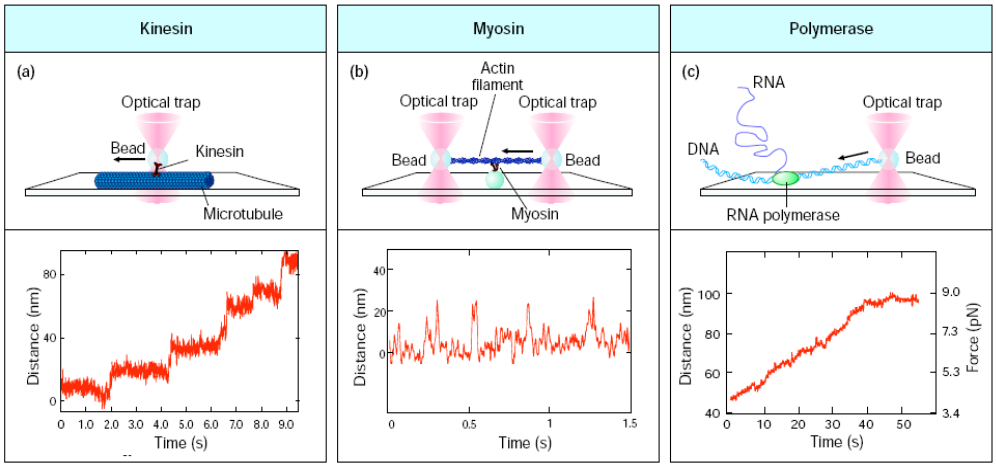

Figure 8.5: Comparison of different optical tweezers-based assays. **(a)** *Interaction assay.* Low concentrations of polystyrene microspheres are diffusing in the sample chamber, sparsely coated by kinesin. One bead is captured by the optical trap and is then brought in proximity of a microtubule attached to the glass surface. The force and displacement produced by the individual molecular motor as it walks along the microtubule are resolved by determining the displacement of the bead from the center of the trap (Block et al., 1990) **(b)** *Dumbbell assay*. An actin filament is suspended in between two optically trapped beads and it is approximated to a third bead, stuck on the slide surface, which is sparsely coated with Myosin (Finer et al., 1994; Capitanio et al., 2006). **(c)** *Tethered assay*. A single RNA polymerase is attached to the slide surface and the free end of the DNA template is attached to an optically trapped bead. As the DNA is transcribed, the RNAp pulls the bead along the DNA template (Yin et al., 1995). In the lower panels the ordinate is the distance moved by the trapped bead. Adapted from (Simmons et al., 1996).

Besides the high versatility and precision afforded by optical tweezers, there are also some limitations and drawbacks that must be carefully considered, such as the lack of selectivity and exclusivity. Basically, any dielectric particle near the focus of the trapping beam will be trapped, and the number of particles that can be simultaneously trapped can be large. This has some implications: the freely-diffusing objects to be trapped must be in low concentrations to prevent trapping of additional undesired objects. Moreover, the cleanness of all the objects and components of the sample cell is crucial for a good trapping and position control, since trapped impurities can distort or mask the position signal. Another drawback of optical tweezers is local heating, due to the high intensity of the trapping laser at the focus (typically 10^5-10^8 W cm^{-2}). Local heating can influence enzymatic activity and change the local viscosity of the medium.

8.3 Brief theory of Optical tweezers

As described above (paragraph 8.2), the overall net force acting on a trapped dielectric particle result from a balance between scattering and gradient forces. Scattering forces are proportional to the light intensity and act in the direction of the propagation of the incident beam. This force is a consequence of the momentum delivered by the scattered photons. Gradient forces, on the other hand, as indicated by their name, arise from the spatial gradient in light intensity and act in the direction of the gradient (i.e. towards the center of the beam). Trapping beams focused by a high numerical aperture lens, have a Gaussian intensity profile to achieve the smallest focal spot and produce the largest optical gradient.

In developing a theoretical description of optical trapping, one must consider the size of the trapped object. When the object's dimension (d) is much larger than the wavelength of the trapping light ($d >> \lambda$) the *"ray-optics"* regime applies. In this case, diffraction effects can be neglected and the trapping forces of the light can be understood in terms of geometric or ray optics. When the trapped object is much smaller than the wavelength of the trapping laser, i.e $d << \lambda$, the conditions of *Rayleigh scattering* are satisfied; in this case, the optical forces can be calculated by treating the trapped particle as a point dipole, since the electromagnetic field is constant on the scale of the particle. When the dimensions of the trapped particle are comparable to the wavelength of the trapping laser ($d \sim \lambda$), the regimes pointed above are not valid and it's possible to get a numerical approach with the *Mie regime*. A complete theoretical treatment of the Mie regime has been derived (Rohrbach et al., 2002). For illustration purposes, the simpler cases of Ray-optics and Rayleigh regimes are described below.

"Ray-optics" regime (d >>λ)

We can get a qualitative picture of the trapping using simple ray optics by decomposing a light beam into individual rays, each one with appropriate intensity, direction and state of polarization, which propagate in straight lines in media of uniform refractive index (Ashkin et al., 1992). These rays can change their direction when they refract at boundaries of media with different refraction indexes (in this case the trapped sphere and the surrounding medium). Figure 8.6 points out the action of the optical trap on a dielectric sphere in terms of the total force due to a typical pair of rays *a* and *b* of the converging beam, under the simplifying assumption of zero surface reflection. The picture shows that, for a generic displacement of the particle centre from the bead focus, a net restoring force counteract that displacement, pulling the particle to the centre of the beam, as described by the potential well on chapter 8.2.

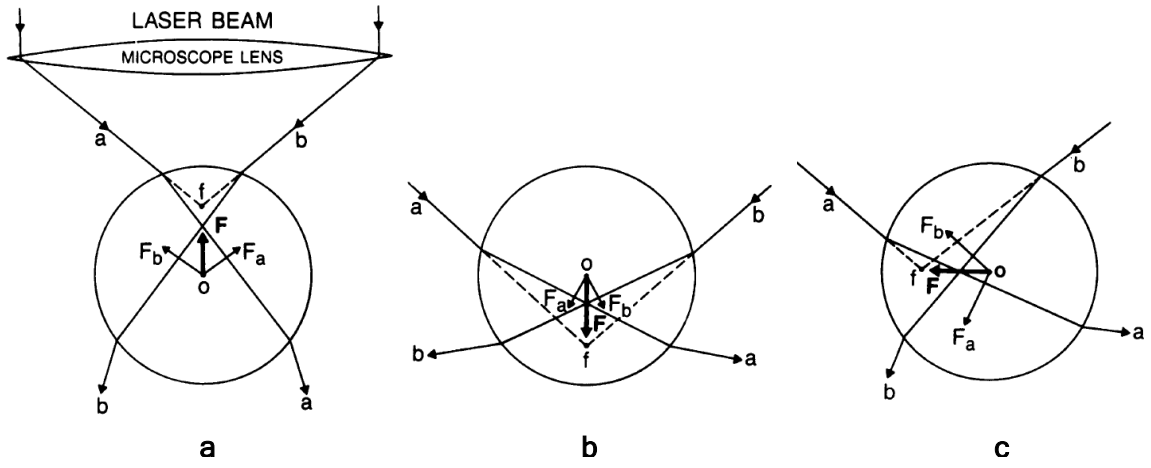

Figure 8.6: Qualitative description of the scattering forces acting on a dielectric sphere in the ray-optics regime. The incident trap beam is represented by two rays (a and b) that converge at the focal point *f* of the objective. Refraction at the water/beam interface gives rise to the scattering forces F_a and F_b. The sum of these forces, F, is the trapping restoring force and always pulls the center of the bead (o) towards the trap focus, when the bead is displaced along the optical axis (**a** and **b**) or laterally **c**). Note that the scattering component due to the reflection by the particle is not indicated. (Ashkin et al., 1992)

Note that in this regime, the focus of the incident beam is considered a dimensionless point, because its actual finite size of λ/2NA is negligible for spheres much larger than λ.

The force acting on the sphere is due to the change in the momentum carried by the light, at the sphere/water interface owing to refraction (figure 8.7). By Newton's third law, an equal and opposite momentum change is imparted to the sphere; the force on the sphere (F_{sphere}) is given by the rate of the momentum change ($\Delta\vec{q}$):

$$F_{\text{sphere}} = -\frac{dq}{dt} \qquad (7)$$

When the refraction index of the trapped particle is higher than that of the surrounding medium, the optical force arising from refraction is in the direction of the intensity gradient. Nevertheless, for a lower index, the force is in the opposite direction of the intensity gradient and the refractive forces become repulsive.

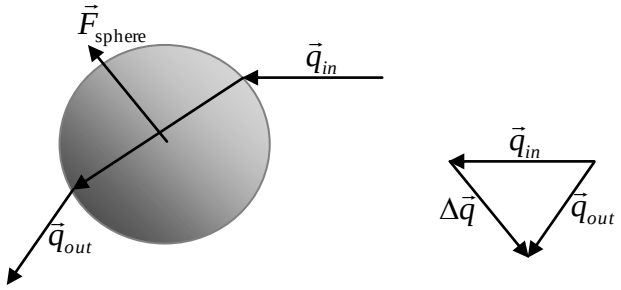

Figure 8.7: Representation of the force acting on a trapped dielectric microsphere (d >>λ), due to the refraction of a single light beam (reflection phenomena are not considered).

Rayleigh regime (d <<λ)

In the Rayleigh regime, objects can be represented as induced dipoles and point scatterers so that the electromagnetic field can be regarded as uniform across the dielectric particle. Nonetheless, the focus cannot be represented as a dimensionless spot or a point, but as a diffraction-limited region with diameter close to λ. The scattering force acting on a sphere with radius r is given by

$$F_s = \frac{I_0 \sigma n_m}{c} \qquad (8)$$

where

$$\sigma = \frac{128\pi^5 r^6}{3\lambda^4}\left(\frac{m^2-1}{m^2+2}\right)^2 \qquad (9)$$

is related to the scattering cross section and to the scattering function (van der Hulst et al., 1957), I_0 is the intensity of the incident light, c is the speed of light in vacuum, λ the wavelength of the trapping laser, n_m is the index of refraction of the medium and m is the relative refractive index (the ratio of the index of refraction of the particle to the index of the medium (n_p / n_m). Therefore, the scattering force is due to absorption and reradiation of light by the dipole; it is in the direction of propagation of the incident light and is proportional to the intensity.

Gradient force is due to the interaction of the induced dipole and the electromagnetic field. It is given by:

$$\vec{F}_g = \frac{1}{2}\alpha\vec{\nabla}(E^2) \tag{10}$$

where E is the electric field and α is the polarizability of the particle given by

$$\alpha = n_m^2 r^3 \left(\frac{m^2 - 1}{m^2 + 2} \right) \tag{11}$$

From equation 10 the gradient force is proportional and parallel to the intensity gradient and points up the gradient when m >1, i.e. when $n_p > n_m$. Stable trapping requires a gradient force greater than the scattering force along in $\hat{Z}$ direction. To achieve this, a tight focus is required, with a significant fraction of the incident light coming in from large angles. The maximum incident angle is determined by the NA of the microscope objective used to focus the trapping laser:

$$NA = n_m \sin\theta_{\max} \tag{12}$$

where n_m is the medium refractive index and $\theta_{\max}$ is half aperture angle (maximum incidence angle), as shown in Figure 8.8. Note that to obtain a stable trap, the incoming laser beam must overfill the back aperture of the objective, so that sufficient convergent, high-angle rays are supplied to counteract the scattering force.

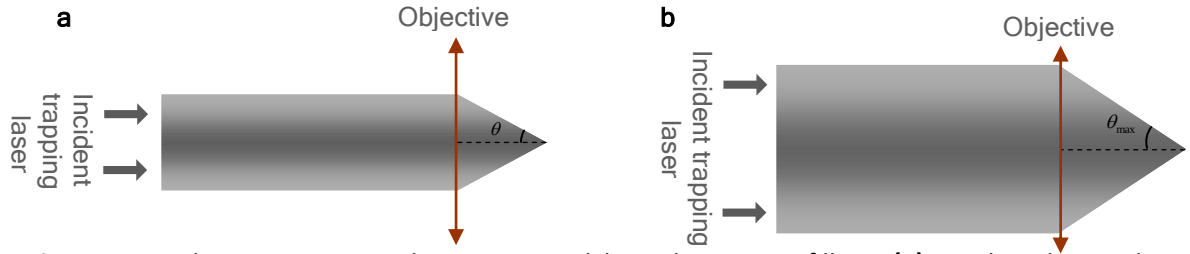

Figure 8.8: Objective numerical aperture and laser beam overfilling. **(a)** Incident beam does not overfill the back aperture of the objective. The highest-angle rays (θ) are smaller than θ_{max} **(b)** Expanded trapping beam that exploits completely the objective high NA. In this case, the scattering force is more efficiently counteracted.

9. Single DNA molecule manipulation: DNA mechanical properties and the application of double optical tweezers

9.1 DNA Elasticity

The elastic properties of DNA are unique among other natural or synthetic polymers. DNA characteristic base stacking and braided architecture lead to an unusual intrinsic stiffness, making the molecule resistant to sharp bending. For this reason DNA is commonly described as a *semi-flexible* polymer. DNA elasticity influences a large variety of cellular processes, especially protein-induced bending, looping or twisting. *RNA polymerases* and *helicases* (enzymes that move along DNA duplex using the energy released by ATP hydrolysis to unwind the two strands, required during replication and transcription of DNA) have evolved as motors to translocate along torsionally constrained DNA molecules. *Topoisomerases* control the number and topology of supercoils and release torsional strains in DNA by breaking and rejoining its strands. The biological relevance of DNA bends has also been demonstrated by the enhancement of DNA recombination and gene transcription observed when specific target sites for activators are replaced by intrinsically bent DNA sequences (Krogh et al., 1991; Muller et al., 1994). DNA, as a polymer with small bending

rigidity, can adopt a more compact "coiled-coil" conformation resulting in an average end-to-end distance much shorter than its contour length. Pulling the molecule into a more extended chain is entropically unfavourable because reduces the number of possible conformations but tension of at least 0.1pN are needed to significantly extend DNA (a force of about 6pN is needed to extend DNA to 95%of its contour length, *Lc*). The elastic properties of DNA (from which all biological process involving protein-DNA interaction depend) have been widely investigated by single molecule pulling experiments, which represent the strictest test to date of DNA elastic behaviour.

The first single-molecule DNA stretching experiment was performed in Bustamante's laboratory in 1992 (Smith et al., 1992). When DNA is pulled from both ends, its elastic behaviour goes through different phases, as evidenced experimentally by measuring a force-extension curve (FEC), as shown in figure 9.1.

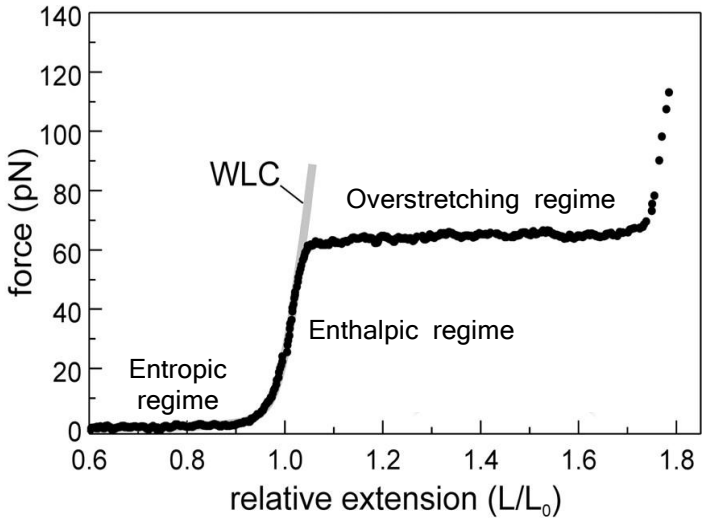

Figure 9.1: Typical force-extension curve of DNA. Elastic behaviour of double-stranded DNA undergoes distinct phases as the molecule is pulled to larger extensions. Entropic and enthalpic regimes can be fitted by the extensible worm-like chain model (gray curve) (see text for further details). Adapted from van Mameren et al., 2009.

DNA in solution is slack and its ends are much closer than the DNA contour length[3]. In the absence of an external force, the semi-flexible polymer adopts and end-to-end distance

[3] The contour length of a polymer represents the length measured following its profile, whereas the end-to-end distance simply measures the direct separation between the two extremities. The contour length of dsDNA is obtained by multiplying its length in base pairs (bp) by 0.34nm (the size of a nucleotide pair).

(*L*) allowing the highest number of polymer conformations (i.e. maximizing the entropy of the system). Theoretically this corresponds to *L*=0. Extending the molecule lowers the number of allowed conformations: this reduction of entropy requires the application of an external force, proportional to the extension to be impelled to the molecule, determining the so-called entropic elasticity. At higher forces, when DNA is almost pulled taut ($L \sim L_c$), one starts to stretch the DNA backbone; the chemical structure of the molecule is altered and the elastic response is no longer exclusively entropic. This is the *enthalpic* regime, where the end-to-end distance of DNA becomes longer than its actual contour length; the molecule behaves as a stretchable solid and this stretching occurs linearly with extension, as for a Hookean spring.

The entropic regime can be mathematically described by the worm-like chain model (WLC) (Bustamante et al., 1994):

$$F = \frac{k_B T}{L_p}\left[\frac{1}{4(1-L/L_c)^2} - \frac{1}{4} + \frac{L}{L_c}\right] \qquad (13)$$

where *F* is the force, *L* the end-to-end extension of the DNA molecule with a contour length L_c. $k_B T$ represents the thermal energy, the parameter L_p is the DNA persistence length, a temperature-dependent measure of the bending rigidity of a polymer (50nm for dsDNA at physiological ionic conditions, i.e. 150mM Na^+). Later on, to include also the enthalpic regime, a further parameter was considered, the DNA stretch modulus (*S*)[4] (Wang et al., 1997; Marko et al., 1995), to get what is called the extensible WLC model:

$$F = \frac{k_B T}{L_p}\left[\frac{1}{4}\left(1 - \frac{L}{L_c} + \frac{F}{S}\right)^{-2} - \frac{1}{4} + \frac{L}{L_c} - \frac{F}{S}\right] \qquad (14)$$

that equals approximately to 1000pN [100]. Figure 5.3 shows a fit of the DNA FEC data to the extensible WLC model (equation 16).

When the DNA molecule is subject to forces ~ 65pN, it stretches up to ~ 70% beyond its contour length without the requirement for increasing force. In this so-called *overstretching* regime, there's a characteristic phase transition in which DNA changes from its B-form - the canonical form of DNA in solution - to its S-form, i.e. an overstretched DNA form with exposed bases (figure 9.2). This remarkable feature is reversible and it was first reported in 1996 (Smith et al., 1996; Cluzel et al., 1996). Above the narrow range of forces in

[4] The stretch modulus S of a simple elastic rod of radius r is related to its intrinsic persistence length, L_p, as: $L_p = Sr^2/4k_BT$.

the overstretching plateau, S-DNA melts into single strands, exhibiting the characteristic force-extension behaviour of single stranded DNA (ssDNA).

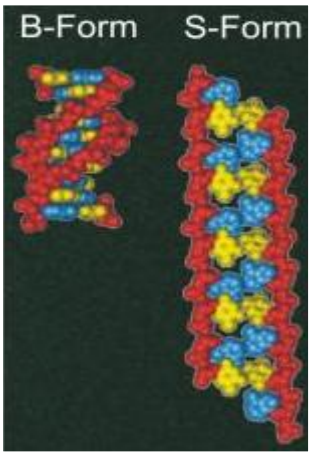

Figure 9.2: B- and S-form of DNA. Figure adapted from http://www.nanoscience.ch/nccr/information/media/sni_newsletter/nanonews_04/cover_story/optical_tweezers.

9.2 Advantages of Tethering one DNA molecule between two optically trapped beads: the "dumbbell assay"

The dumbbell configuration consists in anchoring the target DNA molecule between two optically trapped beads (figure 9.4) (a variation of this geometry has been commonly used by substituting one of the two optical tweezers by a micropipette (Wuite et al., 2000)). This design has been conceived to overcome problems due to the use of flow to extend DNA and due to the proximity of the DNA molecule to a glass surface used in other experimental configurations. Such configurations provide DNA tethering by the attachment of one of its ends to a surface and the application of a shear flow to overcome the entropic forces that otherwise would keep DNA in a relative compact random coil. This configuration has many disadvantages: The drag force acting on the DNA molecule stretched on this way decreases along its length (van Mameren et al., 2008), towards the direction of the free end, making an exact calculation of the applied force difficult; the parabolic Poiseuille velocity profile of the

flow in a thin flow chamber, with zero velocity at the surface (van Mameren et al., 2008). Furthermore, it's well known that the proximity with a surface, mainly when it is not properly passivated, can lead to undesired DNA and proteins interactions. Greene and co-workers (Fazio et al., 2008) have improved this methodology (schematized on figure 9.3) for imaging simultaneously of hundreds of individual DNA molecules.

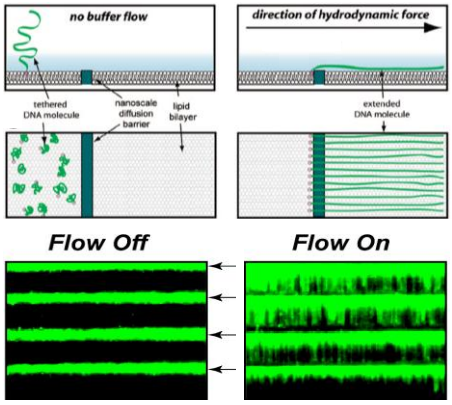

Figure 9.3: Schematic representation of the DNA curtains assay. DNA molecules are tethered to a lipid bilayer and therefore can move in *x* and *y* directions. A diffusion barrier is manually etched into the surface of the flow cell, oriented perpendicularly to the direction of buffer flow. Upper and middle panels represent views from the side and top, respectively. When the flow is applied, DNA molecules are dragged through the bilayer until they encounter the diffusion barrier, at which point they align and form a "curtain" of DNA molecules. Lower panels are images of YOYO1-stained λ-DNA obtained by TIRF microscopy. Arrows indicate the position of diffusing barriers. Adapted from (Fazio et al., 2008).

The "dumbbell assay" implies some evident advantage over flow stretching. First, the mechanical properties of DNA are better controlled (since the molecule is manipulated from both ends with optical tweezers) and the precise end-to-end distance of the molecule (which allows a fine adjustment of the tension and stretching induced to DNA) is accurately measured. This is due to the fact that one or both optical traps (i.e. the infrared trapping beams) can be moved with Acusto Optic Modulators (AOM) or Acusto Optic Deflectors (AOD) which allow a fine tuning of the displacement which in turn allows a fine tuning of the tension applied (generally up to hundreds of pN with an accuracy of tenths of pN accuracy) to the molecule suspended between the beads, in this case DNA. At the same time, if the molecule is changing extension, for example is shortening due to bending or looping caused by interaction with a protein, beads start being pulled and their distance decreases with respect to the equilibrium distance (distance between the traps). The displacement of the beads from the optical traps will thus be proportional to the tension the molecule (this time)

is applying. By measuring the bead position and the stiffness of the trap, it will be possible to accurately measure the force.

At the same time, tethering DNA by both ends, not only overcomes fluctuations of the molecule due to the presence of the flow, but also greatly reduces thermal fluctuation especially in the direction of the DNA axis. This aspect, as will be discussed in a more critical aspect in the next chapter, is a very important advantage when the single molecule manipulation is coupled in the same experimental set-up with single molecule detection. It is intuitive that the precise localization of a fluorescently tagged protein on DNA will suffer from DNA fluctuation.

Another advantage arises from the position of the traps within the chamber. All the assay components are suspended in a solution-like configuration because the traps can be positioned at a chosen distance (generally some microns) far from the glass surface of the cover slip. This is achieved moving in z direction the stage where the sample is located (or the traps, depending on the configuration of the microscope). Electrostatic effects of the glass surface are thereby overcome. The only limitation is that only one molecule a time can be manipulated, making data accumulation time consuming

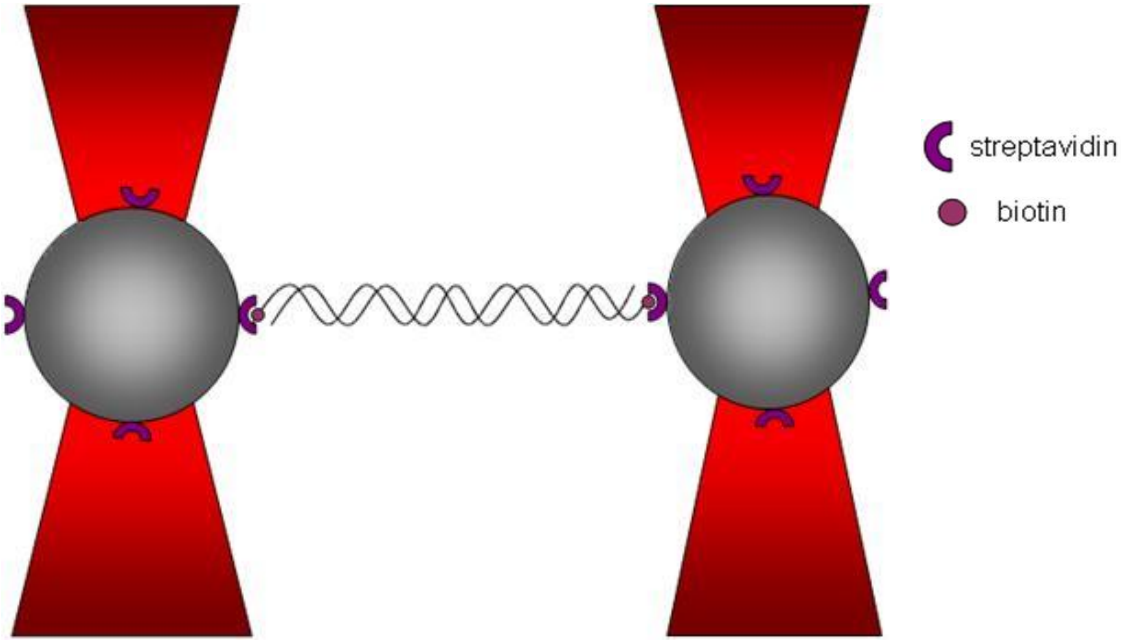

Figure 9.4. A single DNA molecule is tethered between two optically trapped beads in a dumbbell configuration. The attachment of DNA to beads is achieved through the exploitation of the high affinity of streptavidin (on beads) to biotin (on both DNA ends).

10. FIONA and trapping: the FIAT assay

As referred in the preceding chapters, recent advances in single-molecule methodologies are directed towards the combination of both manipulation and detection methods into the same experimental apparatus (van Mameren et al., 2008). This is still challenging since it is not always straightforward to combine different single-molecule approaches with the desired temporal and spatial resolutions, as well as concomitantly getting a good adaptation of the biological system to single-molecule methodologies and a suitable attachment of the chemical labels and/or mechanical handles to the sample (making sure that its functionality is preserved) (Moffitt et al., 2008).

Most part of the works reporting hybrid single-molecule techniques have combined dual optical tweezers with fluorescence but by imaging multiple fluorophores, for example intercalant DNA dyes which label all the double-stranded chain (Quake et al., 1997) or the coating of DNA molecule with various fluorescent DNA-binding proteins, as Human recombinase protein RAD51 (van Mameren et al., 2006), among others.

The first *tour de force* hybrid single-molecule fluorescence detection and optical tweezers experiment was accomplished by Yanagida and coworkers: they imaged single myosin molecules with total internal reflection fluorescence excitation and simultaneously they tethered a single actin filament between two optically-trapped beads (Ishijima et al., 1998) or RNAp on a single tethered λ-phage DNA molecule (Harada et al., 1999). The use of the evanescent wave of total internal reflection to excite molecule implies the dumbbell to stay in the proximity of the coverslide surface for the molecules bound to DNA (or actin) to be excited. Even if this illumination reduces fluorescence background, adds the disadvantage of being obliged to put biomolecules in the proximity of the glass surface.

TIRF excitation can be also characterized by inherent intensity fluctuations due to movement of DNA with respect to the surface.

Wide-field epi-illuminated fluorescence microscopy does not suffer from such intensity fluctuations and allows the excitation of fluorophores in the solution, making possible to maintain the dumbbell far from the coverslide glass surface (even if the excitation of all fluorophores in the solution enhances fluorescence background which in

turn lowers accuracy of localization, Thompson et al., 2002). In the current thesis I will present an innovative hybrid approach given by the combination of single molecule super colocalization with epi-fluorescence excitation, while the DNA template is suspended and manipulated with dual-tweezers (Chapter 8.2), as schematized in figure 10.1. The proof–of-principle of our method of combining Fluorescence Imaging And Trapping (*FIAT assay*) was done previously by localizing with FIONA a single fluorescence probe (a Quantum dot) bound to an actin filament extended between double optical tweezers (Capitanio et al., 2007), and it is illustrated in figure 10.2. The relatively high rigidity of the actin polymer compared to a more flexible polymer (such as DNA) enables a much easier assembly of dumbbells, since extension of the polymer via flow is not required.

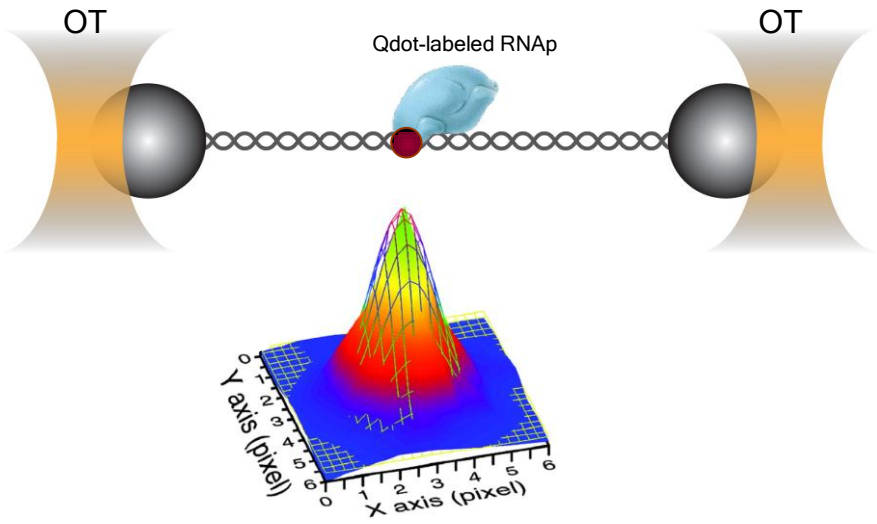

Figure 10.1: FIAT assay applied to a single RNAp transcribing a DNA molecule suspended between two optically trapped beads. The localization of the RNAp is obtained with FIONA technique, represented by the PSF shown in the lower panel.

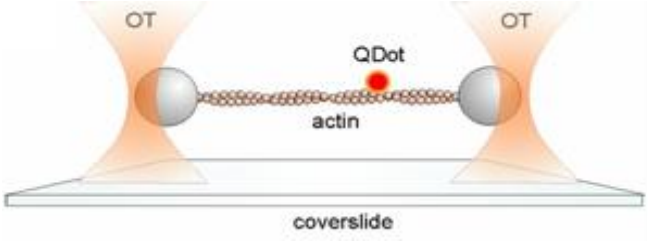

Figure 10.2: Schematic representation of FIAT assay, with an actin filament suspended between two optical tweezers. A fluorescent probe, Quantum dot, is attached to filament and it's position is detected with nanometer accuracy by FIONA (drawings not in scale).

The advantages of combining single molecule localization and manipulation with a double optical trap system can be summarized as follows:

- Electrostatic effects of the glass surface could interfere not only with DNA but also with DNA-protein interactions.
- Forces which could generate from protein-DNA interactions, as for example from protein-mediated DNA looping or bending, can be measured.
- It is possible to appreciate the effects of forces applied on DNA, on protein-DNA interactions and their dynamics.
- Stretching DNA dramatically reduces its thermal fluctuations, especially in the direction of its axis. DNA fluctuations negatively affect the localization accuracy of a molecule bound to DNA which not only depends on diffraction limit, pixel size and fluorescence background (Thompson et al., 2002) but also from the mechanical oscillations of the system.

11. Experimental FIAT Setup

Combining nanometer-stable double-optical trapping and high-resolution single-molecule fluorescence detection is technically challenging (Dijk MA et al., 2004, Brau RR et al., 2006). The position detection of optically trapped objects and single fluorescent probes at nanometer level is affected by various sources of mechanical and acoustic noise and by thermal drifts. The high stability required for nanometer-precision localization and trapping critically depends on a good isolation from these sources of noise. Our custom-built setup was first described in Capitanio at al. 2005 and later on modified for FIAT experiments (Capitanio et al., 2007) and it was specifically designed to obtain high mechanical stability and makes use of optics suited for both double-optical tweezers and fluorescence detection.

The microscope mechanical structure and optics pathway were mounted on an optical table equipped with active isolators (Melles-Griot), which limits the mechanical vibrations. The mechanical structure, illustrated in figure 11.1, is made of ERGAL (Erbium, Gallium, Aluminium) and it is mounted on four elastomeric isolators (newdamp, Newport) that significantly reduce mechanical resonances, as well as acoustical and mechanical noise.

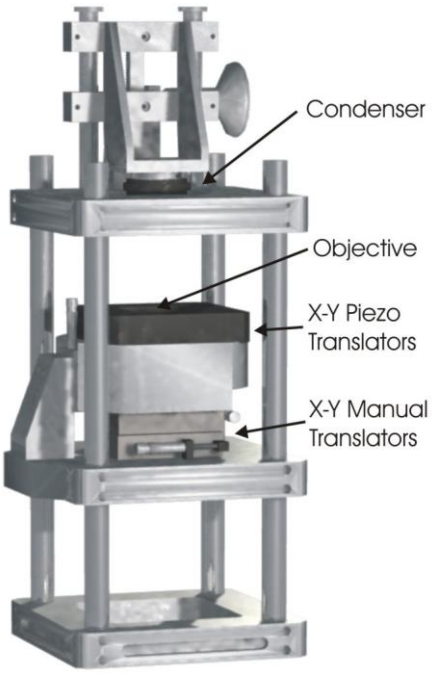

Figure 11.1: Mechanical structure that constitutes the optical microscope.

The structure is composed by three 250 × 250 × 30 mm bored platforms held by four stainless steel columns: the center of the platforms coincides with the optical axis of the microscope and the lower platform serves as a basis for the whole microscope. On the middle platform, two manual translators (M-014 Physik Instrumente) allow gross movements of the sample in the *xy* plane (25 mm of excursion in each direction), while a *x-y* piezoelectric translator (P-527.2CL Physik Instrumente), mechanically coupled to the manual ones by means of a ERGAL platform, allows fine movements (200 µm of excursion, 1 nm minimum displacement). The objective (Nikon Plan-Apochromatic 60X, NA 1.2, W.D. 0.2 mm, water immersion[5]) sits over a piezoelectric translator for *z* movements (P-721.20 Physik Instrumente, 100 µm of excursion, 1 nm minimum displacement). The higher platform serves as a basis for the position-detection system and the support structure for the condenser (Olympus U-AAC, Aplanat, Achromat, 1.4 NA, oil immersion) .

Figure 11.2 represents a schematic drawing of the experimental apparatus, which is equipped with two CCD cameras for brightfield microscopy, with 200x (Hamamatsu XC-SC70CE) and 2000x magnification (Ganz ZC-F11C3) and a EMCCD camera (electron-multiplied CCD, photometrics cascade II) for high-sensitivity wide-field fluorescence microscopy (200x magnification). The use of a high quantum efficiency and electron-multiplied CCD is essential to reach the high signal-to-noise ratio required for nanometer-precision localization of biomolecules. Illumination for fluorescence microscopy is supplied by a frequency-doubled Nd:YAG laser (Coherent, Verdi V-10, 532 nm wavelength) through a polarization-maintaining optical fibre, whereas illumination for brightfield microscopy is supplied by a halogen lamp (Schott KL1500LCD, 150W). A motorized mirror placed on the emission path directs the image alternatively to the CCD or to EMCCD cascade II cameras when brightfield or fluorescence microscopy is desired, respectively.

Double optical-tweezers are obtained by splitting a single beam from a Nd:YAG laser (Spectra-Physics Millennia IR, 1064 nm wavelength) into two beams with orthogonal polarizations. An optical isolator (OI) is placed in the laser path, close to the source, to

[5] High numerical aperture objective lenses are essential for optical trapping as explained in chapter 4.4; even if maximum NA can be achieved with oil-immersion objectives (up to 1.4), the refractive index mismatch between the immersion oil (η= 1.512) and the aqueous sample, i.e. the trapping medium (η~1.32) leads to significant spherical aberrations that would deteriorate the performance of the trap, when the distance of the focus to the sample surface increases. To allow good trapping deeper into solution and equally stable at any distance from the surface, water-immersion objectives are required, at the expense of a lower NA (typically equal to 1.2 for water-immersion objectives).

(nearly) abolish random amplitude fluctuations in the trapping laser, due to optical feedback phenomena from back-reflections of the beam. The two traps can be finely and independently moved within the sample along the *x* direction with two acousto-optic modulators (AOM, A&A DTS-XY 250) placed on the path of the beams, conjugated to the back focal plane of the objective. By controlling the frequency of the acoustic wave in the AOMs crystals through Direct Digital Synthesizers and a computer-controlled board, beams can be tilted in the AOM crystal and in the conjugated point in the back focal plane of the objective. This corresponds to translation of the beams (along the *x* direction) in the sample plane. The position of the trapped object is detected with nanometer resolution with two quadrant detector photodiodes (QDPs, UDT DLS-20) placed in the back focal plane of the condenser. The choice of well-separated wavelengths for trapping and fluorescence excitation is essential for an efficient separation of the two laser beams through dichroic mirrors and filters. To further reduce mechanical and acoustic noise, the apparatus is enclosed in a chamber of plastic panels which are able to slide in order to make the setup accessible during operation and sample assembly and to be completely closed during measurements. Moreover, the optical path is enclosed into boxes to minimize air turbulences, which critically affect the point stability of the trapping laser.

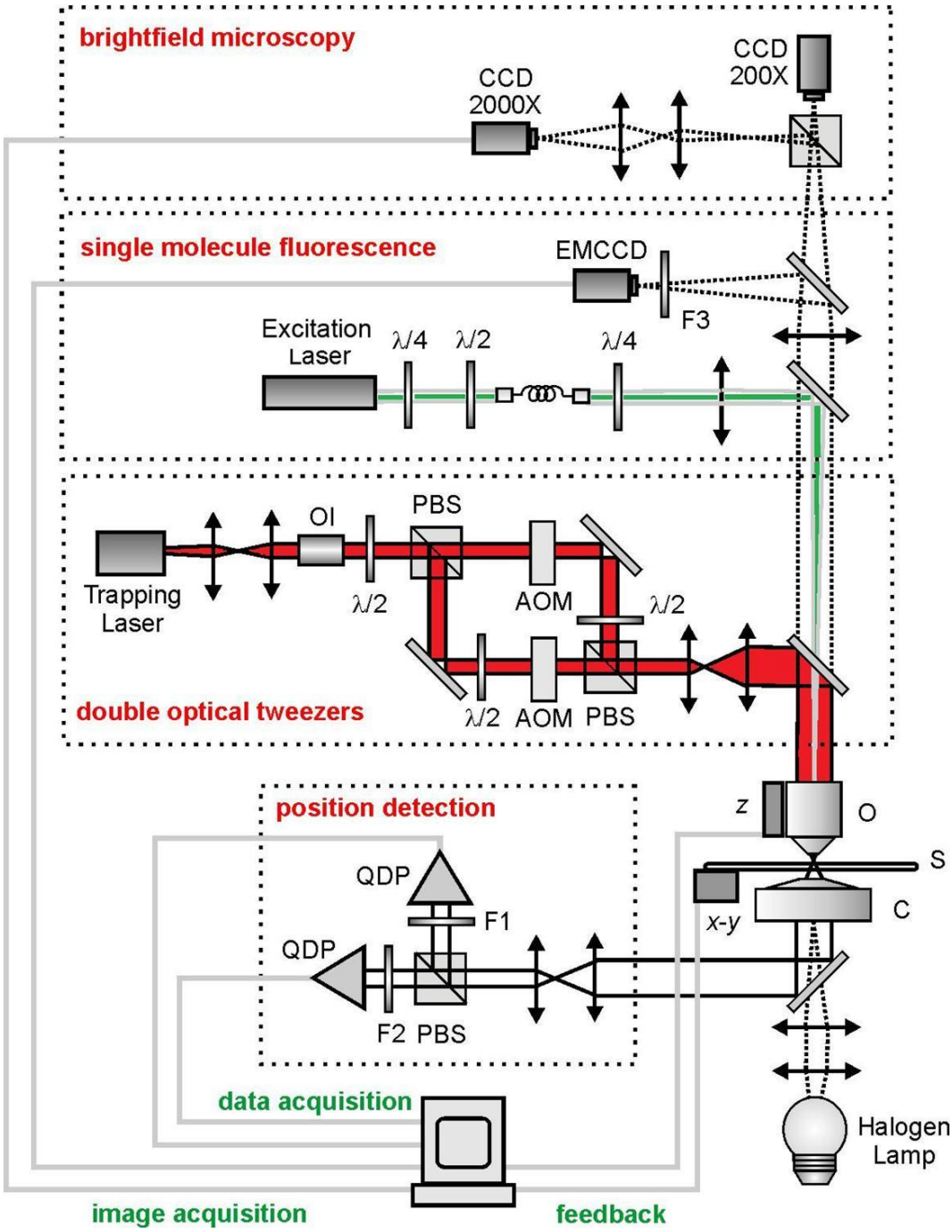

Figure 12.2 .Schematic representation of the experimental setup for combining fluorescence imaging and trapping (FIAT). Illumination for wide-field fluorescence microscopy is supplied by a Nd:YAG duplicated laser (532nm wavelength) and double optical tweezers are obtained by splitting the beam from a Nd:YAG (1064nm wavelength) into two beams with orthogonal polarization. OI: Optical Isolator, PBS: Polarizing Beam-Splitter Cube, AOM. Acousto-Optic Modulator, ʎ/2 and ʎ/4: half and quarter waveplate, O: Objective, S: Sample, C: Condenser, x-y and z: piezo translators, QDP: Quadrant Detector Photodiodes, F1 and F2 interferential filters at 1064nm, F3 emission filter.

11.1 Optical tweezers force calibration and detection

As explained in chapter 8.2, an accurate position calibration of the trapped bead is crucial to compute the external forces acting upon the trapped object. Since it is often hard or even impossible to predict those forces with the current theory available, one must determine them experimentally.

To calibrate the laser trap, two parameters must be taken into account: *k*, the tweezers spring constant and β, the position detector calibration factor (Capitanio et al., 2002) (since the detector reads the displacements of the bead as voltage rather than nanometers). For small displacements of the bead from its equilibrium position in the trap (±400nm), the force exerted by the trap is harmonic ($F = -kx$) and the position detector response is linear (Figure 11.3). Therefore, one can write

$$x = \beta V \qquad (15)$$

where *x* is the bead displacement and *V* the voltage output of the position detector.

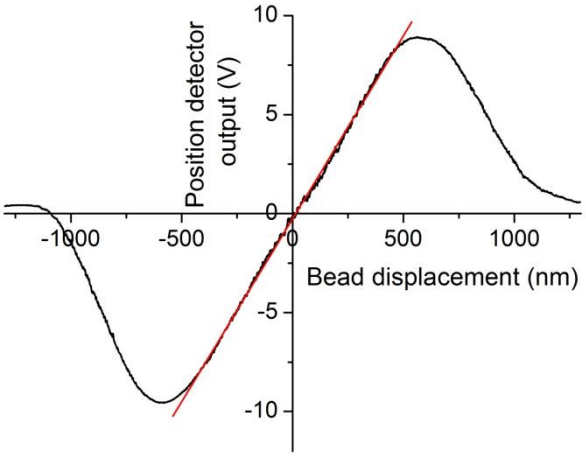

Figure 11.3: Position detector output (*V*) versus displacement in *x* direction from the center of the trap of 1µm diameter polystyrene bead (black curve). For small displacements (±400nm), the detector response is approximately linear (red fit curve).

Several methods to calibrate the optical trap and determine *k* and β have been described (Capitanio et al., 2002; Svoboda et al., 1994; Gittes et al., 1998). The method we have used is based on the confined Brownian diffusion of the trapped particle. A bead held

in optical tweezers, rather than being perfectly steady, shows some fluctuations due to forces acting on the bead itself upon the constant random collisions of the surrounding solvent molecules. Considering the theory of confined Brownian diffusion of a particle in a harmonic potential (Wang et al., 1945), these position recordings can be used to measure the parameters β and *k*, since the amplitude and frequencies of the bead oscillations about the equilibrium point are related to the trap stiffness. Considering a bead of radius *R* into a fluid with a viscous coefficient η at temperature *T* and held in an optical trap with stiffness *k*, the power spectrum of the thermal fluctuations $S_x(f)$ along the spatial coordinate *x* is described by (Gittes et al., 1998):

$$S_x(f) = \frac{k_B T}{\gamma \pi^2 (f_C^2 + f^2)} \tag{16}$$

where k_B is the Boltzmann constant, γ is the viscous drag coefficient of the bead, calculated using Stokes' law:

$$\gamma = 6\pi\eta R \tag{17}$$

and

$$f_C = \frac{k}{2\pi\gamma} \tag{18}$$

is the characteristic corner frequency.

Equation 16 represents a Lorentzian function; its behaviour at low and high frequencies is given by:

$$\begin{cases} f << f_C \Rightarrow S_x(f) \approx S_0 = \dfrac{k_B T}{\gamma \pi^2 f_C^2} = \dfrac{2 k_B T}{\pi k f_C} \\ f >> f_C \Rightarrow S_x(f) = \dfrac{k_B T}{\gamma \pi^2 f^2} \propto \dfrac{1}{f^2} \end{cases} \tag{19}$$

At low frequencies ($f << f_C$), the power spectrum is roughly constant, while at high frequencies ($f >> f_C$) it falls off like $1/f^2$; this means that on short time scales the particle does not "experience" the confinement of the trap, showing a behaviour characteristic of free diffusion.

Nevertheless, as already mentioned, in practice the detector reads "uncalibrated" displacements fluctuations *x(t)* as voltage rather than displacements in nanometers. The two

parameters are matched in equation 15 and the power spectrum of the signal *V(t)*[6] has a Lorentzian shape (figure 11.4):

$$S_V(f) = \frac{1}{\beta^2}[S_x(f)] = \frac{1}{\beta^2}\frac{k_B T}{\gamma\pi^2\left(f_C^2 + f^2\right)} \qquad (20)$$

The *V* subscript indicates that it is the power spectrum of a voltage signal and it is equivalent to (16) but with the multiplicative factor 1/ β^2 .

Figure 11.4 shows a typical power spectrum of the position signal from a trapped bead, acquired at 200 kHz for 8 seconds. Power spectrum is fitted with equation 20 to get *k* and *β*.

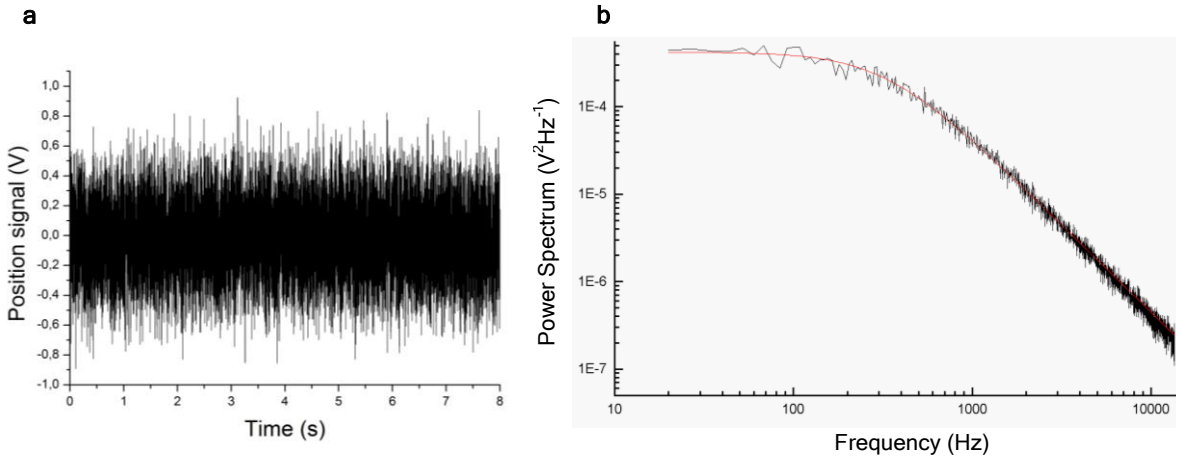

Figure 11.4: Calibration of trap stiffness and force-detector sensitivity using thermal fluctuations of a trapped bead. (a) Raw recordings of the signal in Volt of a 1,87 µm diameter bead at thermal equilibrium in the optical trap, using the voltage output from the quadrant photodetector. (b) Power spectrum of the trace in (a). The red curve is the Lorentzian fit.

Note the importance of γ for this method of optical tweezers calibration. In the case of surface proximity as, for example the glass coverslide or a second bead, γ can vary significantly from Stokes' law (equation 17). However, measurements and calibrations in this thesis have been carried out at different distances between the two trapped beads (while pulling the DNA molecule) and between beads and the coverslide surface, and this must be taken into account to get a correct trap calibration.

[6] The power spectrum of the bead displacement $S_v(f)$ (Figure 12.4.b) is calculated as square of the modulus of the Fourier transform of the thermal fluctuation data in Volt recorded in the time domain (figure 12.4.a) and it contains the contribution of motions to the thermal force with different frequencies.

In order to understand which are the smallest distances from the glass surface for the Stokes' law (equation 17) to be valid, we measured *k* and β values obtained from fitting of power spectra for different distances *h* between the glass surface and the center of the bead (figure 11.5). We used 935 nm radius beads (Spherotech, Inc). Values of *k* and β obtained for distances *h* greater than 7 μm do not vary more than 3.3% and 1.04%, respectively. From theory, first-order approximation of γ near an infinitely extended surface is given by (Happel et al., 1983):

$$\gamma = 6\pi\eta R\left(1+\frac{9}{16}\frac{R}{h}\right) \tag{23}$$

The correction to the γ coefficient predicted by equation 18 is about 7.5% at a distance of 7 μm and about 2.5% at a distance of 20 μm. We chose to performed trap calibration farther than 20 μm from the coverslide surface to avoid significant errors in the γ value. When this was not possible, we corrected γ values using equation 23.

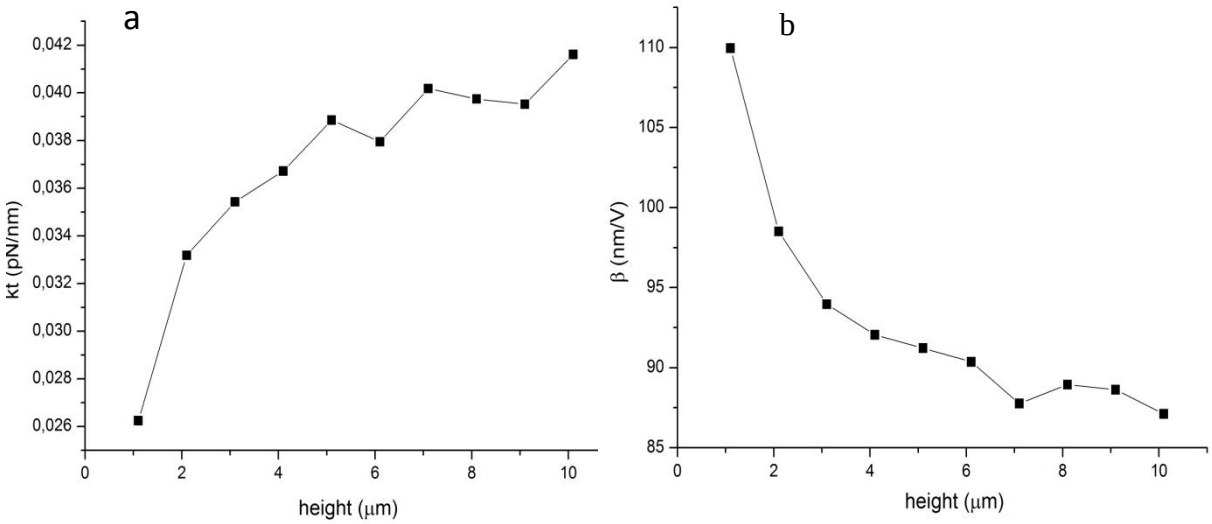

Figure 11.5: *k* (a) and β (b) behaviour versus trap height (i.e distance between the center of the trap and the coverslide surface).

We also measured *k* and β values for different distances *d* between the centre of the beads (935 nm radius) (figure 11.6). Optical traps are displaced through the AOMs (along *x* direction) by setting the frequency of the acoustic waves in the AOMs crystals between 60 and 90 MHz. As explained below, there is a linear relationship between the acoustic wave frequency and trap displacement, with a conversion factor α~1.06 μm/MHz. Values of *k* and

β obtained for distances between beads *d* greater than 1.7 MHz do not vary more than 3.0% and 1.4%, respectively. Therefore, we always performed trap calibrations with distance between the two traps greater than 1.7 MHz to avoid significant errors in the γ value.

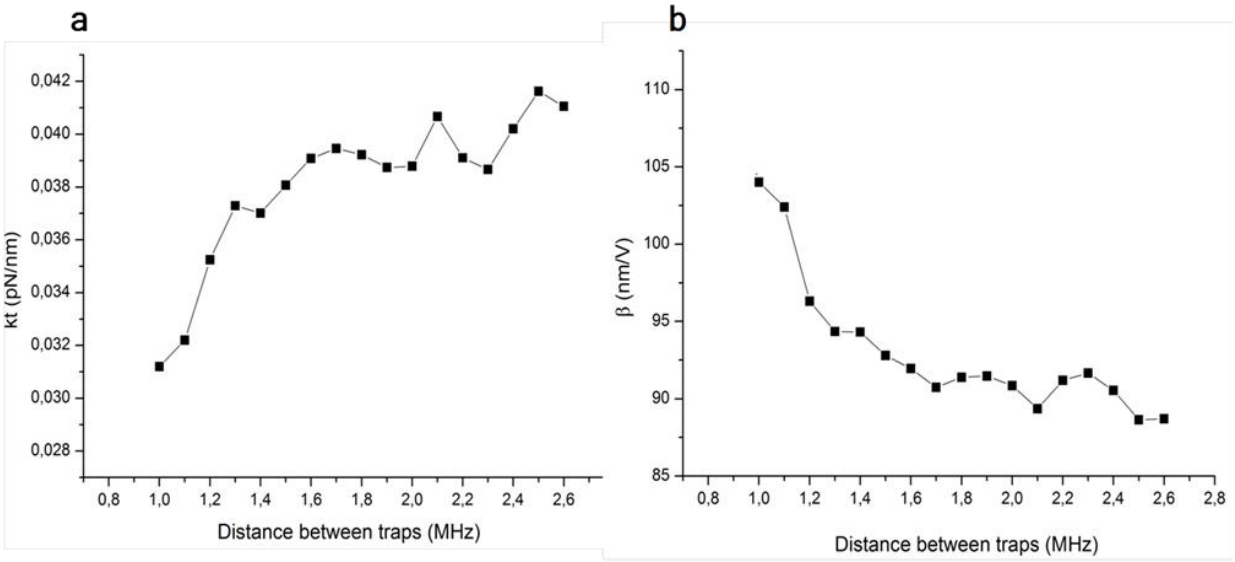

Figure 11.6: *k* (a) and β (b) behaviour versus distance between the center of the two trapped beads.

11.2 AOMs efficiency and force measurements

In the previous paragraphs we discussed the methods and cautions adopted for optical tweezers calibration. In a DNA-pulling experiment, traps are moved away from each other through AOMs. Since AOMs efficiency (i.e. laser power of the diffracted laser beam) is not constant with the acoustic wave frequency and depends non-linearly on the acoustic wave amplitude, this must be taken into account when measuring forces exerted on the DNA molecule.

Optical tweezers calibration was done before each experiment using the power spectrum method by acquiring the position signal of the trapped beads with both QDPs for different frequencies of the acoustic wave of the AOMs, corresponding to the different trap positions along the *x* direction, required for DNA pulling experiments. Calibration was completely automated through a custom written Labview program. The distance between

the traps during the calibration measurements is 1.85 MHz (1.96µm), far enough to avoid significant deviations of γ from Stokes' law due to the vicinity of the beads The software varies AOM frequencies between 75 MHz and 80 MHz, with steps of 0.2 MHz.. The signal of the trapped beads is acquired with both QPD for 8 seconds at the rate of 20 kHz for each frequency of the AOM acoustic wave. For each signal, an average between 32 power spectra is calculated and fitted with a custom-written Matlab routine, by minimizing χ^2 to obtain *k* and *β*. Bead radius and the distance between the centre of the beads and the surface of the slide is also taken into account, according to equation 20, in cases in which the distance could not be greater than 20 µm.

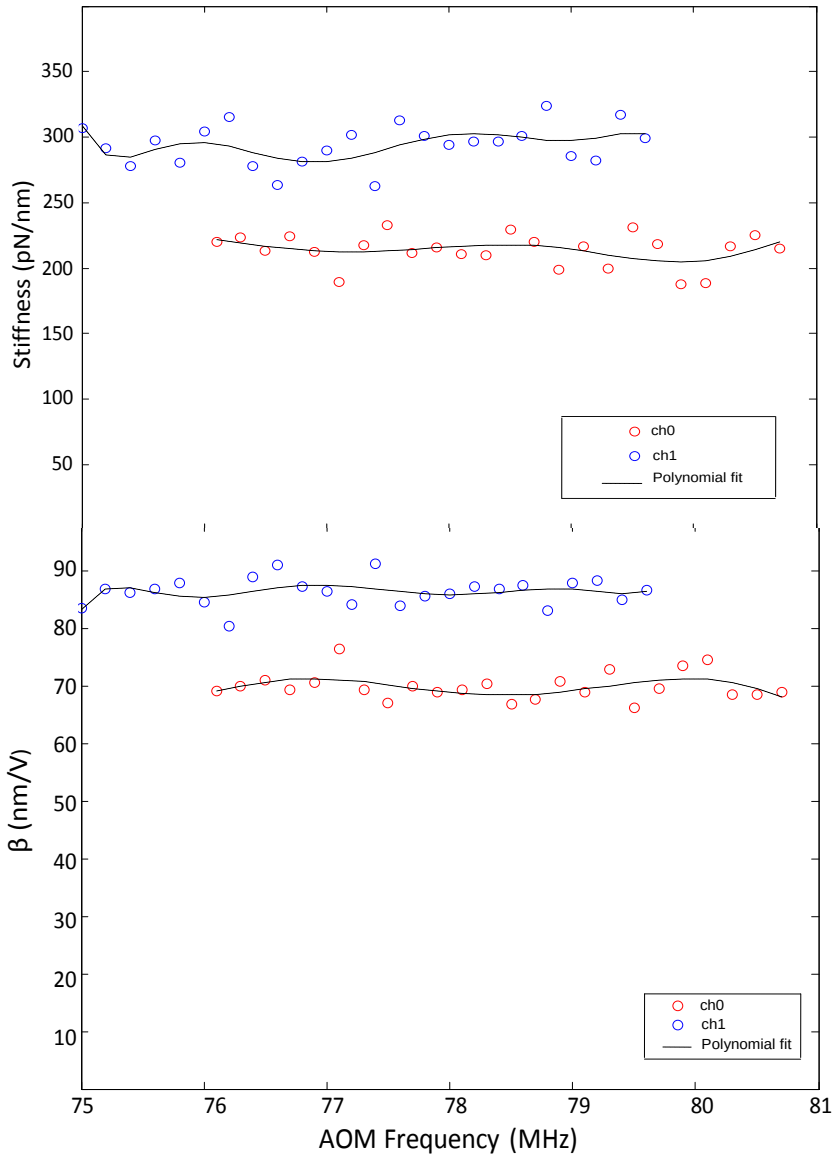

Figure 11.7: Plot of *k* (a) and *β* (b) values for both traps (ch#0 and ch#1) versus acoustic wave frequencies of the AOMs.

Figure 11.7 shows *k* and *β* for both traps obtained from such calibration. *β* is almost independent of the traps position (when the optics are well aligned), whereas *k* depends on the AOM diffraction efficiency. AOM efficiency was assessed by measuring the laser power at the entrance and exiting from the AOM, as a function of the frequency of the acoustic wave. We have aligned the optics in order to obtain a highest and most constant AOM efficiency in the range of AOM acoustic wave frequency of interest (75 - 80 MHz), as shown in figure 11.8.

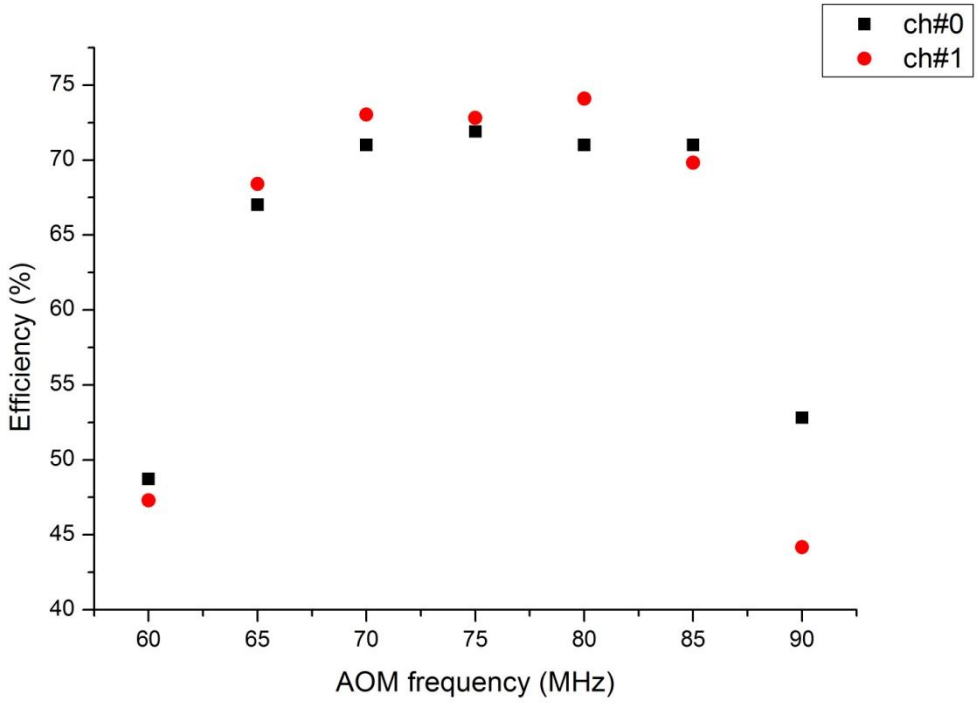

Figure 11.8: AOM first order diffraction efficiency, obtained from the ratio between the laser power exiting and entering the AOM, in function of the acoustic wave frequency.

The power of the diffracted beam varies with the amplitude of the acoustic wave in the AOM crystal (figure 11.9). This can be varied through a 12-bit control of the DDS signal amplitude. The efficiency values have a linear dependence just for the "central" amplitude values of the acoustic wave; the non-linear behaviour was taken into account and approximated by a 3rd degree polynomial curve (figure 11.7).

Labview and Matlab programs automate the experimental procedure, from traps calibration to DNA-pulling and FIAT experiments. After calibration, the curves *k* and *β* versus AOM wave frequency are fitted with 6th-degree polynomials. Coefficients of these polynomials are then loaded into the Labview program that automates traps control. In this

way, for each value of laser power, AOM wave frequency and amplitude, the stiffness of the traps is known and the force applied on the DNA molecule can be calculated.

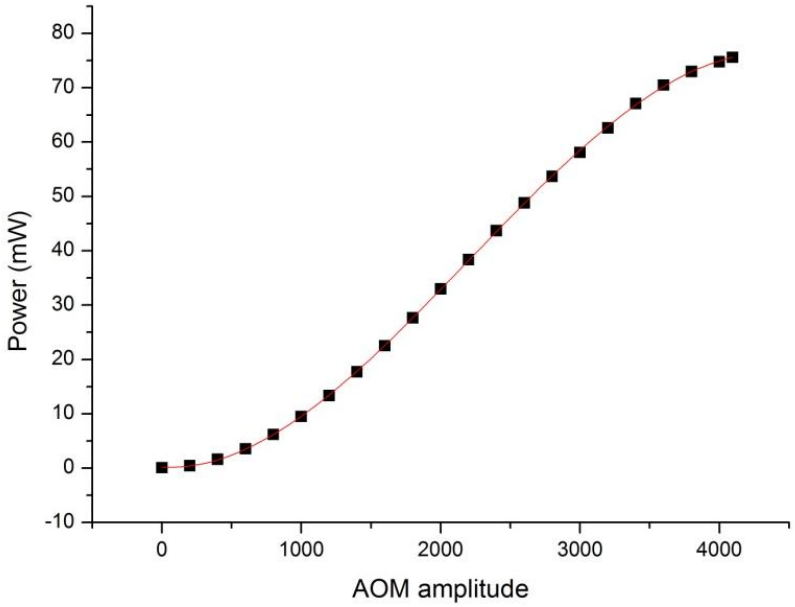

Figure 11.9: Behaviour of the power of the trapping laser versus the amplitude of the acoustic wave generated by the AOM. The red curve shows a 3rd –degree polynomial.

11.3 Laser pointing stability

In order to maximize the position stability of the suspended DNA and allow precise localization of DNA-binding proteins, the optical tweezers must provide a firm support for the dumbbell onto which the fluorescent probes are anchored. To this end, as described in section 11.2, many cautions were taken to minimize mechanical and acoustic noise, as well as air turbulence that could affect pointing stability of the trapping laser beams. The pointing stability of our optical tweezers was measured by focusing the laser on a 1.1 μm polystyrene bead (Spherotech, Inc.) stuck to the microscope coverslide surface (Capitanio et al., 2007). Figure 11.10 shows the position fluctuations of the trapped bead measured with the QDPs.

In these measurements, in order to compensate thermal drifts of the sample, the *feedback system* (Capitanio et al., 2005) used is based on a high-magnification image of the same 1.1 µm diameter polystyrene bead stuck to the microscope coverslide surface. The image of the bead (from the 2000x CCD camera) was first acquired by the digitalization board on the PC. Then, the bead position along *x*, *y* and *z* directions was calculated by centroid analysis of the inverted and threshold-processed image. Subsequently, the feedback system drives the piezoelectric translators to compensate for drifts (with a bandwidth of 25 Hz, limited by video acquisition rate). The feedback system stabilizes the microscope stage within 1nm.

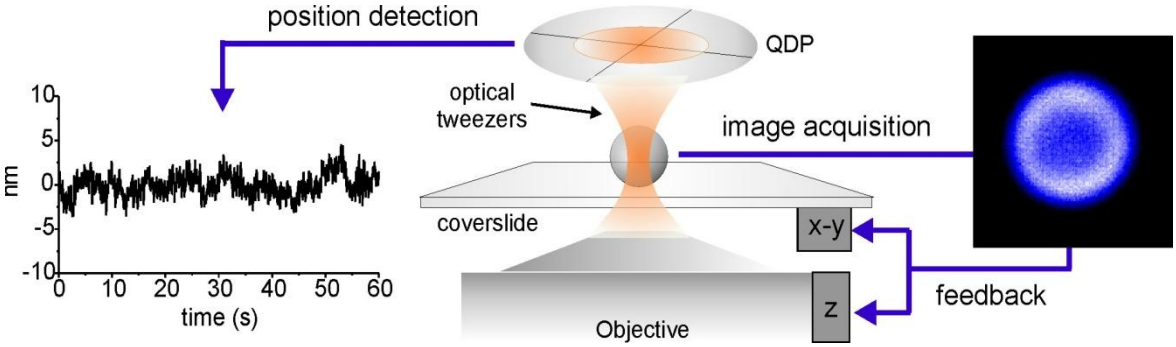

Figure 11.10: Configuration used to quantify the pointing stability of the optical tweezers. In the center: a schematic drawing of the experimental procedure. On the right: image of a bead stuck on the coverslide surface, acquired with the 2000X CCD, inverted and thresholded. The image is used by the feedback system to correct thermal drifts of the sample by moving the piezo translators (x-y and z). On the left: one minute recording of the trap position, acquired with the QDP.

The measurement of the laser pointing stability gave an rms noise very similar to the stage noise (~1nm over the bandwidth of interest, 0.1-25 Hz), demonstrating that the laser pointing stability is of the order of ~1 nm. We have seen no significant drifts with respect to the sample image during the 100 s measurement (the left panel of figure 12.10 shows the first 60 seconds). This measurement demonstrates that the suspended dumbbell configuration not only avoids interaction of the sample with the surface, but it also provides a drift-free assay for fluorescence localization with nanometre accuracy.

11.4 DNA force – extension curve calibration

As explained in chapter 9.1, as soon as a dumbbell[7] is formed, the DNA is pulled from its ends (in length steps of 50 nm) and the DNA extension versus applied force is monitored to check the presence of a single molecule and its integrity. The forces are measured as explained above, and two different methods were tested to precisely measure the DNA extension. In case the distance between the center of the two trapped beads (*D*) and the beads radius (*R1* and *R2*) are known, we can easily calculate the DNA extension *L* as *L=D-(R1+R2)* (see figure 11.11). The information on beads radius is provided by the manufacturer (Spherotech, Inc): 935 $\pm$ 46 nm. Therefore, we only need to measure the distance D between the centers of the two trapped beads.

The first method relies on the fact that we know the position of the traps center ($x1_0$ and $x2_0$, set by the AOMs frequencies), and that we can measure the displacements of both beads from the traps center (x1 and x2) using the traps calibrations described previously. Referring to figure 11.11, we can write:

$$D = (x2_0+x2)–(x1_0+x1) \qquad (24)$$

The relation between AOM frequency and trap displacement is linear in the range of frequencies considered. The nm/MHz conversion factor (1061.06 nm/MHz) allows the conversion of the distance $x2_0$-$x1_0$ between the center of the two traps (figure 11.11) from MHz to nm . The displacements *x1* and *x2* of the beads from the center of the traps are measured through the QDPs signals and equation 15. From equation 26 we obtain the precise value in nm of the distance between the trapped beads.

[7] DNA dumbbell assembly protocol is described in detail on chapter 13.

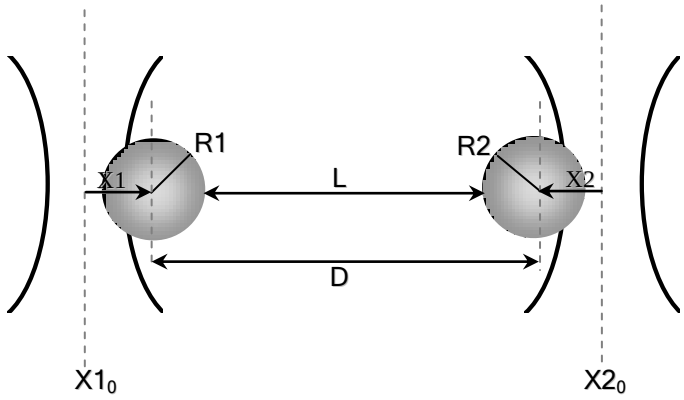

Figure 11.11 : Schematic representation of the DNA extension (distance L between the two trapped beads) calculation. See text for further details.

The second method is based on video microscopy. A snapshot of the position of the trapped beads is taken using brightfield illumination and the 200x CCD in each cycle of signal acquisition, corresponding to different DNA extensions with 50 nm increments. The image is then inverted and threshold-filtered to remove background noise and the distance D between the two beads is directly measured through centroid analysis. The scale factor nm/pixel of the CCD 200x camera for brightfield microscopy is 56,8 nm/pixel and it was obtained by a similar method used for the fluorescence EMCCD cascade II camera calibration (Chapter 11.4).

11.5 EMCCD cascade II camera calibration and detection of the fluorescent probe position

In order to measure displacements of single chromophores or fluorescent probes, the first step is to get an accurate calibration of the pixel size of the EMCCD cascade II camera. The nm/pixel calibration factor was assessed by attaching fluorescent polystyrene beads (0.05 µm, Bangs Laboratories) to the microscope coverslide. The choice of fluorescent beads for the calibration procedure was based not only on their high signal-to-noise ratio, but also on the fact that these probes do not suffer from photobleaching or blinking phenomena, making them a better choice with respect to single fluorophores or quantum dots. A translation of 20 µm of the sample was then effectuated through the piezoelectric stage. The position of a single fluorescent bead was measured before and after the displacement by fitting its point spread function (PSF) with a 2D Gaussian function (as explained in detail below), it was possible to calculate the distance in pixel corresponding to 20 µm. We obtained a value of 230,76 pixel, corresponding to a scale factor of 86,67 nm/pixel.

12. Sample preparation

12.1 DNA labeling

For attaching DNA to beads and form the dumbbell, both beads and DNA have to be functionalized with complementary moieties. Typically, the couple antigen/antibody or streptavidin/biotin are exploited due to their high affinity (Ka= 10^{15} M^{-1} for streptavidin/biotin; one of the highest found in nature), functionalizing one moiety on the bead and the other on the DNA. Generally, beads are coated with an antibody (anti-digoxigenin, for example) or streptavidin, while antigen (digoxigenin) or biotin is covalently linked to both extremities of a linear DNA.

I used a plasmidic (circular) DNA, pFastBac containing the target operator sequences and, for this reason, the first step of DNA labeling is the linearization. Circular DNA is linearized by simple digestion with a restriction enzyme. Figure 12.1 shows the map of the plasmid used. This plasmid contains two identical operator sequences O1 at a distance of 300bp (100nm) and many restriction sites at different positions. When deciding which site to use, one has to consider where the operators will be localized in DNA with respect to the dumbbell. If operators must be in the centre of the dumbbell, digestion shall occur at a site diametrically opposed to operators. Cutting closer to operators will result in operator position shifted towards one of the two beads.

I digested DNA with different restriction enzymes whose sites are in different positions in the plasmid and labeled the resulting linearized DNA with different strategies. These labeling methodologies don't rely on the direct attachment of the label molecule on DNA nucleotides because this would lead to labeling not only at the extremities but along the whole molecule. To achieve selective labeling at extremities, labeled nucleotides are incorporated at extremities through enzymatic polymerization.

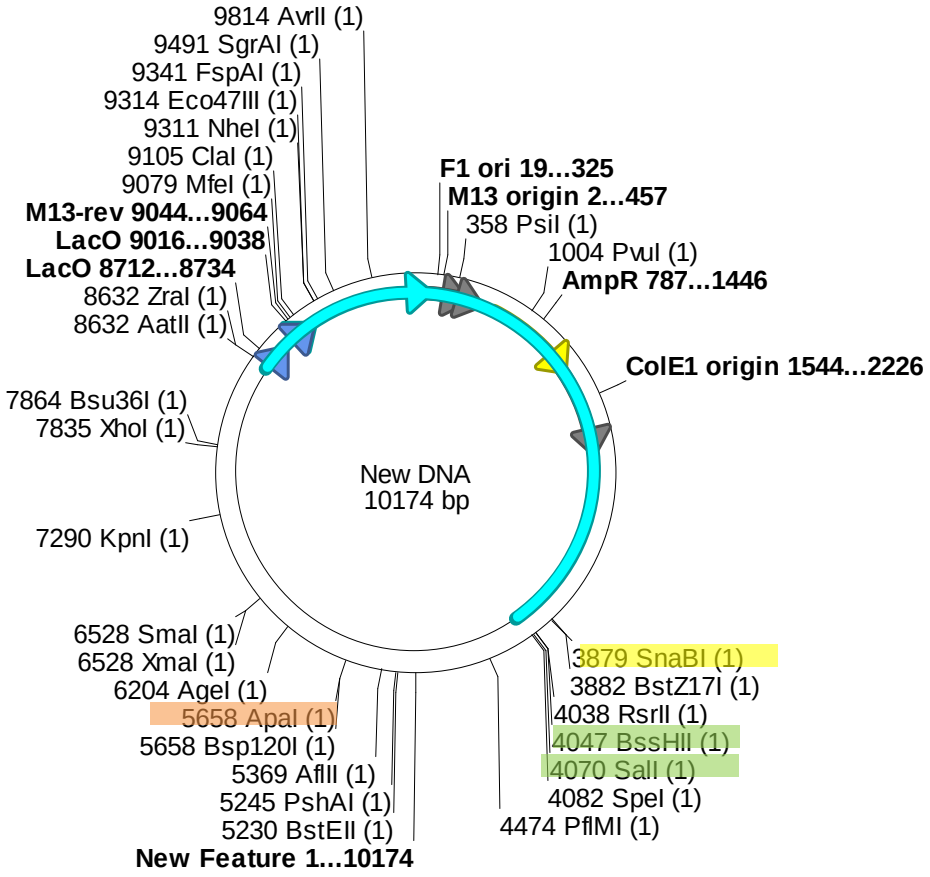

Figure 12.1. Map of sites in the plasmid used, pFastBac containing two operators sequence LacO (blue arrows). In green, orange and yellow are highlighted restriction sites used for linearization of the plasmid.

12.1.1 LABELING WITH KLENOW EXO- DNA POLYMERASE I FRAGMENT

Restriction enzymes used to linearize plasmid DNA, or in general to digest DNA, cut both strands of DNA. If the hydrolysis on the two strands occurs exactly on opposite positions, the resulting DNA ends will be 'blunt'. If the hydrolysis occurs at shifted positions, the resulting ends will be single strand and are called 5' or 3' overhang (depending on whether the last nucleotide of the single strand has a 5' or a 3' free); they are also called sticky ends because can form hydrogen bonds with another complementary overhang DNA extremity (on the same molecule or on another molecule) (figure 12.2).

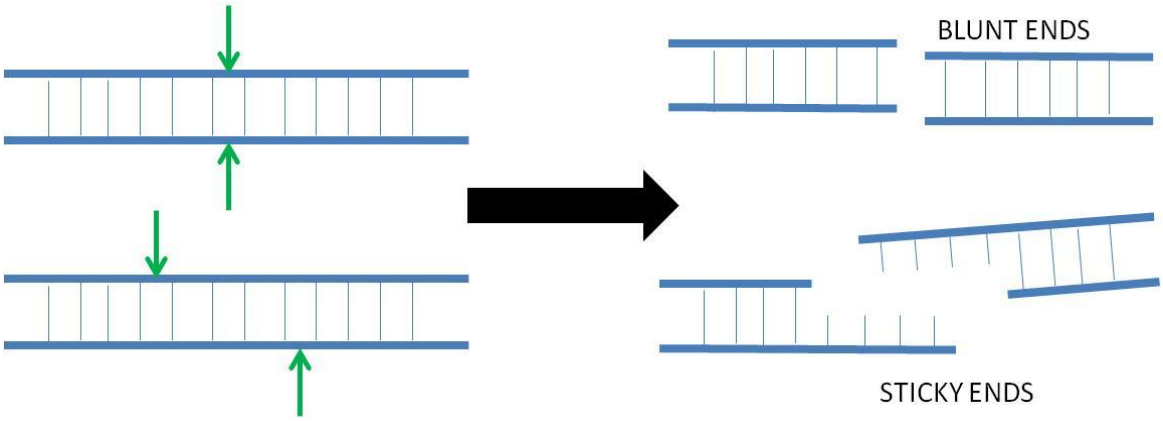

Figure 12.2. The two different possibilities for enzymes to cut (indicated by green arrows) are shown; on opposite sites (top) or on shifted positions (bottom). On the right the products of the two different ways of digestion are presented; when the two strands have the same lengths are called 'blunt ends', while when one strand (overhang) is longer is called 'sticky end'.

The Klenow fragment (Invitrogen, #18012-021) is a proteolytic product of *E. coli* DNA Polymerase I which retains both the 5'→3' polymerase and the 3'→5' exonuclease activities, but not the 5'→3' exonuclease activity of the intact holoenzyme. Therefore, the Klenow fragment retains the polymerization fidelity of the DNA polymerase holoenzyme without degrading 5' *termini*. Its main applications in molecular biology include the ability to synthesize dsDNA from ssDNA templates thus filling-in 5' overhangs (i.e. 5'-protruding ends) on the DNA. The fact that the 5'→3' exonuclease activity is abolished means that the Klenow fragment does not have any capacity for proofreading. Consequently, addition of labelled nucleotides in the polymerization reaction will result in their incorporation in the new DNA strand without being subsequently removed by proofreading. DNA extremities will therefore be labeled.

In order to have the operators in the centre of the linear DNA, two restriction sites close to each other and diametrically opposed to the operator region have been chosen, in particular restriction sites for SalI (NEB, #R0138M) and BSSHII (NEB, #R0199M) (highlighted in green in figure 12.1). A first double digestion step generates a linear DNA with sticky ends. This product is then treated with klenow exo- polymerase in the presence of a mix of deoxynucleotide triphosphates (dNTPs) with the addition of dCTP labeled with biotin (Invitrogen, #19518-018). Since the overhangs generated by the digestion of SalI and BssHII contain the nucleotide dG (see chapter 3.1 for complementarity between base pairs), then a labeled dC will be incorporated. Figure 12.3 shows all the steps of labeling with exo- polymerase and highlights the sequences recognized by the enzymes. This strategy only

allows labeling DNA with biotin because the only commercially available digoxigenin labeled nucleotide is dUTP (Roche, #11209256910). This is a nucleotide typically found in RNA instead of thymine and, as thymine, is complementary to adenine. In order to label DNA with digoxigenin through Klenow fragment, restriction sites with one or more A have to be chosen.

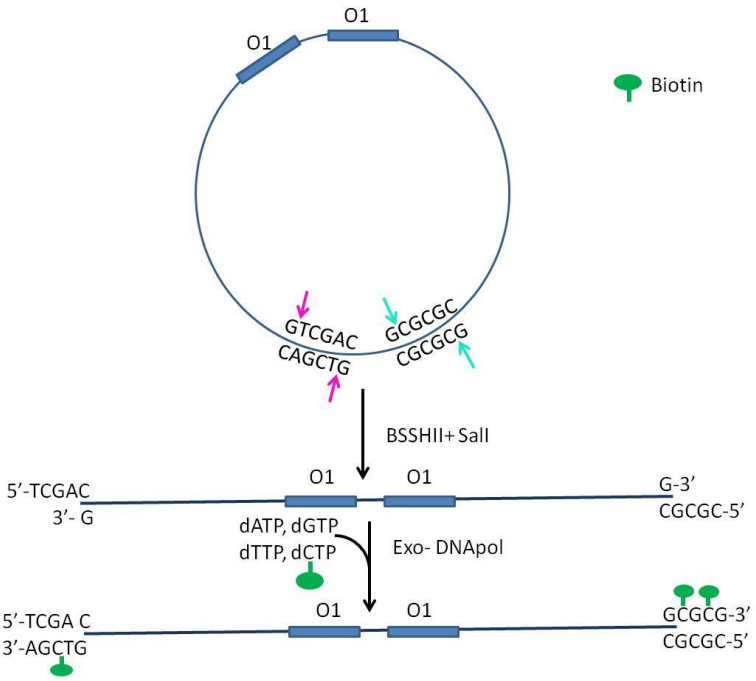

Figure 12.3. BSSHII and PauI digest DNA at their restriction sites between nucleotides indicated by arrows (pink for SalI and light-blue for BSSHII). These sites are diametrically opposed to operators sequences so that once digested and linearized the DNA, operators will be in the centre of the sequence. Digested DNA will have sticky ends which will be filled by exo-DNA polymerase polymerization in the presence of a labeled dCTP (linked to biotin). The new blunt DNA extremities will be, in turn, labeled with biotin.

12.1.2 Labeling with Terminal deoxynucleotidyl Transferase (TdT)

Terminal deoxynucleotidyl Transferase (TdT, Fermentas, #F-203L) is an enzyme able to link up to 130 deoxynucleotides in tandem to DNA extremities, creating a tail of deoxynucleotides. Differently from Exo- which requires 5'-overhang DNA extremities as a substrate, TdT tails 3'-OH of preferably 3'-overhang or, with minor efficiency, blunt ends and doesn't need a template DNA so each kind of nucleotide can be added and that's why it is suitable for labeling (in this case tailing) DNA with digoxigenin-dUTP. For labeling with TdT,

the only prerequisite is that DNA has to be digested with e restriction enzyme which generates 3'- overhang or blunt ends. In the map of the plasmid used, among all restriction sites, there is the site recognized by ApaI, an enzyme generating 3'-overhang or SnaBI which generate blunt ends. ApaI site, (as highlighted in orange in figure 12.1) is not opposed to operators so after digestion operators will be localized closer to one extremity of the linearized DNA while SnaBI is diametrically opposed. Figure 13.4 shows the steps of labeling with TdT; after the first passage of digestion, TdT tailing occurs in presence of a labeled deoxynucleotides. The final product will carry at 3'- a single stranded tail of labeled deoxynucleotides (figure 12.4).

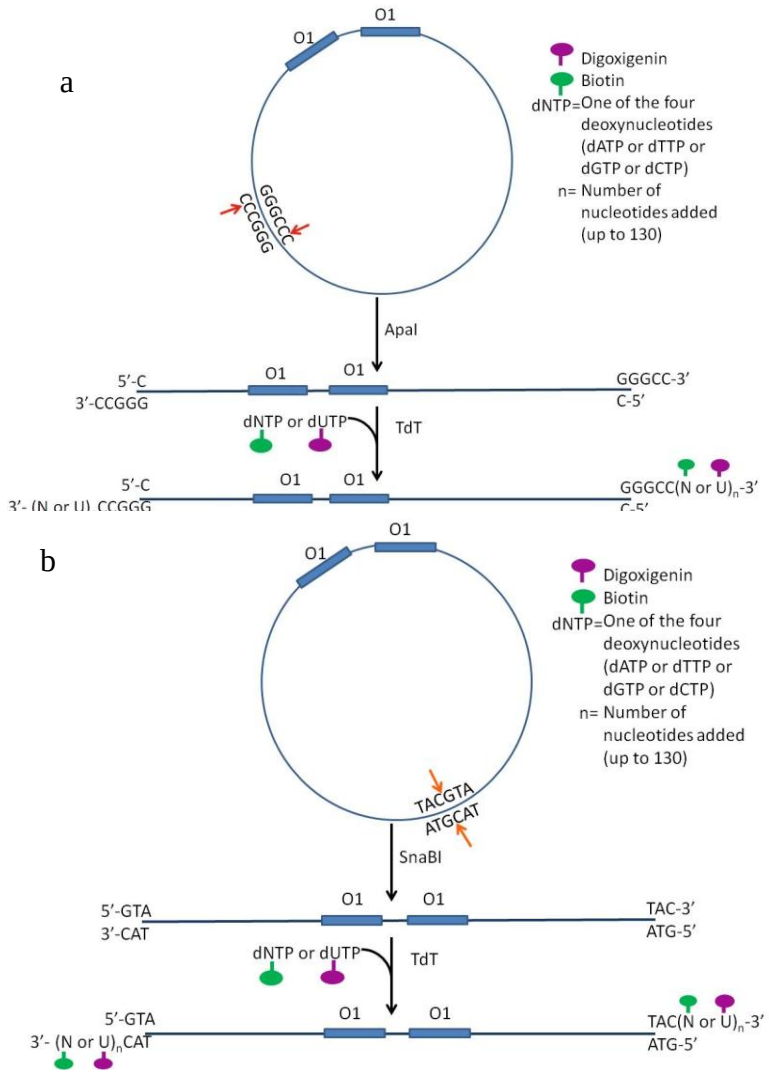

Figure 12.4. (a) Plasmid DNA is digested with ApaI, a 3'-overhang generating restriction enzyme. Terminal deoxynucleotidyl Transferase efficiently links up to 130 labeled nucleotides in tandem to the 3'-OH *terminus* of the DNA molecule independently of the type of nucleotides and label. (b) After digestion with SnaBI, DNA blunt ends are generated and operators will be localized the centre of DNA. 3' of the blunt ends will be tailed by TdT but lower efficiency than 3'-overhang.

12.2 Operators relative positions to determine specificity of binding

Esperimentally, localizing a single molecule means determining the coordinates of the center of the Point-Spread-Function (PSF) arising from the imaging of the fluorescent label tagging the molecule itself. When the fluorescently labeled LacI molecule is bound on DNA containing operators, it is fundamental to know if the protein is specifically bound to an operator sequence or if it is non-specifically bound to non-cognate. The simplest way to have this kind of information, is to measure the ratio between the measured distance between the spot and a DNA extremity (left or right) and the measured total length of the DNA. In the case of specific binding to operator, this ratio must is constrained by the position of the operator relative to the DNA ends, as determined by the restriction site used to linearize DNA. Absolute sequence positions are known from the map of the plasmid. Figure 12.5 reports all the ratios of both operators for all the ways of labeling used. This approach allows not only to distinguish between specific and non specific binding, but also to discriminate on which of the two operators present in the DNA, the protein is bound (since the two operators have significantly different relative positions).

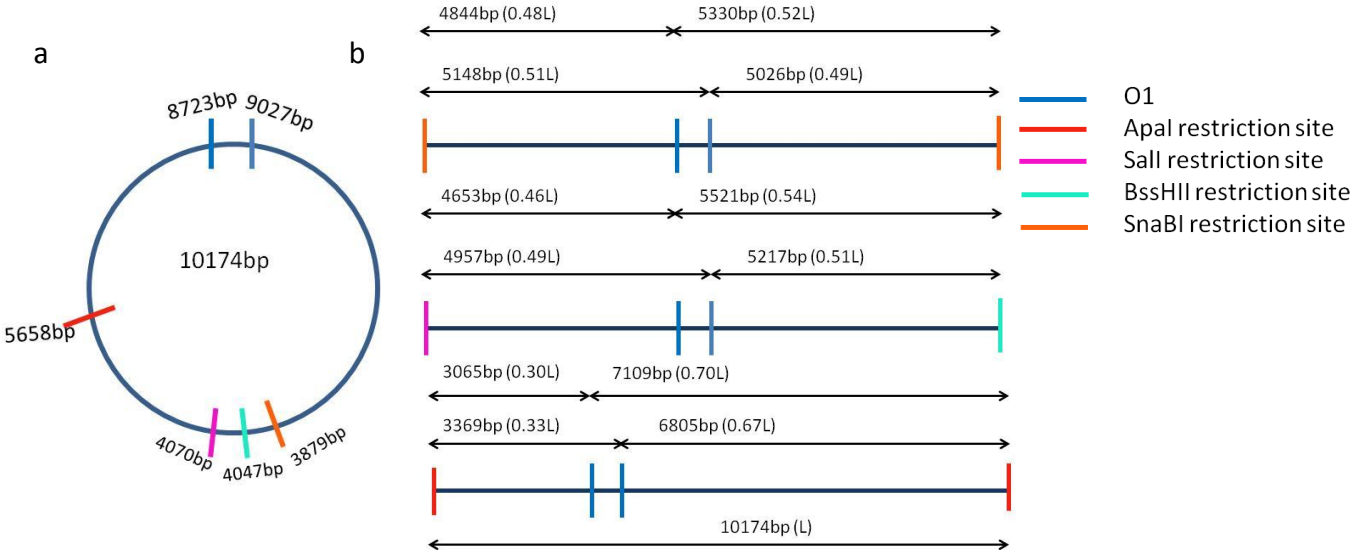

Figure 12.5. (a) Simplified map of the plasmid used with absolute positions of operators (blue bars) and restriction sites used for digest DNA (ApaI, red bar; SalI, pink bar; BssHII light bluebar; SnaBI orange bar). (b) Schematic representation of relative positions of the two operators within the DNA linearized with the different enzymes. L= DNA length and is equal to 10174 base pairs. When digesting with SnaBI, the two operators have relative positions of 0.49L-0.51L and 0.48L-0.52L respectively; when double digesting with SalI and BssHII 0.46L-0.54L and 0.49L-0.51L; when digesting with ApaI 0.30L-0.70L and 0.33L-0.67L

12.3 Protein labeling

12.3.1 Labeling with Quantum Dots

The choice of Quantum dots (Qdots)[8] as the fluorescent probe for FIAT experiments was based on a previous study performed in our laboratory (Capitanio et al., 2007). Qdots (figure 12.6) are inorganic nanoparticles that are very photostable and excitable over a broad range of wavelengths in the UV, with narrow emission bands, centered at a wavelength that depends on the Qdot size (figure 12.6b). In comparison with single organic fluorophores, Qdots are significantly brighter because of their high quantum yield, providing a very high signal-to-noise ratio, which is essential to achieve high localization accuracy (Chapter 7.1). Additionally, Qdots allow extended visualization, since they do not suffer from photobleaching as conventional dyes. However, Qdots exhibit a fluorescence intermittency phenomenon (*blinking*) in which they undergo transitions between fluorescent and non-fluorescent states. Obviously Qdots blinking can be a limitation when the goal is to measure the localization of the probe with continuity over time and with a high time resolution. On the other hand, blinking can be useful as the signature of a single Qdot with respect to multiple Qdots or aggregates that would not display blinking.

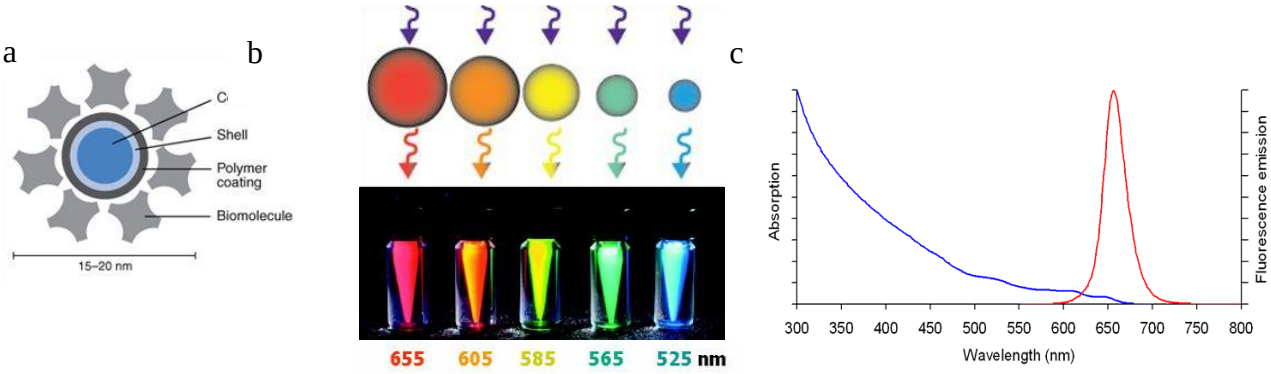

Figure 12.6. Quantum dots nanocrystals. **(a)** Schematic representation of the core-shell structure of Qdots. **(b)** Qdots can be "confined" in their emission by varying their size. Five different nanocrystal solutions are shown excited with the same wavelength UV lamp. **(c)** Absorption (blue) and emission (red) spectra for QDot655. Figures adapted from Invitrogen website (http://www.invitrogen.com/site/us/en/home/brands/Molecular-Probes/Key-Molecular-Probes-Products/Qdot/Technology-Overview.html#size).

[8] Quantum dots nanocrystals have a “core-shell” structure; the core is made of a semiconductor material (cadmium mixed with selenium or tellurium) which has been coated with an additional semiconductor shell (zinc sulfide) to improve optical properties. Other shell layers are made by organic materials that allow the conjugation of Quantum dots to the target biomaterials, without altering their unique optical properties .Qdots are zero-dimensional structures and their electronic states are fully quantized; therefore, their charge carriers and excitations are confined in all three dimensions.

Quantum Dots used for labelling LacI are QDot655 characterized by a broad absorption band and a narrow emission band centred on 655nm (figure 12.6,c) from QDot corporation. Having an emission wavelength (655nm) well separated from the used excitation wavelength (532nm) allows to minimize fluorescence background. The QDot655 used for this work is coated with streptavidin (Invitrogen, #Q10121MP). A bandpass filter (D655/40 nm, Chroma) is mounted in front of EMCCD to collect only photons within the emission band.

The superficial functionalization with streptavidin is useful for conjugating the nanocrytal to the protein of interest if the protein is functionalized with biotin, thus exploiting the high affinity of the streptavidin/biotin pair for labeling the protein. QDots are commercially available in the streptavidin functionalized form, while to couple biotin with the protein a specific sequence, called biotag (with the aminoacid sequence: GLNDIFEAQKIEWHE), musts be added to the protein native sequence through protein engineering; this sequence is then recognized by an enzyme which covalently links biotin to the tag. Briefly, I prepared a plasmid containing gene encoding for LacI followed by the DNA sequence encoding for the biotag. Once bacterial cells are transformed with this plasmid, they over-express LacI protein fused with the biotag.

This target is introduced at the C-*terminus* of the protein not to interfere with the DNA binding activity of the DNA binding domain which is located at the N-*terminus*. The subsequent biotinylation can be performed either *in vivo* or *in vitro*. The *in vivo* approach is generally based on the expression of the protein in a bacteria strain overexpressing biotin ligase to obtain a high level of biotinylation. In other words protein is purified already biotinylated. If wild type strains are used, the physiological pathway of biotinylation is exploited and proteins will be biotinylated but with low efficiency, due to the low concentration of the enzyme in the bacterial cell. *In vitro* biotinylation is performed after protein purification. The biotinylation reaction proceeds through a first step of activation of biotin with AMP and the subsequent covalent link of the activated biotin to the lysine of the biotag (figure 12.7).

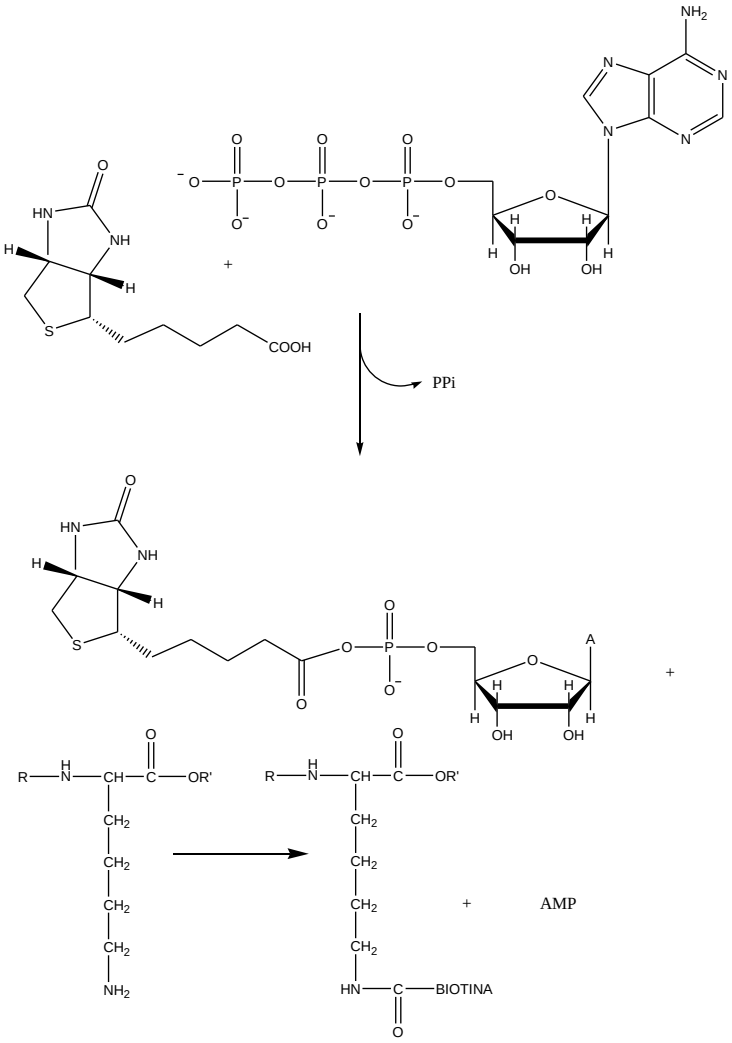

Figure 12.7. Steps of the biotinylation reaction catalyzed by biotin ligase. The first step is activation of biotin through the linking of a molecule of AMP. Once active, biotin is transferred on a lysine of the biotag sequence

As described in chapter 4.1, *lac* repressor is a homotetramer obtained by the self-assembly of the same monomeric structure encoded by a unique gene. Fusing the biotag sequence to this gene will lead to four biotag sequences per tetramer. LacI could be labelled in principle with up to four biotins and eventually with four quantum dots. Since the dimension of a quantum dot is bigger than that of a protein (15nm diameter for quantum dot and 5nm diameter for protein, typically), an overlabeling could alter the physiological and physical properties of the protein (for example, parameters studied like diffusion of the protein which depends on the mass, could be altered from the physiological values). For this specific case, I decided to perform a low efficiency labelling *in vivo* in LacI- bacteria (BLIM) not over-expressing biotin ligase. LacI is thus supposed to carry less than four biotins per tetramer.

12.3.1.1 Preliminary results with Quantum Dots

In order to exploit the high quantum yield of quantum dots, very suitable to get high precision single molecule localization), and for overcoming the problem of photobleaching which limits the acquisition time to some seconds typically, I did the first attempt of protein labelling with quantum dots. As described in the previous chapter, Quantum Dots are linked to LacI through the streptavidin-biotin pair (on the QDots and on the protein respectively). The pair of tags for linking DNA to the beads musts be different to avoid cross-reactions; the two labelling strategies (for conjugating the protein with the fluorescent probe or DNA to the beads) must be bio-orthogonal (not cross-reactive). That's why when conjugating LacI with QDots, digoxigenin-labeled DNA and antidig-beads are used. The first type of experiments to do before studying the dynamics of LacI/DNA interactions (binding and unbinding events with specific and non-specific DNA sequences), are preliminary characterizations by single molecule localization of the conjugated protein in its specifically bound state. This is for determining if the conjugate retains the capability to bind its cognate site and to determine the accuracy of such localization measurements. Basically, a specifically bound LacI is localized and the localization accuracy is measured. From the relative position with respect to DNA it is possible to determine on which of the two operators the protein is bound. At this level of studying specificity is important to avoid non specific binding; this is achieved through a high concentration of salts (200mM KCl) in the buffer. This high ionic strength avoids the electrostatic interaction between negative charges on DNA backbone and positive charges on DNA binding domain of LacI, thus resulting in a ionic exchange effect. If one writes the reaction of exchange:

$$\text{DNA/LacI} + K^+ \rightleftharpoons \text{DNA/K} + \text{LacI} \qquad (25)$$

It is evident that when increasing the salt (in this case KCl) concentration, the equilibrium is shifted to the right, i.e. toward protein detachment. 200mM is sufficiently high for non-specific binding to be negligible (Barkley 1981). In these preliminary experiments, the complex DNA-LacIQDot was formed in a tube, by incubation of the three components (DNA, LacI and QDots), before introduction of the sample in the flow chamber,. In this way,

when a dumbbell is formed, there will also be the bound labelled protein. If LacI is first incubated with QDot to form the conjugate LacI/QDot and then with DNA, no dumbbell formed presented labelled protein bound. Surprisingly, if LacI was incubated with DNA first and QDots were added subsequently, all dumbbell presented labelled protein bound (figure 12.14). Fluorescence videos were acquired with a 10ms exposure time, 532nm laser power on sample of ~20µW and a DNA tension of 1pN. Figure 13.15 shows a typical trace of the position (determined through the MATLAB custom written 2D-Gaussian fit algorithm during time). From the standard deviation of positions it is possible to obtain the accuracy of the localization measurements. Figure 12.14 represents an average image of a video (797 frames); LacI is bound to the centre of the DNA, because that DNA was in fact double digested with SnaBI (and labelled with digoxigenin-dUTP tail by TdT), resulting in an operator position at the centre of the DNA. From a qualitative point of view, one can suppose that this binding is effectively specific. To confirm such specificity the relative distance from DNA extremities were measured and compared to the values expected on the basis of the DNA sequences. The example reported in figure 12.14 shows a relative distance from one end of 0.49L the measured total length of DNA (L) and 0.51L to the other end of DNA, thus matching one of the two operators sequence position, present on DNA. It was confirmed that LacI was bound to the specific cognate site.

Accuracy determined by the standard deviation of the position resulted to be 9.8±0.6nm (mean±standard error, N=6). This value is far from the expected nanometer level. That's because these first experiments were done with a Y shaped flow-cell (detailed description of the flow-system will presented in the next chapter) allowing to introduce in the flow cell just two solutions; one must always be beads and the other, in this case, was represented by the complex DNA, protein and QDots; video are thus acquired in this channel (and not in a buffer only channel) where diffusing probes determine a high level of fluorescence background which, in turn, decreases localization accuracy.

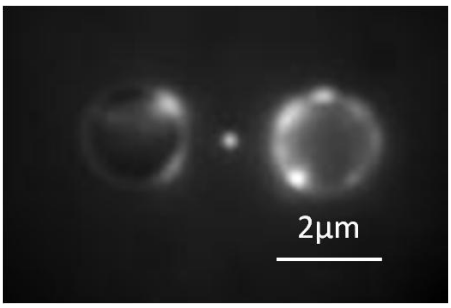

Figure 12.14. Average image (797 frames) of QDot labelled LacI specifically bound to DNA. In this example, DNA was double digested with SalI and BssHII resulting in an operator position in the centre of DNA. Namely, LacI was bound at the centre of DNA molecule, as expected.

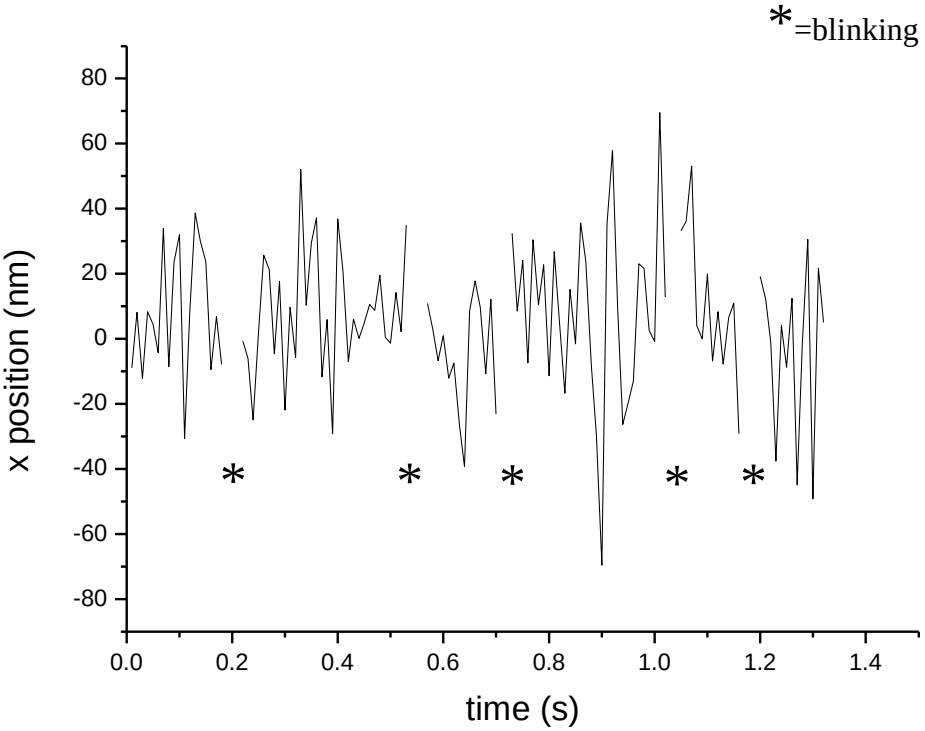

Figure 12.15. A typical trace of position vs time of LacI specifically bound to operator. Position was obtained from a 2D-Gaussian fit of the bright spot, with an exposure time of 10ms. As described previously, a single QDot particle alternates states of emission with states of non-emission, the 'blinking' phenomenon (stars). A trace of QDot will thus show gaps in correspondence of non-emission states.

Despite QDot conjugation to LacI/DNA complex does not alter the stability of the complex, it is not clear if the QDot/LacI conjugate retains the capability to bind DNA. In fact, when mixing QDot and protein first and then DNA (before introduction of samples in the chamber) no dumbbell presented labelled proteins bound. It can be supposed that the binding of QDot to free LacI could affect the capability of binding DNA. On the other hand, when QDot is mixed after DNA/protein binding has occurred, the protein remains bound but

when dissociates (thus resulting in a free, unbound state), likely loses its ability to bind again. The observed bound states obtained mixing components in the order: DNA, protein, QDots could be attributed to a stabilization of the native structure of the protein by DNA which prevents destabilization by QDots when DNA/protein complex is preformed. Also waiting for up to one, no binding event of the LacI/QDots complex was detected. Also when mixing DNA and LacI first and then QDot but with a lower concentration to reduce fluorescence background (and thus to increase localization accuracy), no labelled protein was detected bound to DNA.

These findings led to the necessity of evaluating another type of fluorescent probe, for example an organic fluorophore. These kinds of dyes are very small compared to the size of a protein so they are less likely to affect the protein activity. Unfortunately, these dyes are also less bright and photobleach on a short time scale (typically on the order of seconds) at the excitation power typically used for single molecule detection. I decided to use an Atto dye which is, among all the organic dye, one of the brightest and most photostable. Also a new, multichannel flow-cell has been realized and discussed in next chapters.

12.3.2 Labeling LacI with ATTOdye

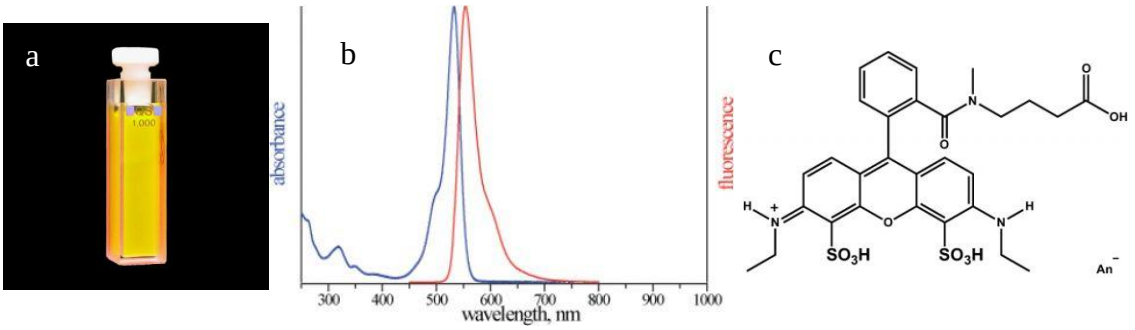

Figure 12.8. (a) Picture of a solution of Atto532. (b) Absorption and emission spectra (blue and red respectively). Absorption has a maximum at 532nm while fluorescence at 553nm. (c) Molecular structure of Atto532. Images from https://www.atto-tec.com/attotecshop/product_info.php?info=p102_ATTO-532.html&XTCsid=sbkv0esqfmuqt4306bukcga597.

ATTO532 is a fluorescent label related to the well-known dye Rhodamine 6G. Characteristic features of the label are strong absorption, high fluorescence quantum yield,

high photostability, and excellent water solubility. Figure 12.8 shows absorption and emission spectra and the molecular structure of the dye. The fluorescence is excited most efficiently in the range 515 - 545 nm. The molecule is available with different reactive groups in order to covalently link it to specific functional groups in the protein, in particular protein amino- or sulfhydryl groups.

The most commonly used amine-reactive ATTO derivatives are N-hydroxysuccinimidyl(NHS)-esters (SIGMA, #88793-1MG-F). NHS-esters readily react with amine-modified oligonucleotides or amino groups of proteins, i.e. the ε-amino groups of lysines or the amine terminus, forming a chemically stable amide bond between the dye and the protein (figure 12.9, a).

For labeling thiol groups the most popular and commonly used dye derivatives are maleimides. ATTO-maleimides (SIGMA, #68499-1MG) react with thiol groups of proteins to form a stable thio-ether bond (figure 12.9, b).

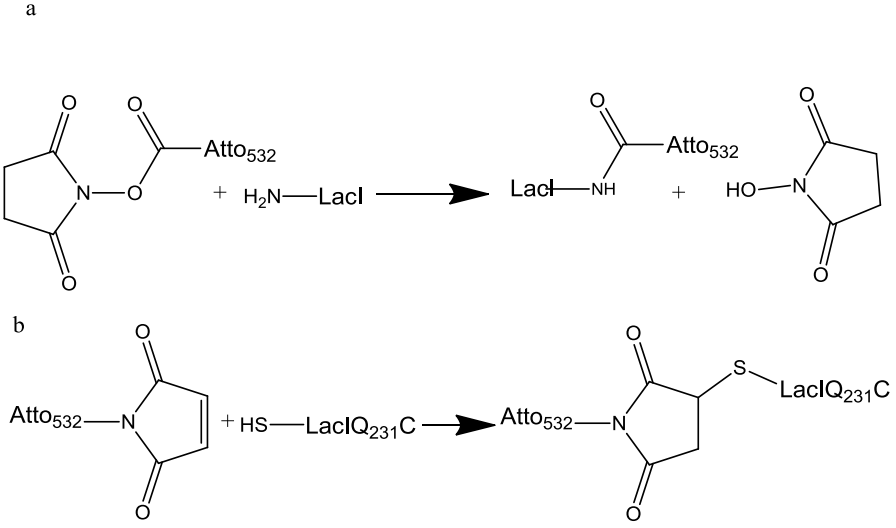

Figure 12.9. (a) General scheme of the reaction of coupling of LacI amino groups with Atto532 through the formation of an amide bond with the NHS-ester moiety of the dye. (b) General scheme for the formation of a stable –C-S- covalent bond between a sulfhydryl group on the protein and the maleimide moiety of the dye.

For coupling of amino groups, wild type LacI was used while for coupling sulfhydryl group, a mutant of LacI, LacIQ231C (figure 12.10), was used. All cysteines (C) present in the wild type have been removed in this mutant protein, while a single cysteine per monomer was introduced at position 231 instead of a glutamine (Q). LacIQ231C has been used previously in looping measurements (Rutkauskas et al., 2009) and it is known that chemical modification at position 231 does not interfere with the DNA binding activity

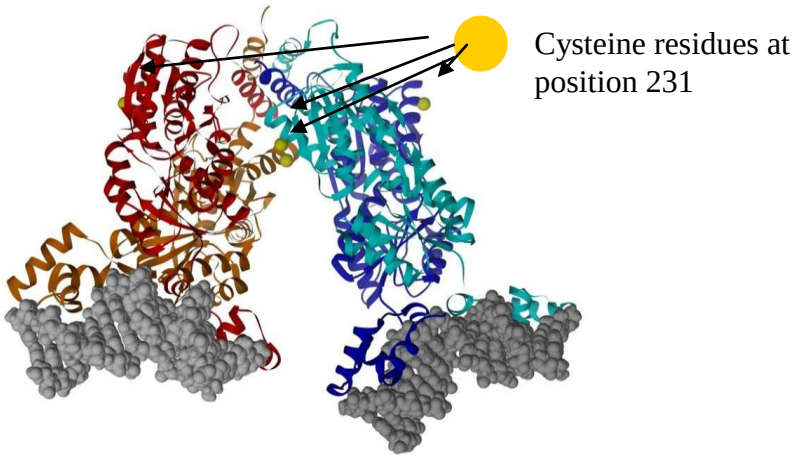

Figure 12.10. Structure of tetrameric LacIQ231C (ribbons).Each monomer is represented with a different colour while the cysteine residues introduced at position 231 are represented with a yellow ball. Grey spacefilling models are two DNA fragments bound simultaneously by the two DNA binding domain of the protein (Lewis et al., 1996).

13. The flow system

To achieve precise control of buffer exchanges and dumbbell assembly during FIAT experiments, a microfluidic system was custom-built. The system is composed of a pressure reservoir (figure 13.2), a pressure control system and a microfluidic flow chamber (figure 13.1). The flow chamber is a sandwich between: a microscope slide with five 1mm-diameter holes (four inlets and one outlet) connected to appropriate tubing by the attachment of NanoPorts Assemblies (#N-333, Upchurch Scientific Inc); parafilm which is manually cut to obtain the desired path of flows and in such a way that the four merged channels perfectly match with the holes in the microscope slide (see Fig. 13.1a), and the slide. The sandwich is heated at 130°C for 30 minutes while being pressed with a weight (see Fig. 13.1b) to make the parafilm melt and attach the two slides. Due to the presence of the NanoPorts glued to the slide, the flow cell is not flat. To overcome this drawback, and in order to apply constant pressure all over the flow cell during the heating process, we have designed and realised a

holder in the mechanical workshop at LENS in which the flow cell fits perfectly upside-down, as shown in figure 13.1b.

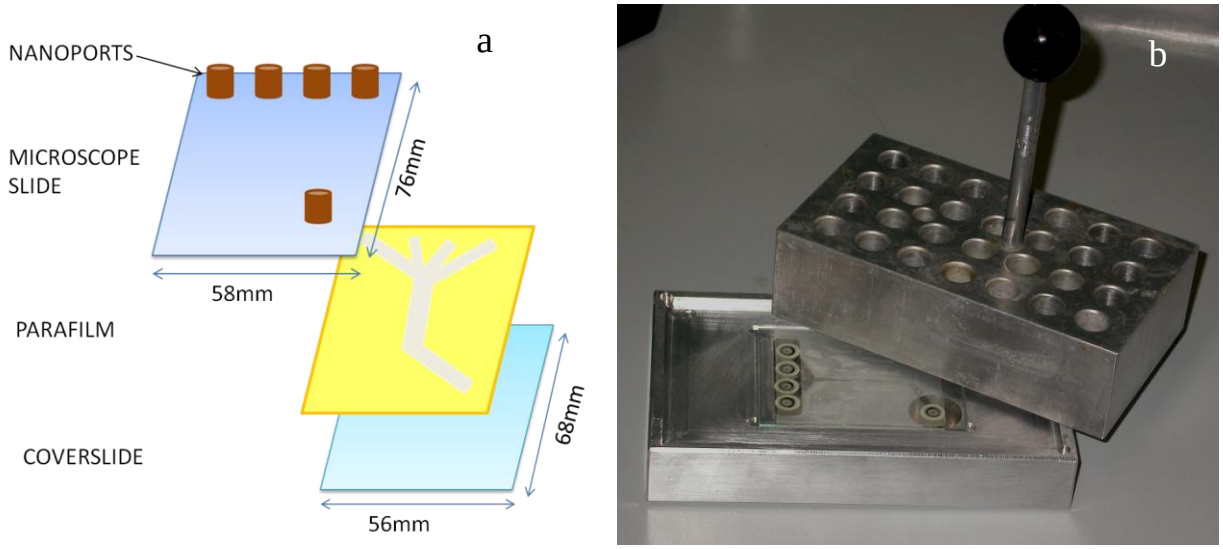

Figure 13.1. (a) All components of microfluidic flow cell are represented, in the order they are assembled to obtain the "sandwich". (b) Sandwich is heated at 130°C in a metallic holder to make parafilm melt and thus stick the slides.

The Plexiglas® pressure reservoir has six independent solution containers (5 x2.5 mL and 1x6 mL capacity) (figure 13.2). The buffer containers consist of sterile and disposable luer lock-tip syringes (2,5 and 6 mL) (Terumo®), with the plungers removed. The connections between the syringe barrels and the flow chamber were made with PEEK™ tubing and flangeless fittings (Upchurch Scientific, Inc.). The fact that syringe containers and Plexiglas® pressure reservoir are transparent helps considerably the flow cell handling, buffer volume control and the monitoring of the possible presence of air-bubbles in the system. Solutions were perfused through the flow cell by pressurizing the Plexiglas® reservoir. Fine control of the flow speed was obtained by adjusting the air pressure with two computer-controlled solenoid valves (ET-2-H-M5, Clippard, Cincinnati, OH, USA): one connected to a +0.5 atm

pressure source and the second to atmospheric pressure. The pressure exerted on the pressure reservoir, and therefore on the solutions, was monitored by a pressure transducer (PTX 1400, Druck LTD) and controlled with custom-written software. The pressure- or atmospheric- solenoid valves were opened for approximately 7 ms to increase or decrease the pressure in the line until the desired value was reached. This approach was adapted from Carlos Bustamante (Wuite GJ et al., 2000), and it yields a smoother flow than using a stepping motor syringe pump (Brewer LR et al., 2008). Moreover, the total volume of fluids in the buffers containers was small compared with the air volume inside the pressure reservoir, which permitted a smooth and stable flow. Typical working pressures were on the order of 20 mBar.

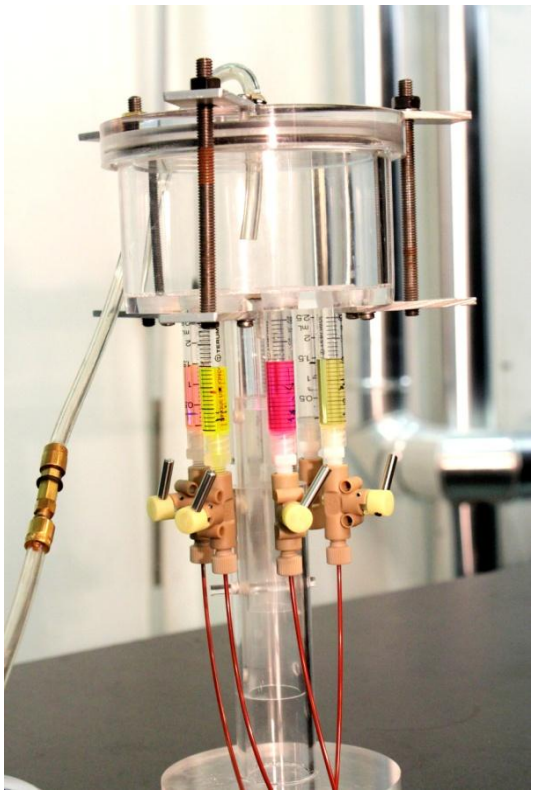

Figure 13.2. Pressure reservoir endowed with a six syringes system.

The first (upper) channel of the flow chamber was used for the polystyrene beads (Streptavidin-coated, 1.87 µm diameter, #SVP-15-5, Spherotech), the second for DNA, the third for protein solution and the last for imaging buffer. Beads and DNA are always dissolved in simple Lactose repressor Binding Buffer (LBB) while LacI is dissolved in Imaging Buffer, consisting of LBB with the addition of oxygen scavenging system (catalase, glucose oxydase, glucose and DTT) in order to the reduce photobleaching which affects all organic

fluorophores and which is reduced in the absence of oxygen. While the pressure system is on, two beads are trapped first; then, moving the stage perpendicularly to the flow, all components are added; DNA is extended by the flow and can bind to both streptavidin-coated beads with its biotin-labelled extremities; finally, the dumbbell is moved into the LacI solution to make protein bind and then either start the acquisition for dynamics experiments or move into the imaging buffer for high precision colocalization measurements (figure 13.3).The hydrodynamic flow was just required to extend DNA molecules and achieve a rapid and efficient attachment to the two optically-trapped polystyrene beads. Once in the final channel, pressure was turned off through Shut-off valves (#P-732, Upchurch Scientific Inc) prior to starting acquisition. In this way, no drag force was applied to the molecule during the subsequent measurements.

Noise reducing practices included filtering buffers with 0.2 µm syringe filters (Nalgene®, #190-2520) and washing microspheres by buffer exchange via centrifugation at maximum velocity (14.000 rpm) for 2min. These cleaning procedures enabled a drastic reduction of submicroscopic particle contaminants that could potentially fall into the trap, thus modulating the level of scattered light and altering the apparent bead position. It was also observed that not all beads were perfectly spherical, and therefore irregularly shaped beads that may be caught with the traps were immediately discarded, and new perfectly round beads were chosen before moving into the DNA channel.

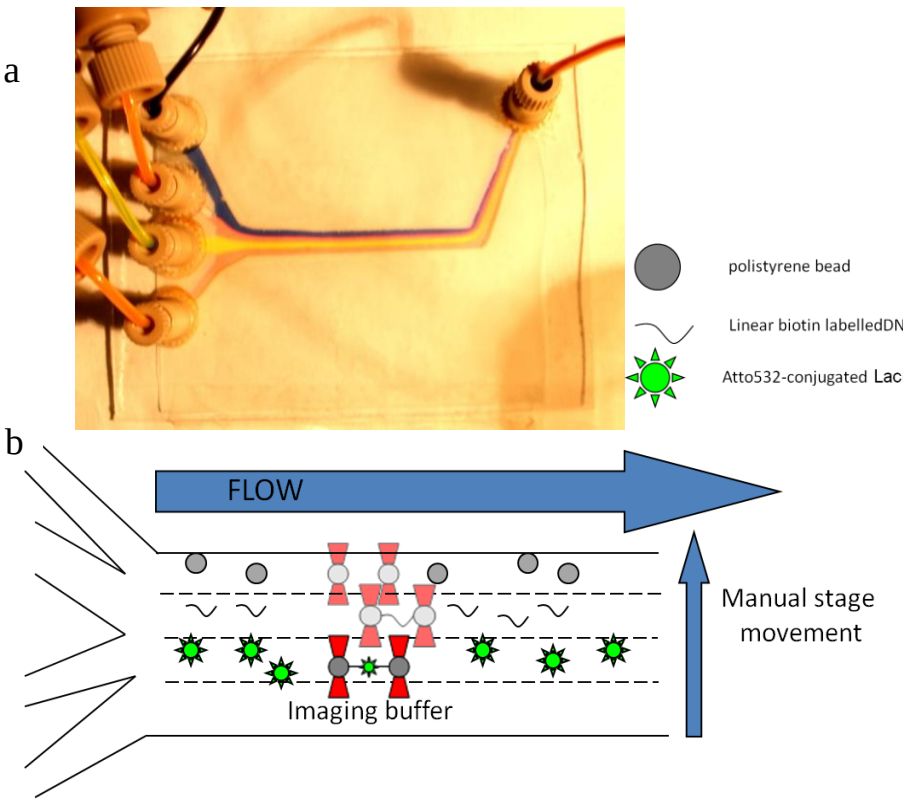

Figure 13.3. (a) Photo of the home-built flow-cell with four independent inlets (on the left) and one outlet (on the right). Four different solutions are pushed in the cell by pressure. Once converged in the same channel, they form four laminar flows without mixing. (b) Two beads (grey) are trapped with the double optical tweezers (red). Moving the stage to the DNA channel, dumbbell formation is achieved by flow extension. With a further displacement dumbbell is moved into the labeled protein channel (green). Flow is now turned off and the acquisition started.

Each flow cell was used for one day of experiments. After that, parafilm and coverslide were detached using acetone or ethanol, and the slide with glued NanoPorts was reused to make a new flow cell. Tubings are instead washed with 30% ethanol and used again.

14. Characterization of ATTO532 dye

As mentioned above, Atto is an organic dye and thus presents the problem of photobleaching which limits the duration of acquisition to the duration of the dye lifetime. The other limit of organic fluorophores is that they are not very bright; in order to collect a sufficiently high number of photons to get enough signal for single molecule detection, one can increase the excitation laser power or the exposure time. In principle to have a high signal to noise ratio, it would be better to increase the exposure time, because increasing laser power enhances background and photobleaching. When investigating biological processes, and in particular the dynamics of single biomolecules, it is fundamental to have a high spatial and temporal resolution to resolve the spatio-temporal details of the dynamics investigated. It is intuitive that the exposure time is a very critical parameter to set for localization of single biomolecules, since it determines the temporal resolution of the measurement. For example, if a protein is moving within the exposure, in that frame there will be a unique, deformed spot centred on a position which will be the average of positions travelled by the particle during exposure time. On the other hand, since laser power reduces fluorophores photobleaching time, a compromise between exposure time and laser power has to be found in order to have a signal to noise ratio which allows a high accuracy of localization with a useful temporal resolution.

Nevertheless, a commonly used trick to slow down the photobleaching rate is to reduce the amount of oxygen dissolved in the imaging buffer. As described in chapter 7, dye

molecules may cross from a singlet excited state S* to the long-lived triplet excited state T*, a process that permits these molecules to interact with their environment for a much longer time. Interaction between O_2 and dye triplets may generate singlet oxygen according to $T^* + {}^3O_2 \rightarrow S + {}^1O_2$. Singlet oxygen has a longer lifetime than the excited triplet states of the dyes. Moreover, several types of damaging oxygen free radicals can be generated when it decays. These reactive, long-lived species can react and oxidize exposed chemical groups and the dye itself. Oxidized dyes are no longer fluorescent and protecting them from reacting with environmental molecular oxygen thus lowers the observed rate of photobleaching (Bernas et al., 2004).

The system used in this thesis to reduce the dissolved oxygen concentration is commonly used (Blanchard et al., 2004; Munro et al., 2007; Joo et al., 2007; Harada et al., 1990) and is based on enzymatic reactions in the presence of glucose. The two enzymes employed are glucose oxidase (which uses molecular oxygen to oxidise glucose) and catalase (which convert hydrogen peroxide produced from the oxidase reaction into molecular oxygen and water). Since catalase converts two molecules of hydrogen peroxide into one molecule of oxygen, two glucose molecules and thus oxygen have to be consumed by oxidase. In summary, the number of oxygen molecules is halved each round of reactions (figure 14.1).

$$2\beta\text{-D-Glucose} + 2O_2 \xrightarrow{GOx} 2\ \text{Gluconic acid} + 2H_2O_2$$

$$2H_2O_2 \xrightarrow{CAT} 2H_2O + O_2$$

Figure 14.1. Scheme of oxygen scavenging by glucose oxidase (GOx) and catalase (CAT).

To measure photobleaching rate at a given laser intensity, a microscope slide is prepared with the dyes attached on the surface. Then a video is acquired and for each spot the intensity profile is obtained. For a single dye molecule, the measured intensity drops down to background in a single step upon photobleaching (figure 14.2). The experimental conditions evaluated were: an integration time of 100ms and 532nm laser intensity on sample of 200W/cm^2 and the band pass filter used is Chroma D600/100. In these conditions, signal to noise ratio was equal to 10. The distribution of the time before bleaching, measured on many spots (N=22) (figure 14.3), shows an exponential decay; fitting these data allows determining the characteristic time for photobleaching, that was found to be equal to 5.7±0.6 s.

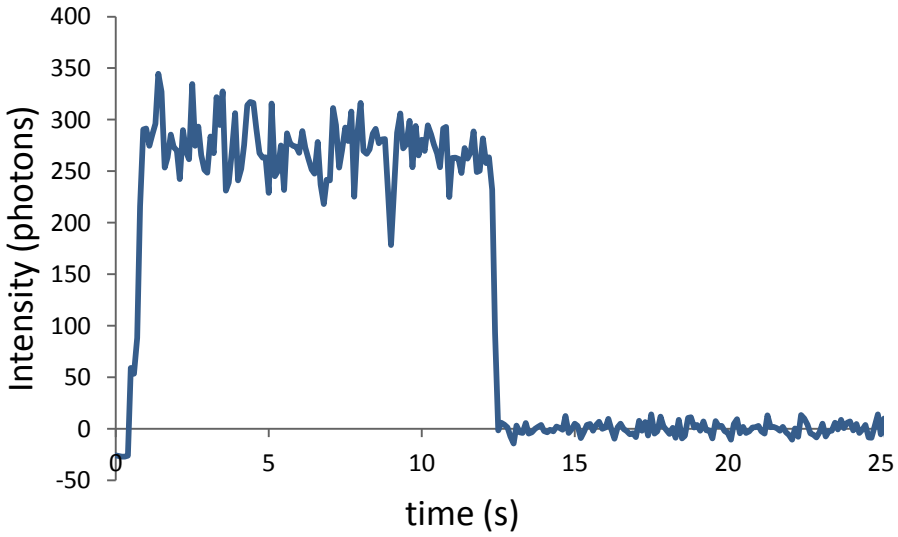

Figure 14.2. Intensity trace of a single dye attached on microscope slide. The dye emits, on average, 270 photons per frame (100ms) before bleaching after 11.3 seconds. The total number of emitted photons results to be equal to 30510 photons.

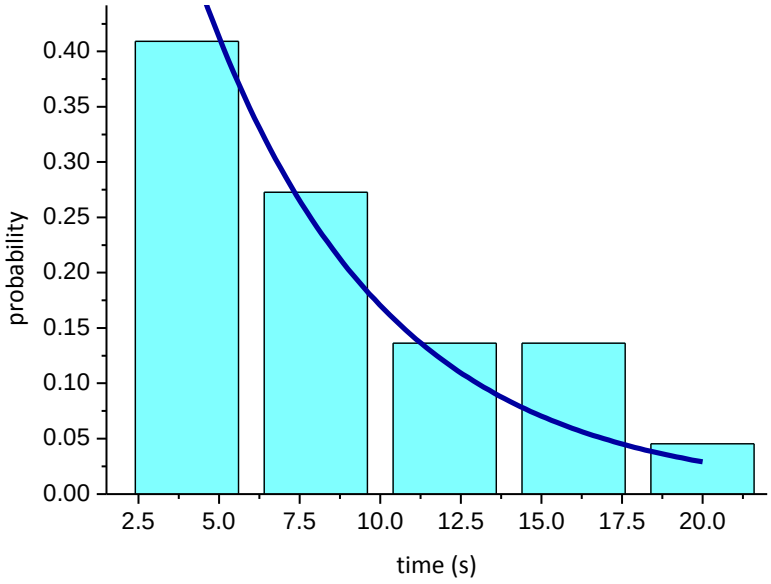

Figure 14.3. Distribution of Atto dye photobleaching times (N=22) at a 532nm laser intensity on sample of 200W/cm^2 shows an exponential decay with a time constant of 5.7±0.6s.

As mentioned in the previous chapter, I tried to link Atto532 to LacI amino groups through a NHS ester functionalized dye and to link Atto532 to a LacI Q231C mutant. In order to test, from a qualitative point of view, if these labelling strategies altered the capability of the proteins to specifically bind to DNA, ATTOLacI (both types of conjugates) are pre-mixed with DNA prior to introduction in the flow cell in order to obtain, if possible, an already labelled protein bound to the dumbbell. This was the case for the mutant LacI but not for the wild type labelled to the amino groups. From the intensity traces of labelled LacIQ231C, in particular from the number of photobleaching steps, it is possible to measure the number of dye molecules bound. Since the protein carries four cysteines, the number of dyes bound should be at maximum four (or less according to the efficiency of the reaction of labelling). Figure 14.4 reports an example of an intensity trace of LacI Q231C bound to operator.

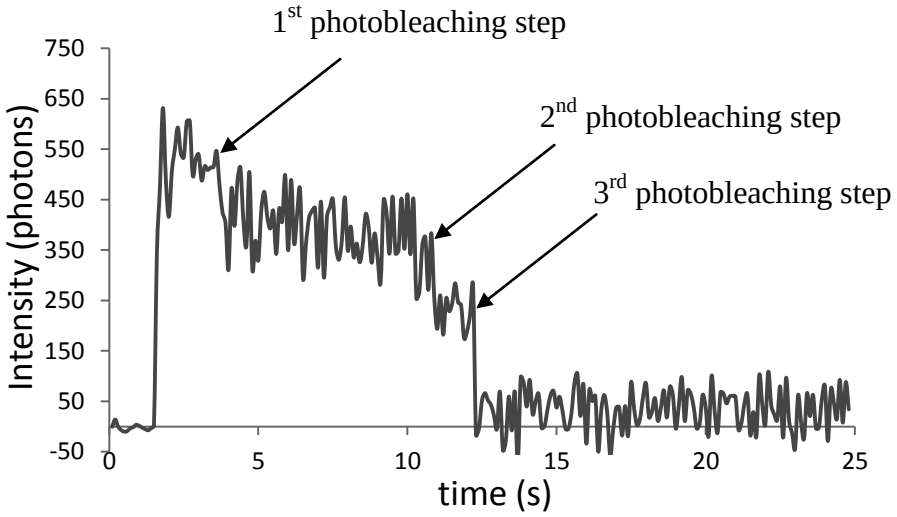

Figure 14.4. Intensity trace of a LacIQ231C labeled with Atto532 through covalent bonds with cysteines sulphydryl groups. The trace shows three distinct photobleaching steps, indicative of the number of dyes bound to the protein.

15. Single molecule kinetic constants measurement

As mentioned above, the step of labeling is a crucial step in that it could alter the structure, and thus the activity, of the protein. It is important to know if the protein retains, after labeling, its native activity. I decided to measure, with the single molecule techniques, kinetic constants for binding and unbinding and compared them to the known values for LacI. One can write the reaction of association between LacI and operator O1 as:

$$\text{LacI} + \text{O1} \underset{off}{\overset{on}{\rightleftharpoons}} \text{LacIO1} \qquad (26)$$

The association reaction is commonly called *on* reaction (from left to right in the equation), while dissociation is commonly called *off* reaction. The rate of the association $v_{on}=k_{on}[\text{LacI}][\text{O1}]$ depends on the molar concentration of O1 and LacI and on the kinetic constant k_{on}. The dissociation rate $v_{off}=k_{off}[\text{LacIO1}]$, on the opposite depends on the molar concentration of the complex LacIO1 and on the kinetic constant k_{off}. The dissociation

constant Kd=[LacI][O1]/[LacIO1] is equal to the ratio between the *off* and the *on* kinetic constants k_{off}/k_{on}. These parameters can be expressed as their reciprocals τ_{off} and τ_{on}[LacI] respectively. τ_{off} and τ_{on} are the characteristic times for dissociation and association, respectively, and correspond to the time the protein spends bound (also called residence time) and to the time the protein spends unbound. These times can also be seen as the time the protein needs to unbind and the time protein needs to bind (that is to encounter) the operator. With the FIAT set-up, it is possible to determine these characteristic times, measuring the time operator is occupied by a LacI molecule and the time operator is unoccupied. For such measurement just three channels of the flow-cell are used: beads, DNA and protein. That's because for measurements of the dynamic interaction (associations and dissociations) the dumbbell must stay in the channel containing protein and not in the buffer without protein. The procedures for these experiments consist of trapping two beads, moving the stage to bring the beads in the DNA channel, form the dumbbell and then move the stage to bring the dumbbell in the protein solution where data acquisition in started. As mentioned in the previous chapter, at a laser intensity on sample of 200W/cm^2, in presence of the oxygen scavenging system, Atto dye shows a characteristic time of photobleaching of 5.7 ± 0.6 s, thus limiting the possibility of measuring the characteristic times for binding and unbinding that are on the order of minutes. To overcome this limitation, I illuminated the sample at discrete time intervals rather than continuously. In particular, I decided to illuminate the sample for 100ms (synchronized with the EMCCD exposure) once a minute (figure 15.1). This gated illumination reduces the illumination of the sample to 1 minute for an acquisition of 10 minutes.

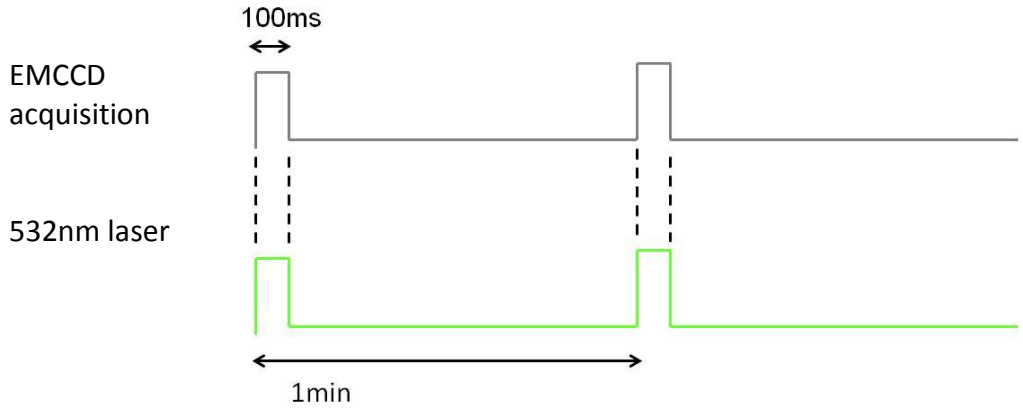

Figure 15.1. Scheme of the acquisition (grey) and excitation (green). EMCCD is synchronized with the excitation laser in order to illuminate and acquire for 100ms (exposure time) once a minute.

During the acquisition a number of frames with LacI bound (figure 15.2,a) and other with LacI unbound (figure 15.2,b) will alternate. An easy way to represent and to visualize all the video in one picture is to transform it into a kymogram. If the frames represented in figure 15.2a-b are rotated by 90° and attached, the resulting image is a kymogram (figure 15.2,c). The kymogram is a representation of *x* coordinate (DNA axis) vs time. This operation is done for all the frames of a video so to visualize them simultaneously (figure 15.3).

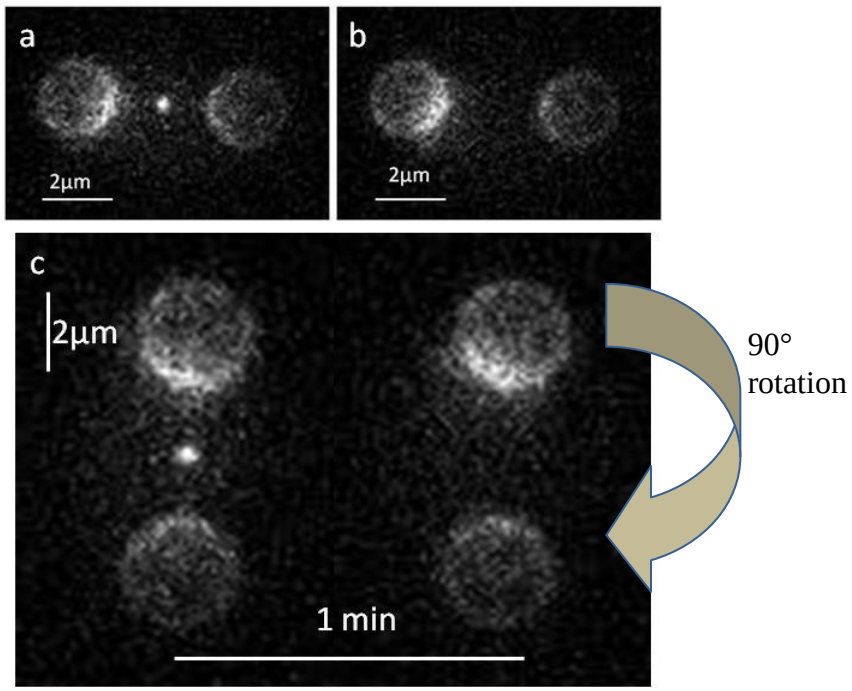

Figure 15.2. Two frames of a track in which bound states (a) alternate with unbound state (b). A 90° rotation of the frames and their juxtaposition gives place to the kymogram representation of the video.

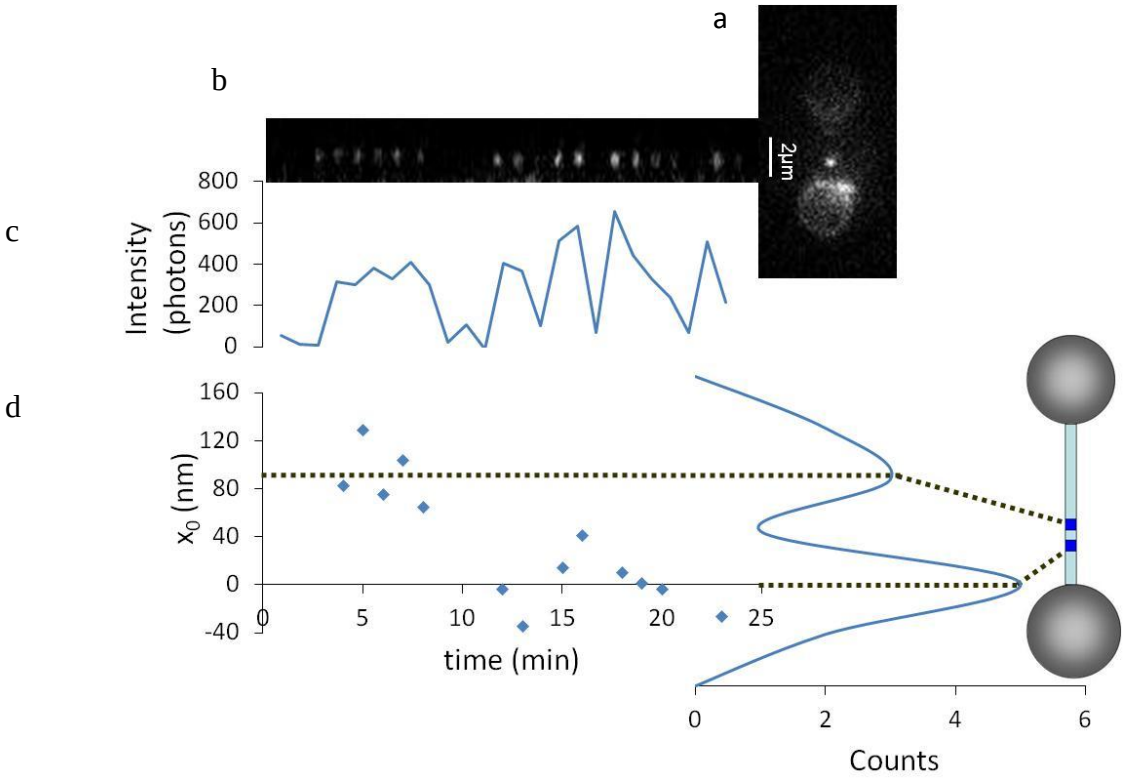

Figure 15.3. Kymogram of a track. (a) single frame of a track from which a region including operator has been cropped. All the cropped frames have been juxtaposed to form the relative kymogram (b). (c) Intensity trace of the kymogram. (d) Positions of LacI in the frames represented in the kymogram. These values are distributed around two averages values separated by a distance of 91±14nm which is consistent with the distance between the two operators. The cartoon on the right is a scheme of DNA (light blue) tethered between the two optically trapped beads (grey) with the operators (blue) shifted from the centre of DNA. In this example DNA was digested with ApaI restriction enzyme.

Given the absolute position of LacI bound to DNA, specificity has to be confirmed from the relative position within the dumbbell. For each position the distance from DNA extremities have been measured (15.4,a) and from the ratio with respect to the total length of DNA (15.4,b), it has been demonstrated the specific binding to operator; also which of the two operators was occupied could be determined (15.4,c).

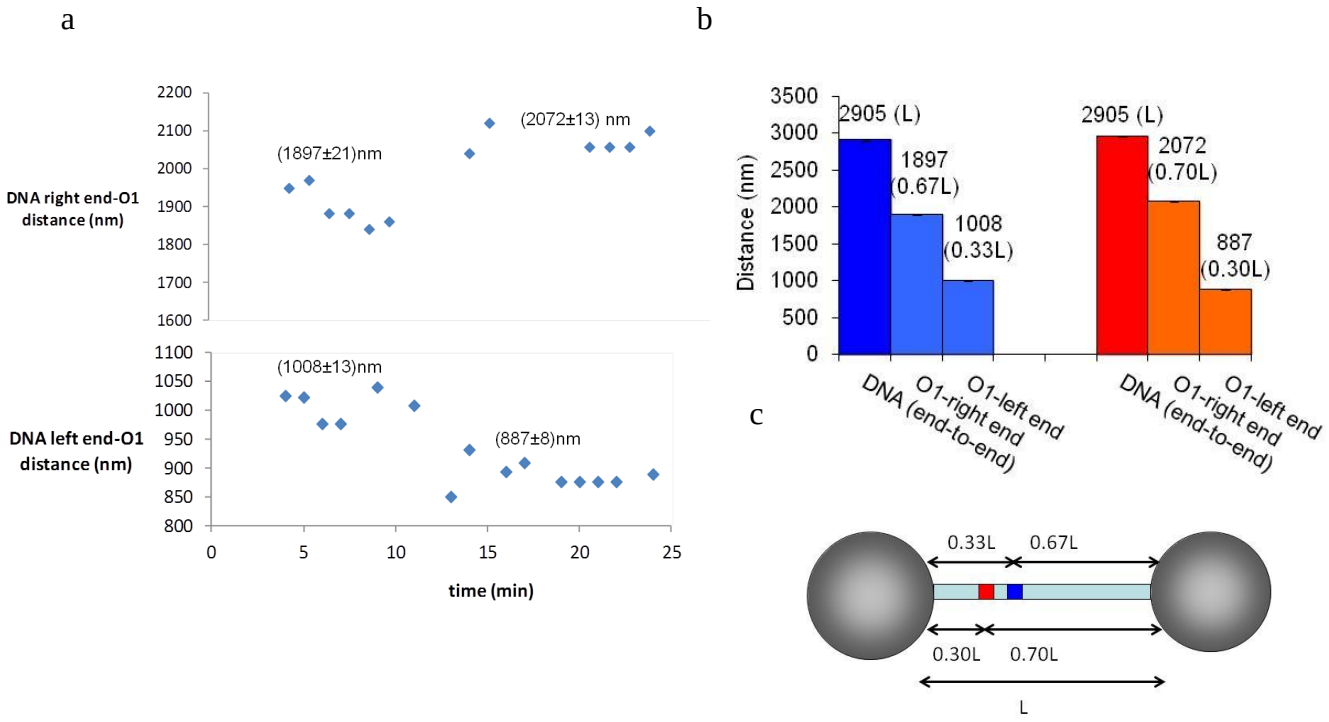

Figure 15.4. (a) Distance of the spot from the right (upper panel) and left (lower panel) extremity of DNA. In the first distribution of position the relative distances are 0.33L and 0.67L while in the second distribution relative distances are 0.30L and 0.70L (b). This distances match with the position of the two operators in a DNA prepared with ApaI (c); the first position occupied was the blue operator of the cartoon and the second position was the red operator of the cartoon.

The precision of the localization, determined from the standard deviation of the positions measured within the same bound state, gave a value of 13 nm (33 frames). The two distributions of times spent bound and freely 3D-diffusing show an exponential decay with characteristic times τoff and τon respectively of 12±1min and 3.3±0.4min (figure 15.5). Considering that DNA construct used contained two Operator sequences, the effective τon to take into account is the double of the value obtained by fitting data, that is 6.6±0.8min.

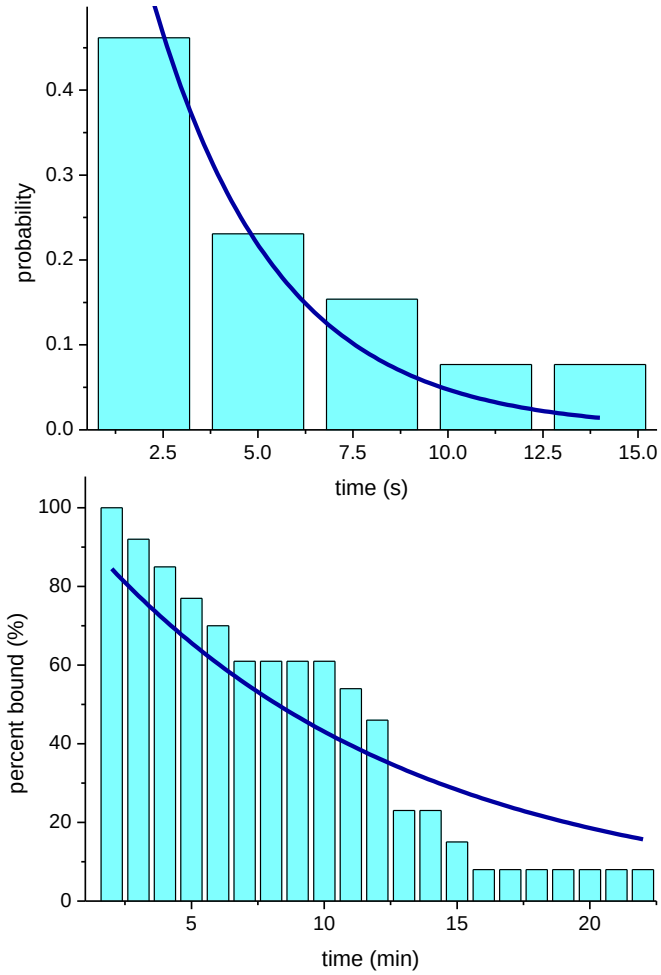

Figure 15.5. Distributions of the durations of states unbound (upper panel) and bound (lower panel). Characteristic times for the exponential decay are respectively 3.3±0.4 min (6.6±0.8 min considering the association to one operator) and 12±1min.

As mentioned above, these times reflect the affinity of LacI for operator. In particular the dissociation constant Kd=τon[LacI]/τoff and given a work concentration of LacI equal to 350pM Kd=396s*350*10^{-12}M/720s=(20±4)*10^{-11}M. This value is in good agreement with value present in the literature (Hsieh et al., 1987), thus confirming that LacIQ231C, retains its normal activity after labelling with Atto532 dye.

16. Effects of exposure time, DNA tension and methodologies used to determine the centre of the PSF on the localization accuracy of an ATTO532LacI specifically bound on DNA

As described in chapter 7.1, the localization of a fluorescently tagged protein is achieved when the centre of its emission pattern (that is the PSF) is determined and the precision associated to this measurement is proportional to the number of collected photons according to Thompson equation (Thompson et al, 2002). Apart from the three terms of Thompson equation (diffraction limit, pixel size and background) there could also be other external factors affecting the localization accuracy as, for example, mechanical vibrations, thermal fluctuations or displacements of the molecule like protein 1D-diffusion on DNA. In this chapter, I show the effects of exposure time, DNA tension and fitting algorithm for determining the centre of PSF on localization accuracy, emphasizing also the relevance of these factors in the determination of biological parameters. The exposure time, as mentioned above, increases the number of collected photons but also lowers the temporal resolution of the measurement. The choice of the exposure time must represent a good compromise between collecting a sufficiently high number of photons and a temporal resolution adequate on a biologically relevant time scale. Three different exposure times were evaluated: 50ms, 100ms and 500ms (figure 16.1).

These measurements were done on ATTO532LacI specifically bound on the operator in the dumbbell configuration. It is intuitive that fluctuations of the DNA molecule (on which the protein is bound) will result in a reduction of the accuracy. As previously demonstrated (Candelli et al., 2011), the highest localization accuracy is achieved for DNA tensions above 1pN, while at forces below 1pN the accuracy of localization is dramatically reduced. This is due to substantial thermal fluctuations of DNA below 1pN which in turn blur and defocuses the image leading to a decreased accuracy; for forces above 1pN, there is not a significant difference in accuracy. In these measurements I used two sets of forces: 1 and 10pN (figure 16.1).

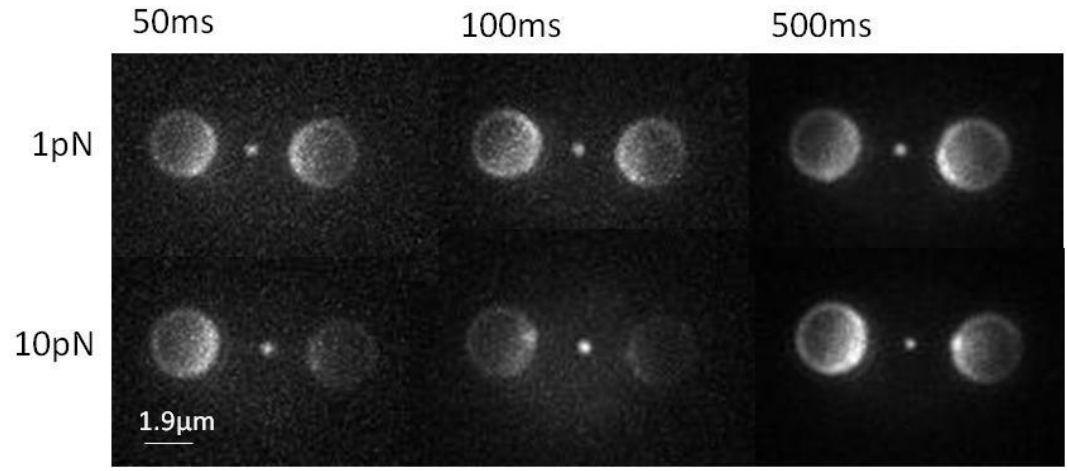

Figure 16.1. Maximum Intensity projections from 100 frames representing LacI specifically bound on DNA. Videos were acquired in imaging buffer (containing oxygen scavenging system enzymes) at 50, 100 and 500 ms exposure time with either 1 pN or 10 pN force applied on DNA.

Regarding the algorithm used for determining the centre of the PSF, even if the most accredited and commonly used is the fitting with a 2D-Gaussian curve, it has some limitations. First, it is slow and requires numerical iterations to determine optimal parameters, and can be prohibitively time consuming for large data sets. Second, the true particle intensity distribution is, in general, not a Gaussian but rather the convolution of the object shape with the Point Spread Function of the imaging system which may not be precisely known. Third, a Gaussian fit has many parameters and, if the only parameter desired is the location of the particle centre, other parameters such as the amplitude and width of the function could represent a superfluous computational cost. Some other methods, like centroid calculation, are fast and do not assume any particular functional form for the PSF but are not so accurate as 2D-Gaussian fit. Recently a new, rapid and accurate method (Ma H. et al., 2012; Raghuveer 2012) has been conceived. This method is based on the concept that the intensity of an imaged particle is radially symmetric about its centre. The localization of the particle centre is thus achieved through an algorithm which determines the point of maximal radial symmetry. The rapidity of the calculation is 100 times faster than Gaussian fit because it provides an analytical expression for the optimal particle centre location, with no iterative fitting steps but with the same accuracy level (figure 16.2).

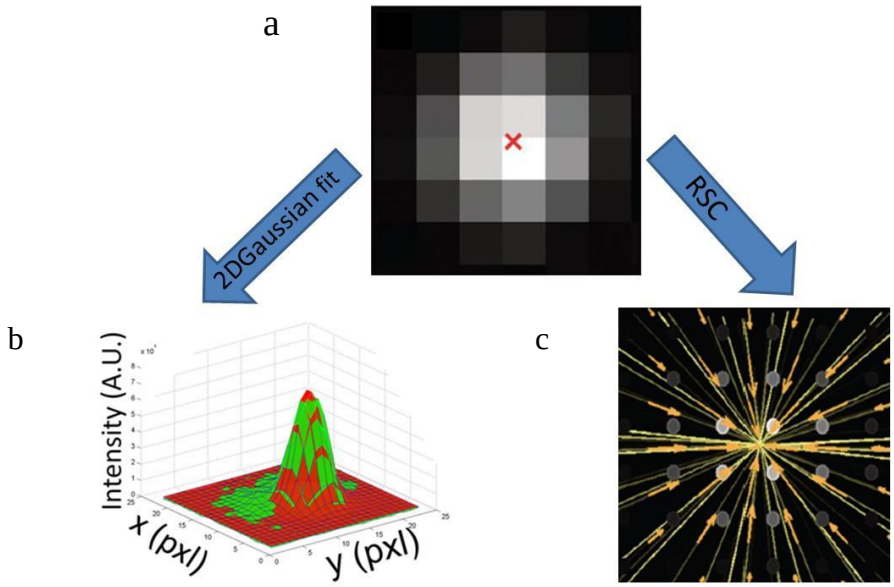

Figure 16.2. The image of a single fluorophore, whose position is indicated by the red 'x' appears as a matrix of pixels with different intensity levels represented as grey scale (a). To localize the single fluorophore with high accuracy, the experimental data which represent the PSF (green) are generally fitted with a 2D Gaussian curve (Cheezum et al., 2001) (b). (c) The gradient of the intensity of (a) (orange arrows) is calculated from the pixel centers represented by the circles. Yellow lines are drawn through each midpoint, parallel to the gradient. The analytically calculable estimate of the centre is represented by the point of minimal distance to yellow lines. Adapted from (Raghuveer 2012).

From the experimental point of view, biotinylated-DNA containing operator sequence is pre-incubated with ATTO532LacI; the complex, streptevidin-beads and imaging buffer containing oxygen scavenging system enzymes are then flushed into the flow cell thus creating only three channels. Once all components are into the flow cell, two beads are trapped and the stage is moved to the complex channel were the dumbbell is formed; DNA is tensioned to a precise value of force (1 or 10pN) measured from beads displacement; to reduce fluorescence background, the dumbbell is finally moved into the imaging buffer channel where data are acquired until the fluorophore photobleaches. For both values of force, video were acquired at three different exposure times: 50, 100 and 500ms.

For each video, the position of the bright spot in all frames before photobleaching was determined with the two different methods presented: 2D-Gaussian fit and the calculation of the Radial Symmetry Centers. For both methods of localization, the measurement uncertainty σ has been evaluated from the standard deviation of the positions within a video (obtained at a given exposure time, DNA tension and method of localization). Figure 16.3 shows the values of localization uncertainty for the *x* coordinate[9], σ_x. Although 2D-Gaussian fit gives slightly lower localization error, the Radial Symmetry Centre calculation provide similar values of uncertainty (as expected from the description of the RSC methods, Ma H. et al., 2012; Raghuveer 2012). For both methods of localization, at a given exposure time, there is a slightly lower error for measurements done at a DNA tension of 10pN with respect to those made at 1pN. The exposure time, increasing the number of collected photons and averaging the fluctuations that blur the image, lowers the error. The best accuracy level is thus achieved for both methods at 500ms exposure time and a DNA tension of 10pN reaching an error of (9.5±1.4) nm for the 2D Gaussian fit and (12.6±2.7) nm for the Radial Symmetry Centre calculation. Nevertheless, the localization accuracy just improves of a factor ~2 ranging from an exposure time of 50ms to 500ms (for example, at 1pN, from (23.1±2.4) nm to (12.9±2.6) nm for 2DGaussian fit and from (25.3±2.7) nm to (14.5±1.3) nm for RSC) at the expense of the temporal resolution which worsens by a factor ten. It is thus crucial to decide, according to the biological aspect to be investigated, whether it is more important having a localization accuracy of 10nm rather than 20nm (in the range of exposure times investigated in this work) or a better time resolution.

[9] The x axis is the axis parallel to DNA in the dumbbell configuration.

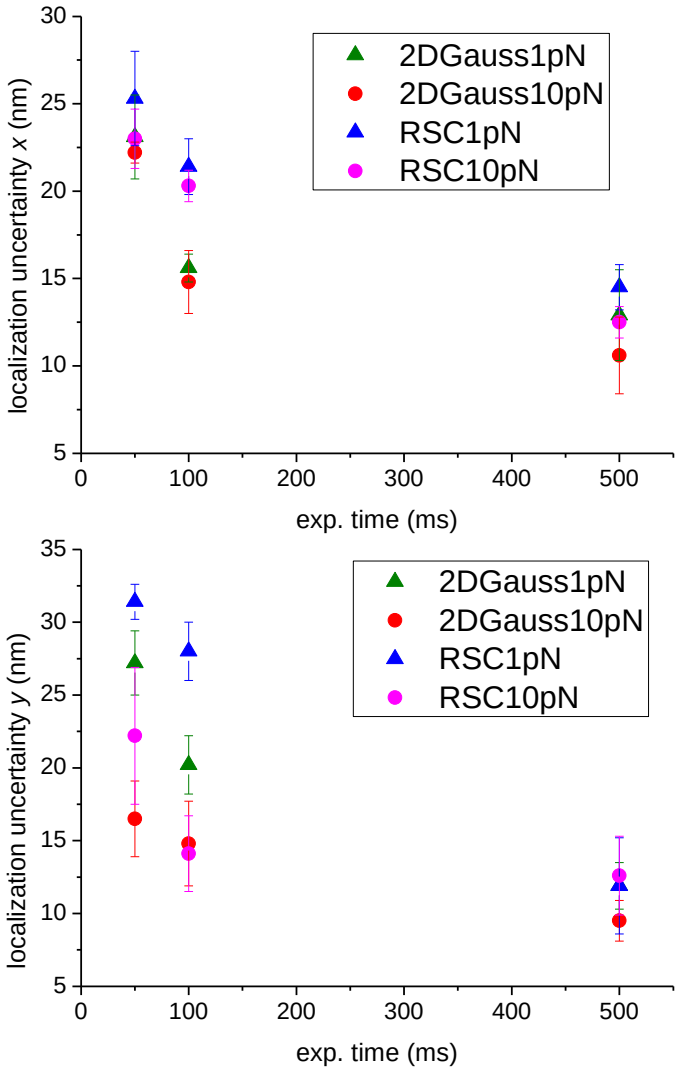

Figure 16.3. The panels show the values of localization uncertainty at three different exposure times (50, 100 and 500ms) and two values of DNA tension (1 and 10pN). Localization has been achieved with two different approaches: fitting the PSF with a bidimensional Gaussian (2DGauss) or calculating the Radial Symmetry Centre (RSC) and the error has been estimated from the standard deviation of the positions during a video. For each combination of force and exposure time, three videos have been acquired and the relative accuracy is thus represented as the average between the three standard deviations of the positions ± standard error of the mean. The upper and lower panel represent the uncertainty along the *x* and y axis, respectively.

In the *y* direction (perpendicular to the DNA axis) the localization error σ_y, as shown in figure 16.3 lower panel, is generally higher with respect to the error in the *x* direction. This is because DNA is tethered along its axis and forces are applied in this direction making DNA more stiff (undergoing less fluctuations) in the *x* direction with respect to the *y* direction. The reduced stiffness in y direction is thus reflected in wider oscillations, that is a lower standard deviation of the position (the localization error). In this case there is a substantial difference in localization uncertainty for measurements done at 1 and 10pN, with a lower error at 10pN because of an increase of the stiffness of the DNA which reduces oscillations. This difference is reduced increasing the exposure time and at 500ms is almost negligible because of oscillations averaging during the exposure.

Thermal fluctuations in the middle of the dumbbell, where the protein is bound, can be theoretically estimated from the equipartition theorem. In fact, considering movements along *x* axis, we can write $\frac{1}{2}k_x\langle x^2\rangle = \frac{1}{2}k_BT$ and thus $\langle x^2\rangle = \frac{k_BT}{k_x}$, where k_x is the combined stiffness of the two traps and of the DNA molecule along the *x* axis (as depicted in figure 16.4), and $\langle x^2\rangle$ is the variance of the *x* position. However, in our measurements, we collected images with a finite integration time so that the fluorescent spot image is averaged during the integration time. This means that, for example considering a 50ms integration time, the bandwidth is limited to about 20 Hz, and the variance of *x* position is smaller than the one calculated using the equipartition theorem. We can estimate the measured *x* variance from the integral of the *x* power spectrum (equation 16), limited to 20Hz:

$$\langle x^2\rangle = \int_0^{20Hz} \frac{k_BT}{\gamma_x\pi^2(f_c^2 + f^2)}df \qquad (27)$$

where $fc = \frac{k_x}{2\pi\gamma_x}$, k_x and γ_x are the total stiffness and drag coefficient along *x* direction, respectively (i.e. the combined *k* and γ of the DNA molecule and the two traps, as illustrated in figure 13.28). Increasing the DNA tension from 1 to 10 pN corresponds to a longitudinal DNA stiffness of ~0.004 pN/nm and ~0.14 pN/nm, respectively. As a consequence, thermal fluctuations decrease from ~8 nm to ~1 nm, with a bandwidth of 20 Hz (50 ms integration time). Higher acquisition times result in a decreased bandwidth and

noise. In any case, as shown in figure 12.27, there is no significant difference between the measured accuracies at 1 and 10 pN, indicating that thermal fluctuations are not limiting the localization accuracy.

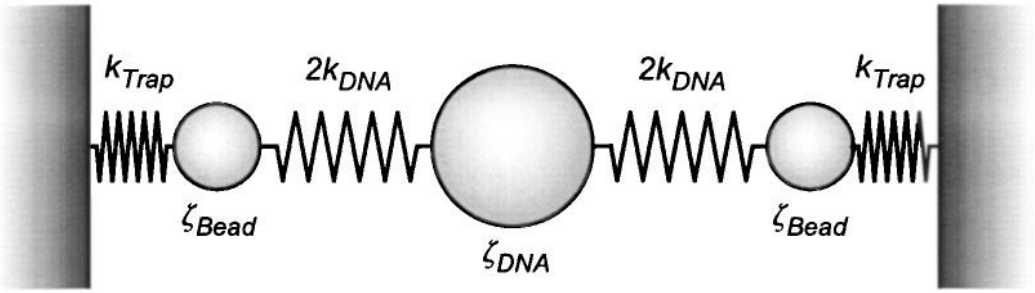

Figure 16.4. Model used to find the spring constant and drag coefficient of the DNA molecule. DNA is modelled as a sphere with a drag coefficient ζ_{DNA} ($\zeta_{DNA,\parallel} = 7.6 \cdot 10^{-9}$ Ns/m; $\zeta_{DNA,\perp} = 17.3 \cdot 10^{-9}$ Ns/m) and two springs in series, each of stiffness $2k_{DNA}$, giving an overall spring constant of k_{DNA} (Meiners et al., 2000).

17. LacI 1D-Diffusion at different DNA tensions

In the last decades, following the discovery (Riggs et al. in 1970) that the experimental association kinetic constant of *lac* repressor is two orders of magnitude higher than the theoretical diffusion-limited value, several models have been proposed. Among these, particularly credited is 1D-diffusion along non-specific DNA, proposed by Berg et al. (1981) and observed by Wang et al. (2006). Briefly, Transcription Factors generally have a high affinity for their cognate sequence and a low affinity for non-cognate DNA; since cognate sequence is just a very small fraction of the whole genome, it is likely that the protein frequently encounters and weakly binds non-cognate DNA before encountering the specific sequence. While non-specifically bound, protein undergoes a 1D-diffusion along DNA. The target search process that could, in principle, enhance association rate to specific target sequence, is given by the alternation of free, 3D-diffusion and 1D-diffusion when non-specifically bound to DNA (see chapter 5 for details).

Nevertheless, there are still some questions that remain unsolved about the mechanism through which non-specific DNA sequences enhance the specific association rate (Halford S.E. 2009). First of all, it has to be taken into account that all experiments until now have always used a salt concentration lower than the physiological one (145mM KCl) and this factor itself enhances association rate (for electrostatic interaction between proteins and DNA); in fact, salt concentration dramatically reduces non-specific interactions, so that non-specific interaction events may not be detectable. Since also the salt concentration used by Riggs et al. (50mM) was lower than the physiological one, it is uncertain if the effective acceleration factor is 100, so it remains still under debate how and how much non-specific DNA sequences act on the acceleration of target search. There are also other controversies around the 1D diffusion model. First is the length of DNA explored in a single sliding event: the longer the sliding length the higher the probability to scan always the same DNA region. Another aspect is that no experiment until now has been done with DNA constructs containing the three natural operators O1, O2 and O3 at specific distances from each other (chapter 4.2).

The aim of the experiments described in this session is to further investigate the 1D diffusion of *lac* repressor exploiting the advantages of the FIAT experimental set-up: DNA is suspended in solution in the flow chamber, far from the glass surface; since DNA is tethered by the optically trapped beads, there is no need to make experiments in the presence of flow (which is only used to introduce samples into the chamber); the use of a dual optical trap system also allows not only to control the mechanical property of DNA but also to apply forces (that is to stretch the molecule) and to study the effect of force on the biological processes, in this case 1D diffusion.

For such studies, I prepared and used a DNA construct containing the wild type operators. Briefly, a 1125bp DNA fragment containing the three natural operators O1, O2 and O3 was amplified directly from the *E. Coli* genome and inserted in the previously used plasmid, between the restriction sites for AatII and AvrII thus replacing the fragment containing the two identical copies of operator O1 (See materials and methods for details of the procedure). A map of the plasmid produced is shown in figure 17.1(a); the highest affinity operator O1 is separated by the other high affinity operator O2, on the right, by 402 bp (~137 nm), while only 92 bp (~ 31nm) separate O1 from O3, at its left. Also for this plasmid are reported the relative distances of operators according to the restriction enzymes used. This information is useful to determine on which operator the protein is specifically bound.

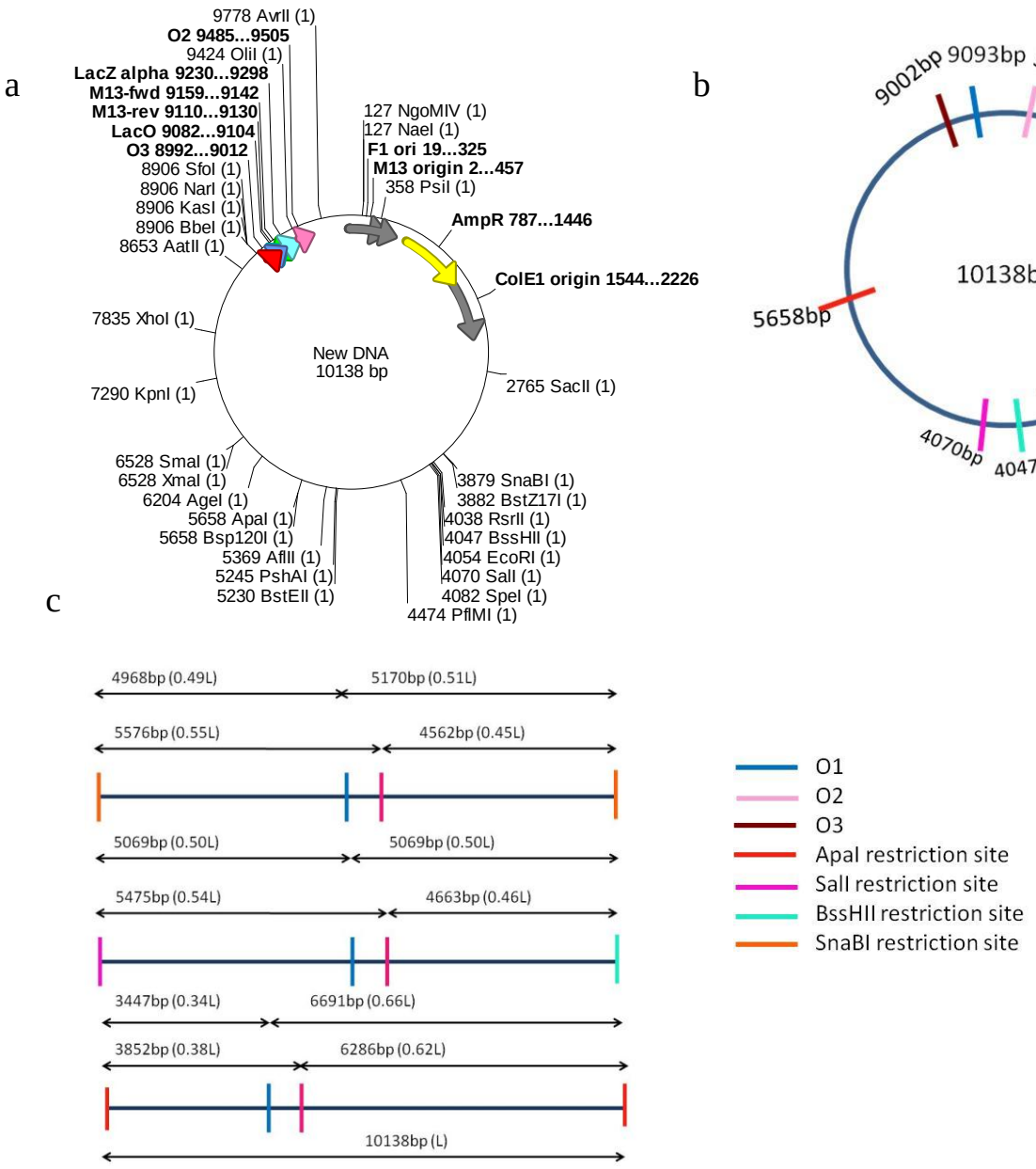

Figure 17.1 (a) Map of the plasmid containing three natural operators O1, O2 and O3 indicated by blue, purple and red arrow, respectively. In the map all restriction sites present in the plasmid are also highlighted. (b) Schematic representation of the plasmid highlighting the positions of operators and restriction site used to linearize the plasmid. (c) Depending on which enzymes are used to digest plasmid, operators will be localized in a different position in the resulting linear DNA, characterized by different relative distances, represented as the ratio between the distance to one extremity and the total length of the molecule, L.

On the other hand, since fluorescence experiments are limited in the time resolution by the bandwidth and since at physiological salt conditions 1D-diffusion is probably too fast to be detected, I used the same buffer (TBE 0.5x (TrisBorateEDTA) pH8.8), with no salt, previously used to detect LacI 1D-diffusion in a different experimental condition (Wang et al., 2006) . In this kind of measurements only three channels are used, for introducing beads,

DNA and the protein. Detecting binding events followed by 1D-sliding, in fact, requires staying in a channel containing the protein; so, the fourth channel, commonly used for imaging buffer is now not needed. Since data are acquired in the protein channel, protein has to be diluted in imaging buffer (TBE 0.5x containing oxygen scavenging system). Basically, once dumbbell is formed, it is moved to the protein channel, flow is switched off and DNA is pre-tensioned to the desired value of force; finally, acquisition is started.

Diffusing LacI is then tracked using the Radial Symmetry Centre calculation and from the trajectories the Mean Square Displacement (MSD) is calculated at different time intervals. MSD is calculated as $<(x(t)-x_0)^2>$ and is related to the diffusion coefficient of the particle (D) according to MSD=2nDt where n is the dimensionality which is equal to 1 for monodimensional diffusion, t is the time interval. Figure 17.2 shows an example of a trace in which a LacI molecule is undergoing 1D-diffusion along non-specific DNA while another is (still) specifically bound. The relative distance of the still molecule, 0.50L (figure 17.2,c) demonstrate that the molecule is bound to primary operator O1.

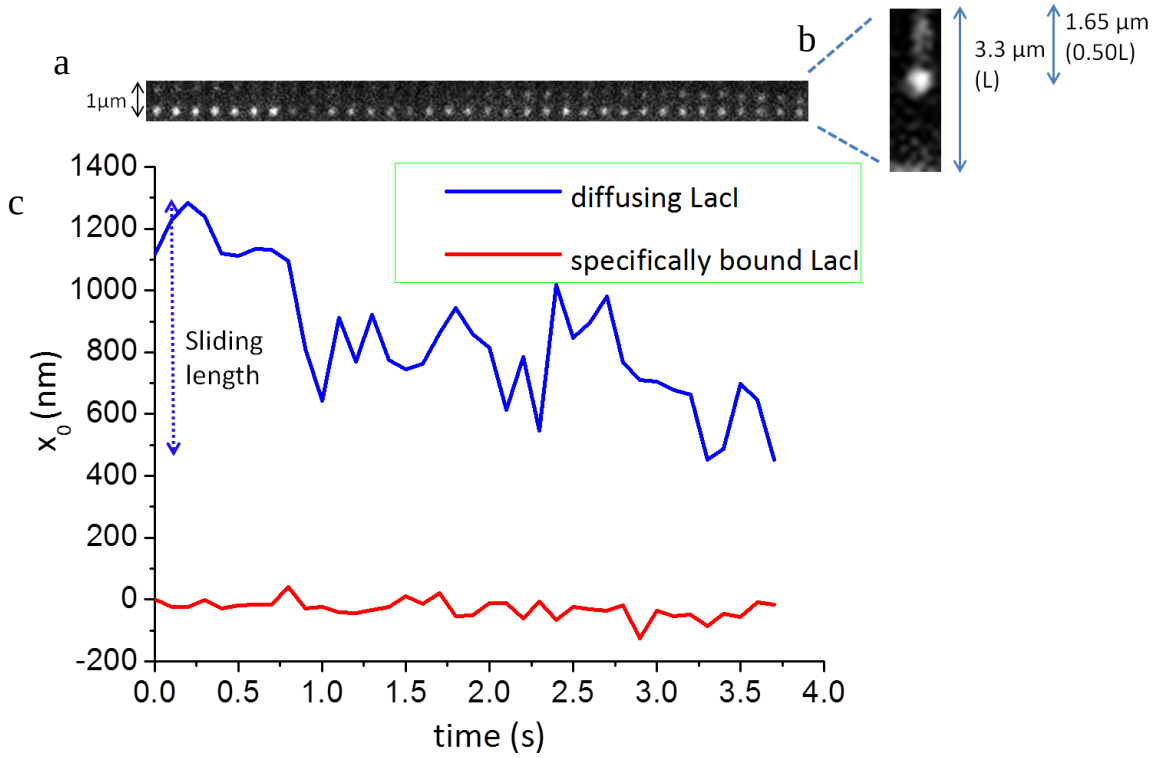

Figure 17.2. (a) kymogram representation of a LacI molecule sliding while another molecule is specifically bound to the operator O1 as demonstrated by the relative distance (0.50L)in (b). Average image (37 frames) of the sliding event in presence of a specifically-bound LacI. (c) Position trace of both diffusing (blue trace) and specifically bound molecule (red trace) which is characterized by a standard deviation of the position of 30nm. This example trace is acquired with a 532nm laser, power on sample of 20µW, 100ms exposure time and a tension on DNA of 20pN.

Figure 17.3 shows the plot of MSD versus time relative to the example reported in figure 17.2. The curve is fitted with a linear function whose slope is equal to 2D, thus giving a value of $D=(173124\pm18525)nm^2s^{-1}$. Trajectories of diffusing LacI have been collected at different forces applied on DNA in order to detect possible effects of the structural rearrangement that occurs when DNA is stretched on 1D-diffusion coefficients. In particular four levels of force have been applied: 1, 10, 20 and 30pN. In addition to the diffusion coefficient, also other parameters that characterize sliding were measured: the sliding length which is the contour distance traveled by the protein during sliding, and the residence time, that is the time the protein spends (non-specifically) bound to DNA during sliding. At a given

force, diffusion coefficient, sliding length and residence time are expressed as mean ± standard error. Increasing the DNA tension leads to a decrease of diffusion coefficients and sliding lengths to a minimum value at a force of 20pN. Unexpectedly, both diffusion coefficient and sliding length rise again at 30pN, showing a similar behavior with respect to DNA tension (figure 17.4). This is probably a consequence of the structural rearrangement of the DNA molecule at higher forces. Instead, residence time linearly decreases with DNA tension thus indicating a reduction of *lac* repressor affinity for (stretched) non-specific DNA (figure 17.5).

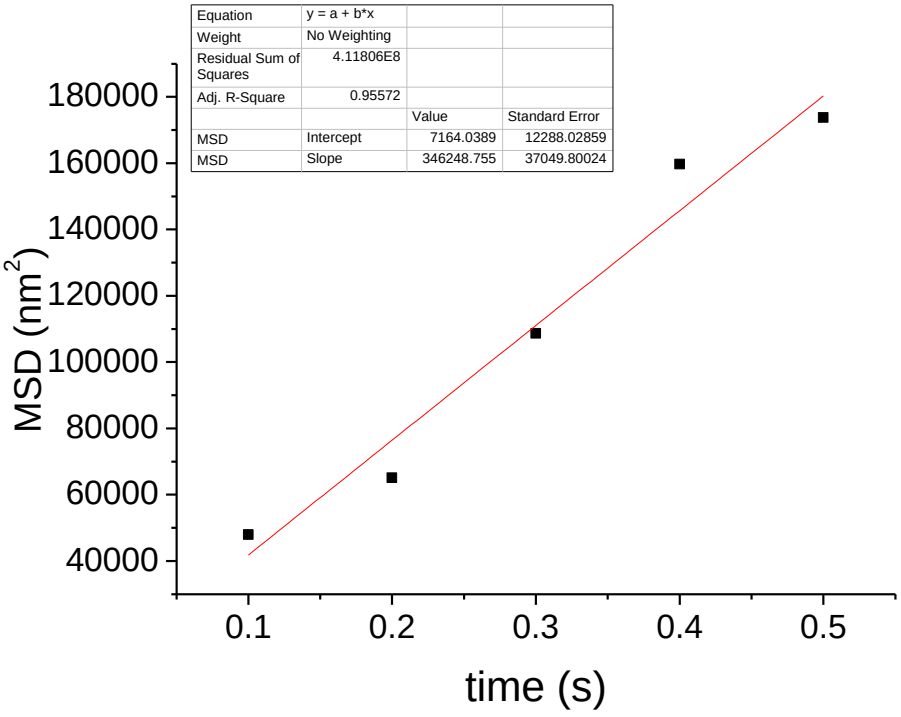

Figure 17.3. MSD vs time plot. The slope of the curve corresponds to 2D thus resulting in a value of D equal to =(173124±18525)nm^2s^{-1}.

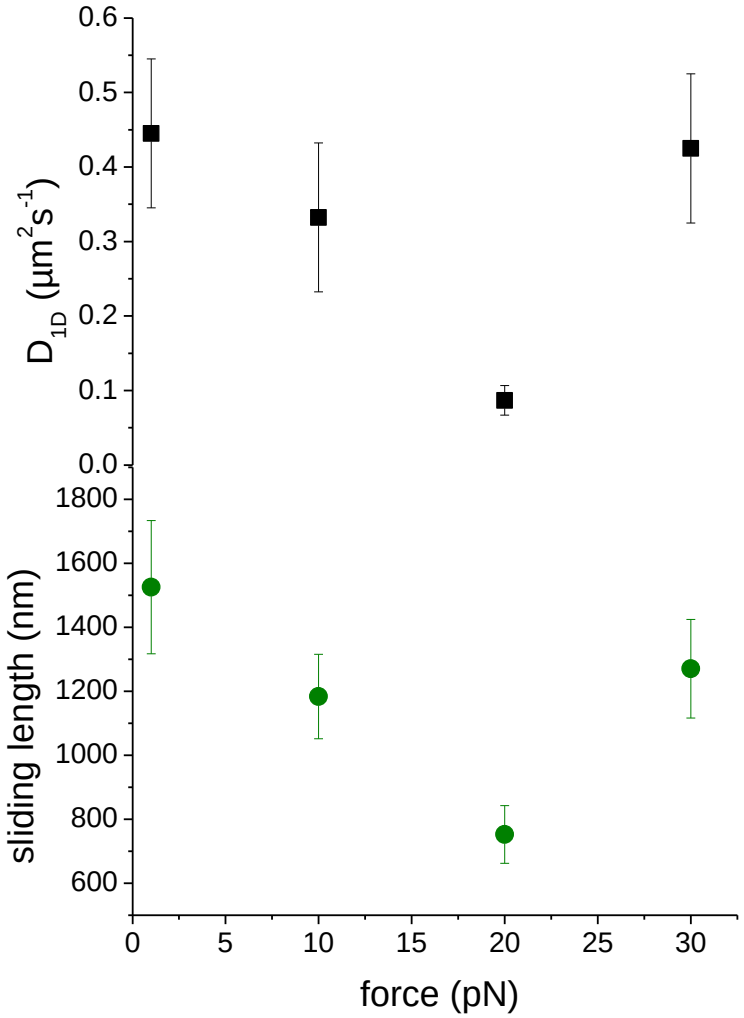

Figure 17.4. LacI diffusion coefficient (black squares) as a function of DNA tension. Dependence of sliding length (green circles) on DNA tension. All measurements are expressed as mean ± standard error (1pN, N=12, 10pN, N=16, 20pN, N=13, 30pN, N=4).

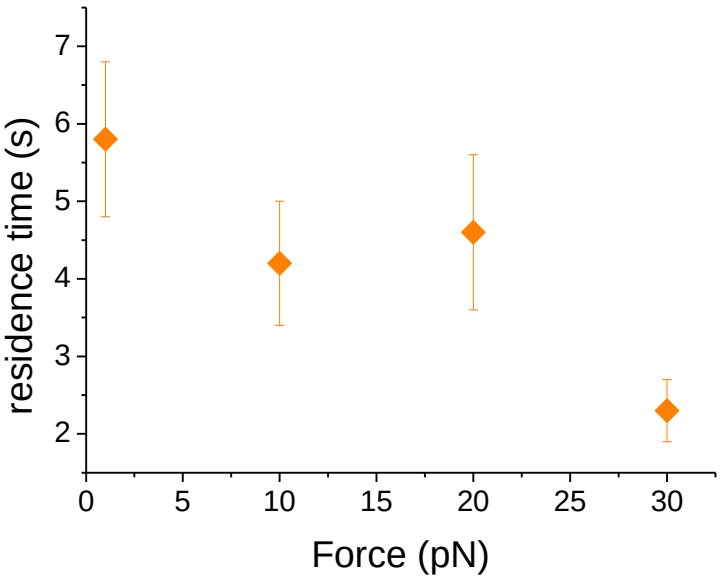

Figure 17.5. Dependence of residence time on DNA tension. All measurements are expressed as mean ± standard error (1pN, N=12, 10pN, N=16, 20pN, N=13, 30pN, N=4).

18. Discussion and future perspectives

In this work of thesis, an experimental set-up that combines single molecule detection and manipulation has been described and results of the application of FIAT assay to the study of protein DNA interaction and preliminary results with the novel ultrafast force-clamp spectroscopy have been presented. To detect and localize a single protein, it occurs to label that is to attach a fluorescent probe. This preparative step is crucial because it musts be taken into account that the object studied is no longer the protein as it is but the protein plus the dye and it is not foregone that, in the conjugated form, protein retains its native structure and activity. I started trying to label *lac* repressor with Quantum Dots because these fluorescent nanocrystals are very bright and don't photobleach. Conjugate was formed just mixing together streptavidin coated QDot and biotin tagged LacI. Addition of such conjugate to DNA didn't give place to binding, as shown by FIAT assay were no bright spot was detected on dumbbell. A change in the order of mixing, in particular mixing first DNA with the protein and subsequently, after the DNA/protein complex formation, addition of the fluorescent probe resulted in a labeled protein bound to DNA. This result suggests a distortion of the protein structure and thus of its DNA binding activity and such distortion is prevented by DNA binding which stabilizes the native structure. This distortion can be attributed to several reasons; QDot has a diameter of 10-15 nm while a typical protein diameter is about 5 nm so the conjugated studied has a mass bigger from that of the protein. LacI is a tetramer and biotinylation can, in principle, lead to four biotins per tetramer and QDot, on the other hand, is coated by about 10 streptavidin molecules leading to the possibility to generate multiple complexes and to distort the protein structure. Another possibility is QDot non-specifically binding to LacI DNA binding domain (when protein is not bound to DNA) because of their negative charge. I then decided to try labeling with a florescent dye, ATTO532, which is a little organic molecule and thus thought to give a negligible mass increase. Parallel, realized a new four channel flow-cell that allow to have components of the experiment is separated laminar flows and to move from one channel to another and to have a channel for buffer, useful to discard fluorescence background deriving from other labeled proteins diffusing in solution. In fact, for example, preliminary results

with QDots were done in a two channels, Y shaped flow cell, where the first chanel was used for beads and in the second all remaining components together: DNA, protein and the probe, although the brightness of QDots, localization accuracy was about 10nm for the high background.

Upon characterization of the new dye, I tried to label LacI amino groups, cysteines of wild type la repressor and of a single cysteine mutant (LacIQ231C) and only the last was successful. In order to determine activity of the labeled protein, I measured characteristic times of association and dissociation through FIAT assay and the measured value of Kd was consistent with the value present in the literature obtained with bulk experiments.

As all organic dye, ATTO532 shows photobleaching after a time that depends on the power of the excitation light; increasing the power reduces dye lifetime. In order to get a high signal to noise ratio, that is a high localization accuracy, exposure time can be increased at expense of temporal resolution. For detecting fast events, it is would be preferable to decrease the exposure time (while lowering the localization accuracy). Also other factor, such as DNA tension can affect localization accuracy acting reducing DNA thermal fluctuations. I measured the effect of such parameters on DNA accuracy, exploring three different exposure times: 50, 100 and 500ms and two DNA tension: 1 and 10pN. Passing from an exposure of 50ms to 500ms there is just a two fold increase in accuracy while temporal resolution is reduced ten times. In the direction parallel to DNA, *x*, there isn't a substantial difference between measurements done at 1and at 10pN while this difference is more pronounced in the perpendicular direction, *y* that generally shows a worse accuracy due to thermal fluctuation of the molecule. Since forces are applied in the same direction of DNA, thermal fluctuations in this direction are reduced. At an exposure time of 500ms fluctuations are averaged thus eliminating difference in accuracy level between the two axes and between measurements made at 1 and 10pN. Nevertheless, calculation of longitudinal stiffness of the system showed a small thermal fluctuation compared to the measured value and a significant difference between 1 and 10 pN (8 and 1nm respectively with an exposure time of 50ms, compared to 23.1±2.4 nm and 22.2±0.6 nm obtained with the 2D Gaussian fit). This comparison clearly indicates that the system is stable from a mechanical point of view and that localization measurements are not limited by its fluctuations.

In these experiments a novel, rapid and accurate algorithm that determines the centre of the spot calculating Radial Symmetry Centre has been evaluated parallel to the

commonly used 2D Gaussian fit. Localization accuracy determined with this new algorithm effectively resulted near to accuracy determined with 2DGaussian fit and also the dependence on exposure time and DNA tension showed the same behavior.

To address target search mechanism, I made experiments with a salt free buffer not to avoid non-specific interactions with DNA. I measured diffusion coefficient, sliding length and residence time of LacI diffusing on a DNA molecule containing the three natural operator sequences and saw the effect of stretching DNA on these parameters that characterize target search. Force values taken into account are: 1, 10, 20 and 30pN.

As suggested by Wang and colleagues (Wang et al., 2006) diffusion coefficients distribution can present a big variance due to the variability in the local (non-specific) DNA sequences. In fact they reported a large distribution of the diffusion coefficient of LacI on a lambda DNA stretched to few picoNewtons, ranging from 0.002 $\mu m^2 s^{-1}$ to 0.1 $\mu m^2 s^{-1}$ and with a mean value of 0.02 $\mu m^2 s^{-1}$. Diffusion coefficient at 1pN obtained with my experiments is different from that reported value and equal to $(0.4 \pm 0.1) \mu m^2 s^{-1}$ (mean ± st. error); this difference can be justified by the fact that I used a different DNA construct thus presenting different non-specific sequences. Moreover LacI used in my measurements is in the native tetrameric oligomerization state while Wang and colleagues used dimeric and monomeric forms of the protein. Finally, the presence of a double optical tweezers allows to keep DNA far from the cover slip (avoiding possible effects due the glass surface) and to precisely tune the tension to be applied on DNA.

Diffusion coefficients and sliding lengths show a similar trend with respect to DNA tension; increasing DNA tension leads to a decrease in both parameters that reach a minimum at a tension of 20pN and surprisingly arise again at 30pN. This funding can be attributed to structural rearrangement DNA molecule undergoes as consequence of mechanical stress. Residence time always decreases increasing DNA tension as a direct consequence of a reduction of affinity for non-specific DNA.

18.1 Ultrafast Force-clamp spectroscopy

To overcome the temporal limitation imposed by the exposure time in fluorescence detection, a novel approach is being developed in our laboratories: the ultrafast force-clamp spectroscopy (Capitanio et al., 2012). This technique uses the same FIAT experimental set-up but does not rely on fluorescence. The flow system described in chapter 13., and used for FIAT experiments can also be used in ultrafast force-clamp spectroscopy measurements. The main difference in the experimental configuration is the presence of a third bead made of silica on which *lac* repressor is anchored. This bead is embedded into a nitrocellulose matrix which coats the cover slide surface. The first component to be introduced in the flow-cell is the protein. Subsequently, the firsts two (upper) channels are used to introduce beads and DNA (and thus enabling to form the dumbbell) while the last two are simply used to introduced buffer. Once dumbbell is assembled, DNA is first stretched and brought in close proximity of the third bead, where LacI is present. In this configuration, equal and opposite forces are applied to left and right beads ($F_L = -F$ and $F_R = +F$) and the net force (F_{tot}) applied to DNA is zero. Second, the force applied by each trap is clamped to two different values, $F_L = -F$ and $F_R = +F + \Delta F$, so that the net force applied to the dumbbell becomes $F_{tot} = +\Delta F$. The forces acting on the two beads are clamped independently by a double-feedback system that moves the traps using acousto-optic deflectors (AODs) to keep the forces constant. Because a force, F_{tot}, is applied to the dumbbell, when molecules DNA and the protein are not bound, the dumbbell moves against viscous drag at constant velocity, $v = F_{tot}/\gamma$ (γ is the viscous drag coefficient of the dumbbell). When the displacement of the dumbbell exceeds a preset value (typically 100–200 nm in our experiments), the force applied by the traps is reversed ($F_{tot} = -\Delta F$), to maintain the two molecules in proximity of each other. The dumbbell, thus, moves in the opposite direction until it reaches the initial position, and the force is switched again to $F_{tot} = +\Delta F$ (figure 18.1,a). Therefore, when the two molecules are not bound, position of the traps over time is a triangular wave. When the molecular bond is formed, F_{tot} is transferred to the protein; as the system is designed to maintain a constant force, the dumbbell suddenly stops. Therefore, the position signal of the traps becomes a flat line (figure 18.1,b). The trace of the position represented in figure 18.1 (b)left (which has a time scale too large to clearly make the triangular wave visible) shows two sets of binding

events between *lac* repressor and DNA whose position distributions are separated by a distance of 96nm (figure 18.1,(b) right), consistent with the distance between operators (305 bp)

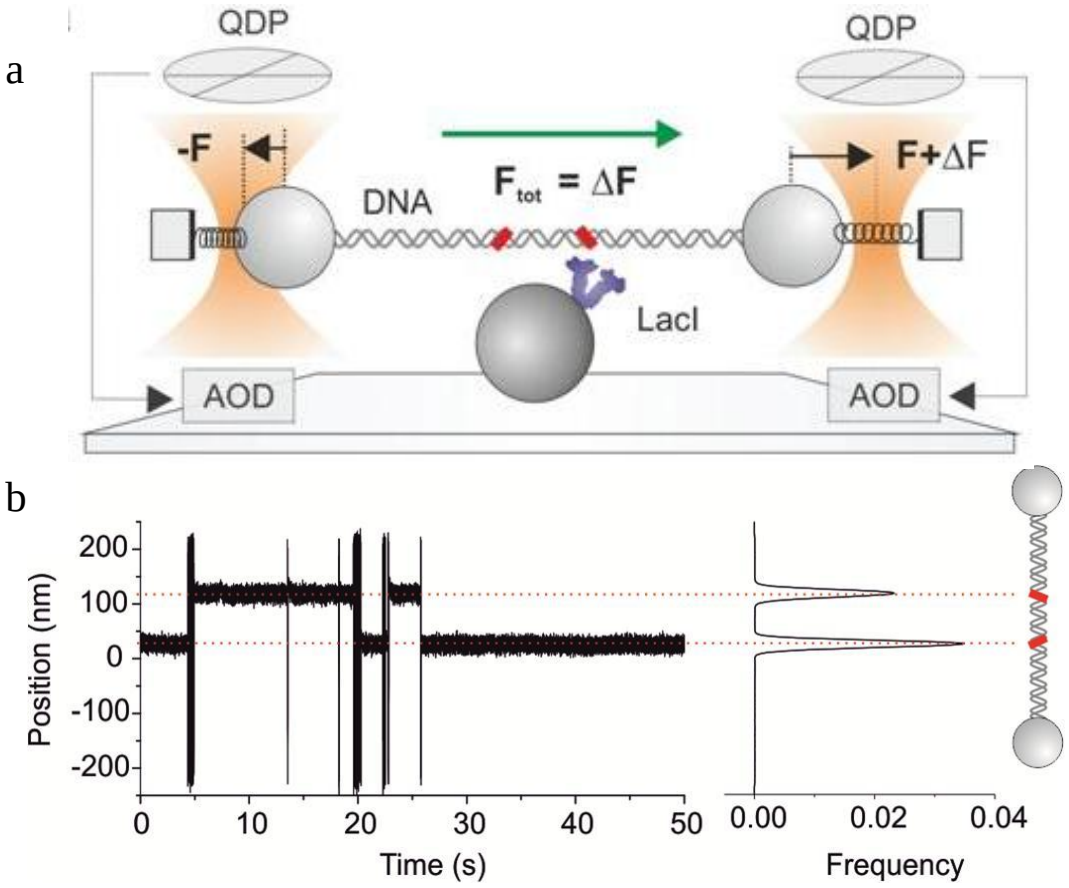

Figure 18.1 (a) Schematic of operational principle of our method illustrating constant F_{tot} = Δ*F* applied to molecule DNA through two feedback systems clamping the force on the left and right bead to −*F* and *F* + Δ*F*, respectively. The force is measured using quadrant detector photodiodes (QDPs) and kept constant by moving the traps through AODs. (b) Typical record of a LacI molecule interacting with a DNA molecule (F_{tot} = 5 pN, ± 200 µm confined dumbbell oscillation; left). The triangular wave is too fast to be visible on the time scale displayed here. Distribution of bound positions (right) shows peaks separated by the distance (~96 nm) between the two LacI operators (red) in the DNA molecule. Drawings are not to scale.

Figure 18.2 displays the clustering of long events at two specific positions along the DNA, separated by 96 nm. Nevertheless, beyond these long interactions, there is another, kinetically well-distinct, population of short interactions with non-operator DNA (which allow rapid scanning of DNA during the target search) even if buffer contained 200mM KCl. This method is thus suitable to map the interaction kinetics along all the DNA sequence;

moreover, the method has a very large dynamic range on the measurable interaction durations (from ~10 µs to tens/hundreds of seconds).

Next steps will thus include the use of this ultrafast spectroscopy technique performing experiments with a physiological salt concentration buffer (145mM KCl, high enough to avoid detection of non-specific interactions by fluorescence) thus trying to disentangle some contradictions on target search kinetics arisen recently (Halford 2009) contesting the fact that experiments present in literature always used a low salt buffer (that itself enhances association rate); also the effect of a wide range of forces on the interaction will be determined.

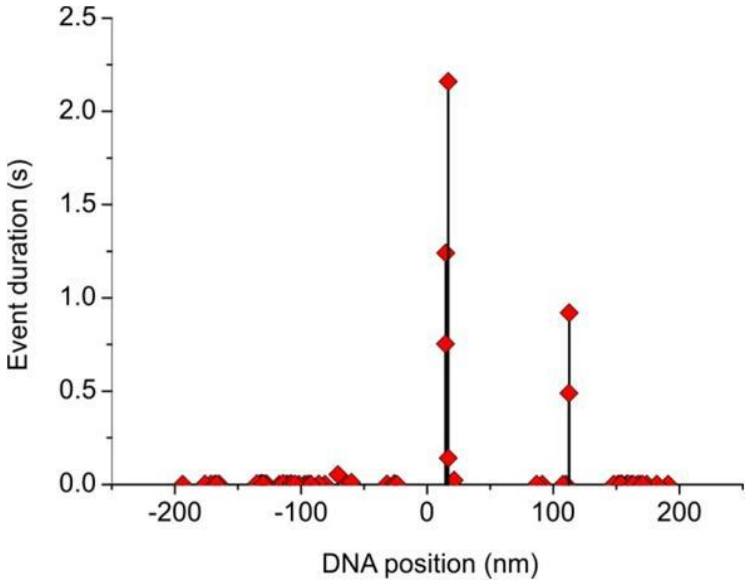

Figure 18.2 The figure shows the durations of the interactions measured on one DNA dumbbell (total recording time 100 s) as a function of position along the DNA molecule. The force applied in this recording was 5 pN.

19. Materials and Methods

Lactose repressor expression and purification

LacI minus cells BLIM are transformed with a plasmid containing gene encoding for LacI; 50µl competent BLIM cells are thawed on ice and then 1µl of plasmid DNA is added and let incubate for 30 minutes. Cells are heat shocked 45 seconds in 42°C water bath and put in ice again for 2 minutes. 400µl LB is added to cells and incubated at 37°C for 1 hour with shaking. 10 and 100µl of transformed cells are plated on two Amp50 plates and incubated at 37°C overnight.

The day after, one colony is picked and inoculated into 50ml LB with 50µg/ml Amp and grown all the day at 37°C with shaking. On evening four two liters flaks are filled with one liter of LB with 50µg/ml Amp and each of them is inoculated with 1ml of the 50ml growth and let grow overnight at 37°C overnight. The growth is centrifuged at 3000 rpm for 30 min into centrifuges bottles. Pellet is resuspended in 30ml cold breaking buffer. Lysozyme is added to a final concentration of 40mg/ml and frozen at -20°C.

Cells are thawed on ice; once lysed they look like a jelly. 10mg/ml DNAse is added and saturated solution of $MgCl_2$ (to a final concentration of 10mM) until the cells are runny and have lost their jelly-like consistency. They are then centrifuged at 8000rpm for 50 minutes. Supernatant containing our protein is saved. Supernatant is transferred on stir plate and ammonium sulfate is added slowly (23.1g $(NH_4)_2SO_4$ per 100g of supernatant). Once fully dissolved, suspension is let stand for 1 hour. Then it is centrifuged for 40 min 8000rpm. Pellet is then gently resuspended in 10ml 0.09M KP.

Dialysis tubing is washed with ddH_2O and soaked in 0.09 M KP. Then one end is clamped and protein solution is transferred inside the tubing, and then also the other end is clamped. Tubing is put in a beaker containing 0.09M KP and let stir for 1hour, then buffer is changed with fresh one and left stir another hour. Buffer is changed again and left stir overnight.

The day after dialysis buffer is changed and let dialyze for 1 hour. Dialysate is centrifuged for 30 min 8000 rpm.

In the meanwhile P-cell column is equilibrated with 0.09M KP until the conductivity of the out going buffer reaches a stable value. Supernatant containing the protein is thus loaded into the equilibrated P-cell column. 0.09M KP is used to elute flow-through.

Absorbance at 280nm is read by an UV detector connected to the column output. Elution with 0.09M KP lasts until UV A280 reaches the baseline again. Then the column is washed with 0.12M KP until there is no protein detected in the flow through. Then a gradient of ionic strength is applied generated with equal volumes of 0.12M KP and 0.3M KP. LacI elutes around 0.18M KP (figure 19.1).

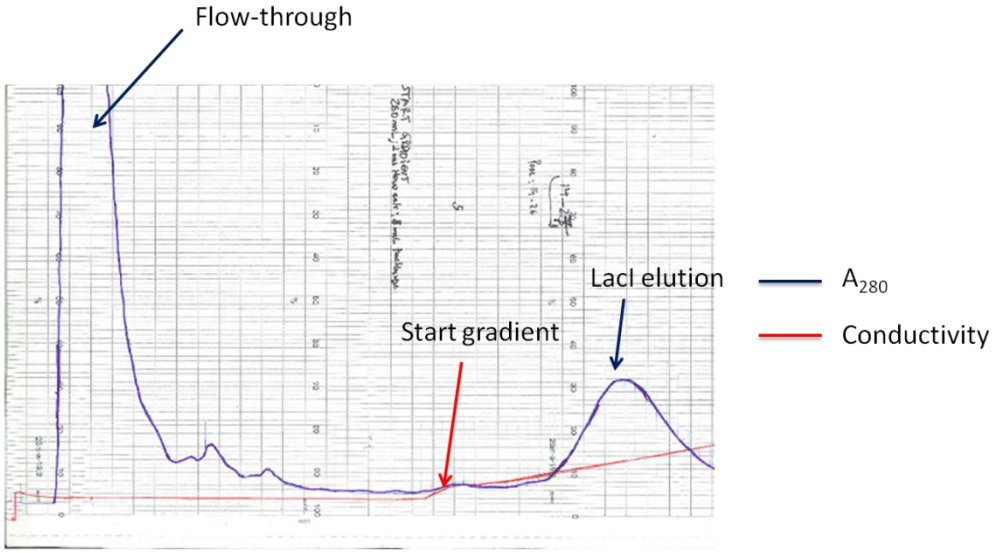

Figure 19.1. Flow chart representing output solution conductivity (red) and Absorbance at 280nm (blue). The first step is elution of all proteins with 0.09 KP. After a gradient of ionic strength is applied and LacI is eluted at a value of conductivity corresponding at about 0.18 KP.

Fractions of eluted LacI are controlled with an SDS-PAGE in order not to include impure fractions in the next step of concentration to smaller volume (figure 19.2).

SDS-PAGE

Resolving gel (10 ml): acrylamide solution 30% (4 ml), H_2O (3.35 ml), resolving gel buffer (Tris/HCl 1.5 M, pH 8.8) (2.50 ml), SDS solution 10% (100 µl), TEMED (10 µl), APS 10% (100 µl).

Resolving gel is put between two glass plates in a gel caster. Then water saturated 2-butanol is added in order to create and parallel to the ground surface of the gel. Solution is left polymerize for 20 minutes. 2-butanol is removed with absorbing paper and water is added and removed to fully remove alcohol traces.

Stacking gel (5 ml): acrylamide solution 30% (0.67 ml), H_2O (3.05 ml), stacking gel buffer (Tris/HCl, pH 6.8) (1.25 ml), SDS solution 10% (50 µl), TEMED (10 µl), APS 10% (50 µl).

Stacking gel solution is added on resolving gel with a comb on the top to create samples wells and left polymerize for 20 minutes and the is possible to remove the comb.

Plates are placed into the electrophoresis tank which is filled with running buffer (3.03g Tris base, 14.4g glycyne, 1g SDS in 1l ddH_2O).

Samples are diluted in sample buffer and boiled for 5 minutes before loading the gel. Molecular weight markers and samples are then loaded into the wells and let run for 1 hour with a potential of 200mV. After run, gel is carefully removed from plates and let stain in staining solution for one hour on a rocket. Gel is the let destain in destaining solution overnight to remove excess of stain.

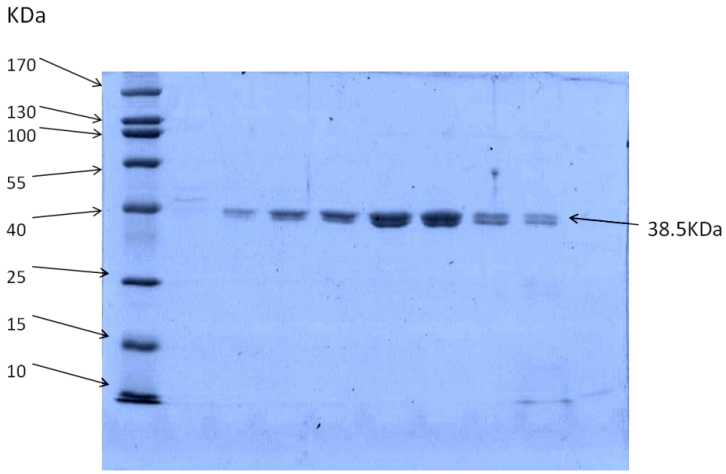

Figure 19.2. SDS-PAGE of fractions corresponding to A280 peak of eluted LacI. On the left there is the molecular weight marker, while spots correspond to sample fractions. Spot molecular weight corresponds to the molecular weight of LacI in the monomeric form (38.5KDa), resulting from denaturation of the native tetramer thus confirming that sample analyzed contain Lac repressor.

Protein labelling with ATTO532 (jena bioscience, #FP-220-532)

100µl of protein (10mg/ml) are mixed with 3µl Tris-(2-carboxyethyl)phosphine hydrochloride (TCEP) (0.1mg/µl) and vortexed carefully. Then 33µl of Atto532 (10mg/ml in DMF) are added. Reaction mixture is vortexed carefully, centrifuged briefly and let incubate 2 hours in a shaker at 20°C protected from light. Reaction is then stopped by addition of 3µl GSH (0.1mg/µl). The conjugate is purified by spin concentration (Amikon Ultra 10K).

DNA labelling with biotin

Terminal Deoxynucleotidyl Transferase (TdT) labelling

Plasmid DNA is first digested with ApaI (Fermentas, #ER1411) for 1 hour 30°C in buffer B (10 mM Tris-HCl pH 7.5 at 37°C 10 mM $MgCl_2$ 0.1 mg/ml BSA), 50µl reaction volume. Alternatively, DNA is digested with SnaBI (Fermentas, # ER0401) for 1 hour 37°C **1X Buffer Tango:** 33 mM Tris-acetate (pH 7.9 at 37°C), 10 mM Mg-acetate, 66 mM K-acetate, and 0.1 mg/mL BSA, 50µl reaction volume. Reactions are stopped by thermal inactivation at 65°C for 20 minutes. Digested DNA is purified with PureLink® PCR purification Kit (Invitrogen, #K3100-01) and then labelled according to the following protocol:

Reagents	Amount
5X buffer	4µl
DNA 3' ends	1-pmol
Biotynilated nucleotides biodATP, biodTTP or biodCTP, biodGTP	130pmol or 60pmol
TdT (fermentas, #EP0161)	1.5µl
ddH_2O	to 20µl

37°C for 15 minutes and 70°C for 10 minutes for thermal inactivation. Labelled DNA is further purified prior to use.

Exo- Klenow fragment labelling

DNA is first double-digested with two restriction enzymes, PauI (Fermentas, #ER1092) and SalI (Fermentas, #ER0642) in buffer O (50 mM Tris-HCl, pH 7.5, 10 mM $MgCl_2$, 100 mM NaCl and 0.1 mg/ml BSA), 50µl reaction volume, and incubating for 1 hour 37°C. Reaction is stopped by heat inactivation at 80°C for 20 minutes.

After purification of digestion, DNA is labelled through incorporation of biotinylated nucleotides by Klenow exo- (Fermentas, #EP0421) with the following protocol:

Reagents	Amount
PauI/SalI digested DNA	6µg
dGTP (Invitrogen, #10218014) 1:10	0.5µl
dTTP (Invitrogen, #10219012) 1:10	0.5µl
Biotin-14-dCTP (Invitrogen, #19524-016)	8µl
Biotin-14-dATP (Invitrogen, #19518-018)	8µl
Klenow DNA polymerase exo-	0.5µl
10x reaction buffer for Klenow exo-	5 µl
ddH_2O	To 50µl

37°C for 30 minutes and 70°C for 15 minutes for inactivation. Labelled DNA is purified prior to use.

Preparation of plasmid containing three natural operators

DNA sequence containing three native operators is amplified from E. Coli through PCR with following primers:

O1O2O3AatII_F aga gag gac gtc tgg gat acg acg ata ccg aag
O1O2O3AvrII_R aga gag cct agg aat cat cat taa agc gag tgg c

reagents	Volume (µl)
Buffer 10X	5
dNTPs (Invitrogen, #4303441)	1
Primer Forward (100µM)	0.25
Primer Reverse (100µM)	0.25
Taq polymerase (Invitrogen, #11708013)	0.4
H_20	38.6

And following thermal cycle:

Temperature (°C)	Duration	Number of cycles
94	6’	1
94	45’’	35
50	30’’	
72	1’30’’	
72	5’	1

Amplified sequence and plasmid DNA are both double digested with AatII (NEB, #R0117S) and AvrII (NEB, #R0174S) in buffer 4 (20 mM Tris-acetate pH 7.9, 50 mM K-acetate, 10 mM Mg-acetate, 1mM Dithithreitol), for 1 hour at 37°C. Reaction is stopped by thermal inactivation at 80°C for 20 minutes.

Amplified sequence is then treated with antarctic phosphatase (NEB, #M0289S) in 1X Antarctic Phosphatase Reaction Buffer (50 mM Bis-Tris-Propane-HCl, 1 mM $MgCl_2$,

0.1 mM $ZnCl_2$, pH 6.0) for 30 minutes, 37°C. Reaction is stopped by thermal inactivation at 65°C for 5 minutes.

Ligation of plasmid DNA with amplified sequence is performed by Quick Ligation kit (NEB,#M2200S) according to the following protocol:

Reagent	Amount
vector	50ng
insert	3fold molar excess respect to vector
Quick ligation buffer	10µl
Quick T4 DNA ligase	1µl
ddH_2O	To 20µl

The products of ligation are then amplified used to transform cell.50µl competent DH5α cells are thawed on ice and then 1µl of plasmid DNA is added and let incubate for 30 minutes. Cells are heat shocked 45 seconds in 42°C water bath and put in ice again for 2 minutes. 400µl LB is added to cells and incubated at 37°C for 1 hour with shaking. 10 and 100µl of transformed cells are plated on two Amp50 plates and incubated at 37°C overnight. 50µg/ml Amp and grown overnight at 37°C with shaking. The day after minicolture is centrifuged in 1.5ml tubes at 12000g to collect pellet. Plasmid is purified from pellets by mini-prep purification kit (Invitrogen, PureLink™ Quick miniprep kit, #K2100-10). All samples are then analyzed by sequencing with the following prmer:

5’-AACGGCATTAAGAAAGTCCTCAAGAA-3’

BUFFERS

Lac repressor Binding Buffer (LBB) (50ml): 121.1mg Trizma base (10mM), 1.491g KCl (200mM), 10µl of 0.5M EDTA (0.1mM final concentration), pH 7.4

TBE 0.5 x (1 liter): 5.4g Tris, 2.75g Boric acid, 2ml 0.5M EDTA pH 8.0, and distilled water up to 1 liter, pH 8.3.

Imaging Buffer (1ml): 878µl buffer (LBB or TBE), 12 µl of 250mg/ml glucose, 20 µl 1M DTT, 40 µl 5mg/ml Glucose Oxydase, 50 µl 1mg/ml Catalase.

Luria Broth (LB) (1L): 10g Trypton, 5g yeast exract, 10g NaCl, distilled water up to 1 liter. pH 7.4

Breaking Buffer: 0.2M Tris-HCl, pH 7.6, 0.2M KCl, 0.01 M Mg acetate, 5% (w/v) glucose, 0.1mM DTT (Glucose and DTT have to be added fresh).

Potassium phosphate (KP) 0.5 M, stock: two solutions of potassium phosphate monobasic and dibasic are prepared separately, both at a concentration of 0.5M. About 2/3 of dibasic and 1/3 of monobasic are mixed until pH reach 7.5

20. Bibliography

A.D. Riggs, S. Bourgeois, M. Cohn, **The lac repressor-operator interaction: III. Kinetic studies**, *Journal of Molecular Biology*, **53**: 401-417 (1970)

Abbondanzieri EA, Bokinsky G, Rausch JW, Zhang JX, Le Grice SF, Zhuang X: **Dynamic binding orientations direct activity of HIV reverse transcriptase**. *Nature* **453**:184-189 (2008).

Abbondanzieri EA, Greenleaf WJ, Shaevitz JW, Landick R, Block SM: **Direct observation of base-pair stepping by RNA polymerase**. *Nature* **438**:460-465 (2005).

Alessandrini A, Facci P: **AFM: a versatile tool in biophysics**. *Measurement Science & Technology* **16**:R65-R92 (2005).

Ashkin A, Dziedzic JM, Bjorkholm JE, Chu S: **Observation of a single-beam gradient force optical trap for dielectric particles**. *Opt Lett* **11**:288 (1986).

Ashkin A: **Forces of a single-beam gradient laser trap on a dielectric sphere in the ray optics regime**. *Biophys J* **61**:569-582 (1992).

Bai L, Santangelo TJ, Wang MD: **Single-molecule analysis of RNA polymerase transcription**. *Annu Rev Biophys Biomol Struct* **35**:343-360 (2006).

Barkley MD, **Salt dependence of the kinetics of the lac Repressor-Operator Interaction: role of nonoperator deoxyribonucleic acid in the association reaction**. *Biochemistry* **20**: 3833-3842 (1981)

Bernas T., Zarebski M., Cook PR, Dobrucki J.W. **Minimizing photobleaching during confocal microscopy of fluorescent probes bound to chromatin: role of anoxia and photon flux**. *J. Microsc*. **215**: 281-296 (2004).

Biebricher A, Wende W, Escudé C, Pingoud A, Desbiolles P: **Tracking of Single Quantum Dot Labeled EcoRV Sliding along DNA Manipulated by Double Optical Tweezers**. *Biophysical Journal* **96**:L50-L52 (2009).

Binnig G, Quate CF, Gerber C: **Atomic force microscope**. *Phys Rev Lett* **56**:930-933(1986)

Blainey PC, van Oijen AM, Banerjee A, Verdine GL, Xie XS: **A base-excision DNA-repair protein finds intrahelical lesion bases by fast sliding in contact with DNA**. *Proc Natl Acad Sci U S A* **103**:5752-5757 (2006).

Blanchard SC: **Single-molecule observations of ribosome function**. *Curr Opin Struct Biol* **19**:103-109 (2009).

Blanchard, S. C., H. D. Kim, R. L. Gonzalez Jr., J. D. Puglisi, and S. Chu. **tRNA dynamics on the ribosome during translation**. *Proc. Natl. Acad. Sci*. USA. **101**:12893–12898 (2004).

Blanchard, S. C., R. L. Gonzalez, H. D. Kim, S. Chu, and J. D. Puglisi. **tRNA selection and kinetic proofreading in translation**. *Nat. Struct. Mol. Biol*. **11**:1008–1014 (2004).

Block SM, Goldstein LSB, Schnapp BJ: **Bead Movement by Single Kinesin Molecules Studied with Optical Tweezers**. *Nature* **348**:348-352 (1990).

Brandenburg B, Zhuang X: **Virus trafficking - learning from single-virus tracking**. *Nat Rev Microbiol* **5**:197-208 (2007).

Braslavsky I, Hebert B, Kartalov E, Quake SR: **Sequence information can be obtained from single DNA molecules**. *Proc Natl Acad Sci U S A* **100**:3960-3964 (2003).

Brau RR, Tarsa PB, Ferrer JM, Lee P, Lang MJ: **Interlaced optical force-fluorescence measurements for single molecule biophysics**. *Biophys J* **91**:1069-1077, (2006)

Brewer LR, Bianco PR: **Laminar flow cells for single-molecule studies of DNA-protein interactions**. *Nat Methods* , **5**:517-525 (2008)

Bustamante C, Bryant Z, Smith SB: **Ten years of tension: single-molecule DNA mechanics**. *Nature* **421**:423-427 (2003).

Bustamante C, Macosko JC, Wuite GJ: **Grabbing the cat by the tail: manipulating molecules one by one**. *Nat Rev Mol Cell Biol* **1**:130-136 (2000).

Bustamante C, Marko JF, Siggia ED, Smith S: **Entropic elasticity of lambda-phage DNA**. *Science* **265**:1599-1600 (1994).

Bustamante C: **In singulo biochemistry: when less is more**. *Annu Rev Biochem* **77**:45-50 (2008)

Bustamante C: **Unfolding single RNA molecules: bridging the gap between equilibrium and non-equilibrium statistical thermodynamics**. *Q Rev Biophys* **38**:291-301 (2005).

C.E. Bell and M. Lewis. **The *lac* repressor: a second generation of structural and functional studies**. *Curr. Op. Struct. Biol*. **11**:19-25 (2001).

Candelli A., Wuite GJ., Peterman EJ., **Combining optical trapping, fluorescence microscopy and micro-fluidics for single molecules studies of DNA-protein interactions**. *PCCP.* **13**: 7263-72 (2011).

Capitanio M, Canepari M, Cacciafesta P, Lombardi V, Cicchi R, Maffei M, Pavone FS, Bottinelli R: **Two independent mechanical events in the interaction cycle of skeletal muscle myosin with actin**. *Proc Natl Acad Sci U S A* **103**:87-92 (2006).

Capitanio M, Cicchi R, Pavone FS: **Position control and optical manipulation for nanotechnology applications**. *European Physical Journal B* **46**:1-8 (2005)

Capitanio M, Cicchi R, Pavone FS: **Position control and optical manipulation for nanotechnology applications**. *European Physical Journal B* **46**:1-8 (2005).

Capitanio M, Maggi D, Vanzi F, Pavone FS: **FIONA in the trap: the advantages of combining optical tweezers and fluorescence**. *JOURNAL OF OPTICS A: PURE AND APPLIED OPTICS* **9:** S157-S163 (2007).

Capitanio M, Maggi D, Vanzi F, Pavone FS:**FIONA in the trap: the advantages of combining optical**

Capitanio M, Romano G, Ballerini R, Giuntini M, Pavone FS, Dunlap D, Finzi L: **Calibration of optical tweezers with differential interference contrast signals**. *Review of Scientific Instruments* **73**:1687-1696 (2002).

Capitanio M, Romano G, Ballerini R, Giuntini M, Pavone FS, Dunlap D, Finzi L: **Calibration of optical tweezers with differential interference contrast signals**. *Review of Scientific Instruments* **73**:1687-1696 (2002).

Capitanio M., Canepari M., Maffei M., Beneventi D., Monico C., Vanzi F., Bottineli R., Pavone F. S., **Ultrafast force-clamp spectroscopy of single molecules reveals load dependence of myosin working stroke.** *Nature Methods* **9**: 1013-9 (2012)

Cecconi, C., Shank, E.A., Bustamante, C. & Marqusee, S. **Direct observation of the three-state folding of a single protein molecule**. *Science* **309**: 2057–2060 (2005)

Charvin G, Strick TR, Bensimon D, Croquette V: **Tracking topoisomerase activity at the single-molecule level**. *Annual Review of Biophysics and Biomolecular Structure* **34**:201-219 (2005).

Cheezum, William F. Walzer, and William H. Guilford, Quantitative **Comparison of algorithms for tracking single fluorescent particles**. *Biophysical Journal*, **81**, 2378-2388 (2001).

Cherney DP, Bridges TE, Harris JM: **Optical trapping of unilamellar phospholipid vesicles: investigation of the effect of optical forces on the lipid membrane shape by confocal-Raman microscopy**. *Anal Chem* **76**:4920-4928 (2004).

Cluzel P, Lebrun A, Heller C, Lavery R, Viovy JL, Chatenay D, Caron F: **DNA: an extensible molecule**. *Science* **271**:792-794 (1996).

Crick F: **Central dogma of molecular biology**. *Nature* **227**:561-563 (1970).

Crick FH: **On protein synthesis**. *Symp Soc Exp Biol* **12**:138-163 (1958).

D. Normanno, M. Dahan, X. Darzacq. **Intra-nuclear mobility and target search mechanisms of transcription factors: a single molecule perspective on gene expression**. *Biochim. Biophys Acta* **6**:482-493 (2012)

Dijk MA, Kapitein LC, Mameren J, Schmidt CF, Peterman EJ: **Combining optical trapping and single-molecule fluorescence spectroscopy: enhanced photobleaching of fluorophores**. *J Phys Chem B* **108**:6479-6484 (2004)

Dumont S, Cheng W, Serebrov V, Beran RK, Tinoco I, Jr., Pyle AM, Bustamante C: **RNA translocation and unwinding mechanism of HCV NS3 helicase and its coordination by ATP**. *Nature* **439**:105-108 (2006).

F.R. Blattner, G. Plunkett, C.A. Bloch, N.T. Perna, V. Burland, M. Riley, J. Collado-Vides, J.D. Glasner, C.K. Rode, G.F. Mayhew, J. Gregor, N.W. Davis, H.A. Kirkpatrick, M.A. Goeden, D.J. Rose, B. Mau, Y. Shao, **The complete genome sequence of Escherichia coli K-12**, *Science*, **277**: 1453-1462 (1997)

Fazio T, Visnapuu ML, Wind S, Greene EC: **DNA curtains and nanoscale curtain rods: high-throughput tools for single molecule imaging**. *Langmuir* **24**:10524-10531 (2008).

Fernandez JM, Li H: **Force-clamp spectroscopy monitors the folding trajectory of a single protein**. *Science* **303**:1674-1678 (2004).

Finer JT, Simmons RM, Spudich JA: **Single myosin molecule mechanics: piconewton forces and nanometre steps**. *Nature* **368**:113-119 (1994).

Finer JT, Simmons RM, Spudich JA: **Single myosin molecule mechanics: piconewton forces and nanometre steps**. *Nature* **368**:113-119 (1994).

Friedman AM, Fischmann TO, Steitz TA **Crystal structure of lac repressor core tetramer and its implications for DNA looping** *Science*. **268**: 1721-7 (1995)

Galburt EA, Grill SW, Bustamante C: **Single molecule transcription elongation**. *Methods* **48**:323-332 (2009).

Galletto R, Amitani I, Baskin RJ, Kowalczykowski SC: **Direct observation of individual RecA filaments assembling on single DNA molecules**. *Nature* **443**:875-878 (2006).
Ghislain LP, Switz NA, Webb WW: **Measurement of Small Forces Using an Optical Trap**. *Review of Scientific Instruments* **65**:2762-2768 (1994).

Gittes F, Schmidt CF: **Interference model for back-focal-plane displacement detection in optical tweezers**. *Opt Lett* **23**:7-9 (1998).

Gittes F, Schmidt CF: **Signals and noise in micromechanical measurements**. *Methods in Cell Biology, Vol 55* **55**:129-156 (1998).

Gosse C, Croquette V: **Magnetic tweezers: micromanipulation and force measurement at the molecular level**. *Biophys J* **82**:3314-3329 (2002).

Grandbois M, Beyer M, Rief M, Clausen-Schaumann H, Gaub HE: **How strong is a covalent bond?** *Science* **283**:1727-1730 (1999).

Graneli A, Yeykal CC, Robertson RB, Greene EC: **Long-distance lateral diffusion of human Rad51 on double-stranded DNA**. *Proc Natl Acad Sci U S A* **103**:1221-1226 (2006).

Greenleaf WJ, Woodside MT, Block SM: **High-resolution, single-molecule measurements of biomolecular motion**. *Annu Rev Biophys Biomol Struct* **36**:171-190 (2007).

Greenleaf, W.J., Woodside, M.T., Abbondanzieri, E.A. & Block, S.M. **Passive all-optical force clamp for high-resolution laser trapping**. *Phys. Rev. Lett.* **95**: 208102 (2005).

Grier DG: **A revolution in optical manipulation**. *Nature* **424**:810-816 (2003).

Grier DG: **A revolution in optical manipulation**. *Nature* **424**:810-816 (2003).

Guo, B. & Guilford, W.H. **Mechanics of actomyosin bonds in different nucleotide states are tuned to muscle contraction.** *Proc. Natl. Acad. Sci. USA* **103**: 9844–9849 (2006)

H. Qian, M.P. Sheetz and E.L. Elson, **Single particle tracking. Analysis of diffusion and flow in two-dimensional systems.** *Biophys. J.* **60:** 910 (1991)

Handa N, Bianco PR, Baskin RJ, Kowalczykowski SC: **Direct visualization of RecBCD movement reveals cotranslocation of the RecD motor after chi recognition**. *Mol Cell* **17**:745-750 (2005).

Happel J, H. B: **Low Reynolds number hydrodynamics: with special applications to particulate media**: M. Nijhoff 1983.

Harada Y, Funatsu T, Murakami K, Nonoyama Y, Ishihama A, Yanagida T: **Single-molecule imaging of RNA polymerase-DNA interactions in real time**. *Biophys J* **76**:709-715 (1999).

Harada Y, Funatsu T, Murakami K, Nonoyama Y, Ishihama A, Yanagida T: **Single-molecule imaging of RNA polymerase-DNA interactions in real time**. *Biophys J* **76**:709-715 (1999).

Harada, Y., K. Sakurada, T. Aoki, D. D. Thomas, and T. Yanagida. **Mechanochemical coupling in actomyosin energy transduction studied by in vitro movement assay.** *J. Mol. Biol*. **216**: 49–68 (1990).

Hinterdorfer, P. & Dufrene, Y.F. **Detection and localization of single molecular recognition events using atomic force microscopy.** *Nat. Methods* **3**: 347–355(2006)

Hough LA, Ou-Yang HD: **Correlated motions of two hydrodynamically coupled particles confined in separate quadratic potential wells**. *Physical Review E* 2002, **65**:020906

Howard, J. **Mechanics of Motor Proteins and the Cytoskeleton**. (Sinauer Associates, Inc., 2001).

Hsieh WT, Whitson PA, Matthews KS, Wells RD, **Influence of sequence and distance between two operators on interaction with the lac repressor**. *J. Biol. Chem*., **262**: 14583-14591 (1987)

Hulst HCvd: *Light Scattering by Small Particles*. New York: Dover Pubblications, Inc.; 1957.Crick FH: **On protein synthesis**. *Symp Soc Exp Biol* **12**:138-163 (1958).

Ishijima A, Kojima H, Funatsu T, Tokunaga M, Higuchi H, Tanaka H, Yanagida T: **Simultaneous observation of individual ATPase and mechanical events by a single myosin molecule during interaction with actin**. *Cell* **92**:161-171 (1998).

Jacob F & Monod J. **Genetic regulatory mechanisms in the synthesis of proteins**. *J. Mol. Biol*. **3**: 318-356 (1981).

J. Kania, B. Müller-Hill. **Construction, isolation and implications of repressor-galactosidase β-galactosidase hybrid molecules**. *Eur. J. Biochem*., **79**:381-386 (1977).

Joo, C., S. A. McKinney, M. Nakamura, I. Rasnik, S. Myong, and T. Ha. **Real-time observation of RecA filament dynamics with single monomer resolution**. *Cell*. **126**: 515–527 (2006).

Kalodimos C.G., Biris N., Bonvin A. M., Levandoski M. M., Guennegues M., Boelens R., Kaptein R., **Structure and flexibility adaptation in nonspecific and specific protein- DNA complexes.**, *Science* **305**: 386-289 (2004)

Kalodimos C.G., Bonvin A. M., Salinas R. K., Wechselberger R., Boelens R., Kaptein R., **Plasticity in protein-DNA recognition: lac repressor interacts with its natural operator O1 through alternative conformations of its DNA binding domain**. *EMBO J.* **21**:2866-76 (2002).

Kapanidis AN, Strick T: **Biology, one molecule at a time**. *Trends in Biochemical Sciences, In Press* (2009)

Kellermayer MS, Smith SB, Granzier HL, Bustamante C: **Folding-unfolding transitions in single titin molecules characterized with laser tweezers**. *Science* **276**:1112-1116 (1997).

Krogh S, Mortensen UH, Westergaard O, Bonven BJ: **Eukaryotic topoisomerase I-DNA interaction is stabilized by helix curvature**. *Nucleic Acids Res* **19**:1235-1241 (1991).

L. Mirny, M. Slutsky, Z. Wunderlich, A. Tafvizi, J. Leith, A. Kosmrlj, **How a protein searches for its site on DNA: themechanism of facilitated diffusion**, *Journal of Physics A: Mathematical and Theoretical*, **42**: 434013 (2009)

Laakso, J.M., Lewis, J.H., Shuman, H. & Ostap, E.M. **Myosin I can act as a molecular force sensor.** *Science* **321**: 133–136 (2008)

Lamerichs RM, Boelens R, van der Marcel GA, van Boom JH, Kaptein R, Buck F, Fera B, Ruterjans H **H NMR study of a complex between the lac repressor headpiece and a 22 base pair symmetric lac operator.** *Biochemistry* **28:** 2985-91 (1989).

Lang, M.J., Asbury, C.L., Shaevitz, J.W. & Block, S.M. **An automated two-dimensional optical force clamp for single molecule studies**. *Biophys. J.* **83**: 491–501 (2002)

Lee GU, Chrisey LA, Colton RJ: **Direct measurement of the forces between complementary strands of DNA**. *Science* **266**:771-773 (1994).

Lee JB, Hite RK, Hamdan SM, Xie XS, Richardson CC, van Oijen AM: **DNA primase acts as a molecular brake in DNA replication**. *Nature* **439**:621-624 (2006).

Liphardt J, Onoa B, Smith SB, Tinoco IJ, Bustamante C: **Reversible unfolding of single RNA molecules by mechanical force**. *Science* **292**:733-737 (2001).

Lu HP, Xun L, Xie XS: **Single-molecule enzymatic dynamics**. *Science* **282**:1877-1882 (1998).

M. Lewis, G. Chang, N.C. Horton, M.A. Kercher, H.C. Pace, M.A. Schumacher, R.G. Brennan, P. Lu, **Crystal structrure of the lactose operon repressor and its complexes with DNA and inducer**, *Science*, **271**: 1247-1254 (1996)

M. Slutcky, L.A. Mirny, **Kinetics of protein-DNA interaction: Facilitated target location in sequence-dependent potential.** *Biophysical Journal* **87**:4021-4035 (2004)

M. von Smoluchowski, **Versuch einer mathematischen theorie der koagulationskinetik kolloier lösungen**, *Z. Phys. Chem*., **92**: 129-168 (1917)

Ma H., Long F., Zeng S., Huang ZL., **Fast and precise algorithm based on maximum radial symmetry for single molecule localization.** *Opt. Lett.* **37**: 2481-3 (2012)

Marko JF, Siggia ED: **Stretching DNA**. *Macromolecules* 1995:8759-8770

Marshall, B.T. *et al.* **Direct observation of catch bonds involving cell-adhesion molecules**. *Nature* **423**: 190–193 (2003)

Meiners JC, Quake SR: **Femtonewton force spectroscopy of single extended DNA molecules**. *Phys*

Mirny L., E. Shakhnovich. **Protein folding theory: from lattice to all-atom models.** *Annu. Rev. Biophys. Biomol. Struct.* 30:361-396 (2001).

Moerner WE: **New directions in single-molecule imaging and analysis**. *Proc Natl Acad Sci U S A* **104**:12596-12602 (2007).

Moffitt JR, Chemla YR, Smith SB, Bustamante C: **Recent advances in optical tweezers**. *Annu Rev Biochem* **77**:205-228 (2008).

Muller HP, Varmus HE: **DNA bending creates favored sites for retroviral integration: an explanation for preferred insertion sites in nucleosomes**. *Embo J* **13**:4704-4714 (1994).

Munro, J. B., R. B. Altman, N. O'Connor, and S. C. Blanchard. **Identification of two distinct hybrid state intermediates on the ribosome**. *Mol. Cell.* **25**:505–517 (2007).

Neher E, Sakmann B: **Single-channel currents recorded from membrane of denervated frog muscle fibres**. *Nature* **260**:799-802 (1976).

Neuman KC, Block SM: **Optical trapping**. *Rev Sci Instrum* **75**:2787-2809 (2004).

Neuman KC, Chadd EH, Liou GF, Bergman K, Block SM: **Characterization of photodamage to escherichia coli in optical traps**. *Biophys J* **77**:2856-2863 (1999).

Neuman KC, Lionnet T, Allemand JF: **Single-molecule micromanipulation techniques**. *Annual Review of Materials Research* **37**:33-67 (2007).

Neuman KC, Nagy A: **Single-molecule force spectroscopy: optical tweezers, magnetic tweezers and atomic force microscopy**. *Nat Methods* **5**:491-505 (2008).
Neuman, K.C. & Nagy, A. **Single-molecule force spectroscopy: optical tweezers, magnetic tweezers and atomic force microscopy**. *Nat. Methods* **5**: 491–505 (2008).

Noji H, Yasuda R, Yoshida M, Kinosita K, Jr.: **Direct observation of the rotation of F1-ATPase**. *Nature* **386**:299-302 (1997).

Normanno D. Vanzi F. Pavone FS, **Single-molecule manipulation reveals supercoiling-dependent modulation of lac repressor-mediated DNA looping**. *Nucleic acids res***. 8**:2505-13 (2008)

O.G. Berg, R.B. Winter, P.H. von Hippel, **Diffusion-driven mechanisms of protein translocation on nucleic acids. 1. Models and Theory**, *Biochemistry*, **20**:6929-6948 (1981).

Oehler S., Amouyal M., Kolkhof P., von Wilcken-Bergmann B., Müller-Hill. **Quality and position of the three lac operators of *E. Coli* define efficiency of repression**. *EMBO J*. **13**:3348-3355

Ozsolak F, Platt AR, Jones DR, Reifenberger JG, Sass LE, McInerney P, Thompson JF, Bowers J, Jarosz M, Milos PM: **Direct RNA sequencing**. *Nature* **461**:814-818 (2009).

Pabo CO, Sauer RT, **Protein-DNA recognition.** *Annual Review of Biochemistry*. **53**: 293-321 (1984)

Perkins TT, Dalal RV, Mitsis PG, Block SM: **Sequence-dependent pausing of single lambda exonuclease molecules**. *Science* **301**:1914-1918 (2003).

Perkins TT, Quake SR, Smith DE, Chu S: **Relaxation of a single DNA molecule observed by optical microscopy**. *Science* **264**:822-826 (1994).

Perkins TT, Smith DE, Larson RG, Chu S: **Stretching of a single tethered polymer in a uniform flow**. *Science* **268**:83-87 (1995).

Quake SR, Babcock H, Chu S: **The dynamics of partially extended single molecules of DNA**. *Nature* **388**:151-154 (1997).

R.A. Alberty, G.G. Hammes, **Application of the theory of diffusion-controlled reactions to enzyme kinetics**, *The Journal of Physical Chemistry*, **62**: 154-159 (1958)

Raghuveer P., **Rapid, accurate particle tracking by calculation of radial symmetry centers**. *Nat. Meth.* **9**: 724-726 (2012)

Reconditi, M. *et al.* **The myosin motor in muscle generates a smaller and slower working stroke at higher load.** *Nature* **428**: 578–581 (2004)

Revyakin A, Ebright RH, Strick TR: **Single-molecule DNA nanomanipulation: Improved resolution through use of shorter DNA fragments**. *Nature Methods* **2**:127-138 (2005).

Rief, M. *et al.* **Myosin-V stepping kinetics: a molecular model for processivity**. *Proc. Natl. Acad. Sci. USA* **97**: 9482–9486 (2000)

Rohrbach A, Stelzer EH: **Trapping forces, force constants, and potential depths for dielectric spheres in the presence of spherical aberrations**. *Appl Opt* **41**:2494-2507 (2002).

Rutkauskas D. Zhan H. Matthews KS, Pavone FS, Vanzi F. **Tetramer opening in LacI-mediated looping**. *PNAS*, **39**: 16627-32 (2009).

S.E. Halford, J.F. Marko, **How do site-specific DNA-binding proteins find their target?** *Nucleic aAcids Research*, **32**: 3040-3052 (2004)

S.E. Halford. **An end to 40 years of mistakes in DNA-protein association kinetics?** *Biochem. Soc.*

Sacconi L, Tolic-Norrelykke IM, Stringari C, Antolini R, Pavone FS: **Optical micromanipulations inside yeast cells**. *Appl Opt* **44**:2001-2007 (2005).

Simmons R: **Molecular motors: single-molecule mechanics**. *Curr Biol* **6**:392-394 (1996).

Smith DE, Tans SJ, Smith SB, Grimes S, Anderson DL, Bustamante C: **The bacteriophage straight phi29 portal motor can package DNA against a large internal force**. *Nature* **413**:748-752 (2001).

Smith SB, Cui Y, Bustamante C: **Overstretching B-DNA: the elastic response of individual double-stranded and single-stranded DNA molecules**. *Science* **271**:795-799 (1996).

Smith SB, Finzi L, Bustamante C: **Direct mechanical measurements of the elasticity of single DNA molecules by using magnetic beads**. *Science* **258**:1122-1126 (1992).

Smith, D.A., Steffen, W., Simmons, R.M. & Sleep, J. **Hidden-Markov methods for the analysis of single-molecule actomyosin displacement data: the variance-Hidden-Markov method.** *Biophys. J.* **81**: 2795–2816 (2001)

Strick TR, Croquette V, Bensimon D: **Single-molecule analysis of DNA uncoiling by a type II topoisomerase**. *Nature* **404**:901-904 (2000).

Svoboda K, Block SM: **Biological applications of optical forces**. *Annu Rev Biophys Biomol Struct* **23**:247-285 (1994).

Svoboda K, Block SM: **Force and velocity measured for single kinesin molecules**. *Cell* **77**:773-784 (1994).

Thompson, Daniel R. Larson, and Watt W. Webb, **Precise Nanometer localization analysis for individual fluorescent probes**. *Biophysical Journal*, **82** 2775-2783 (2002)

Toba S, Watanabe TM, Yamaguchi-Okimoto L, Toyoshima YY, Higuchi H: **Overlapping hand-over-hand mechanism of single molecular motility of cytoplasmic dynein**. *Proc Natl Acad Sci U S A* **103**:5741-5745 (2006).

Tsien RY: **The green fluorescent protein**. *Annu Rev Biochem* **67**:509-544 (1998).

tweezers and fluorescence.*JOURNAL OF OPTICS A: PURE AND APPLIED OPTICS,* **9** S157-S163 (2007)

V. Abkevich A. Gutin E. Shakhnovich. **Specific nucleus as the transition state for protein folding: evidence from the lattice model**. *Biochemistry*. 33: 10026-10036 (1994)

van Mameren J, Gross P, Farge G, Hooijman P, Modesti M, Falkenberg M, Wuite GJ, Peterman EJ: **Unraveling the structure of DNA during overstretching by using multicolor, single-molecule fluorescence imaging**. *Proc Natl Acad Sci U S A* **106**:18231-18236 (2009).

van Mameren J, Modesti M, Kanaar R, Wyman C, Wuite GJ, Peterman EJ: **Dissecting elastic heterogeneity along DNA molecules coated partly with Rad51 using concurrent fluorescence microscopy and optical tweezers**. *Biophys J* **91**:L78-80 (2006).

van Mameren J, Modesti M, Kanaar R, Wyman C, Wuite GJ, Peterman EJ: **Dissecting elastic heterogeneity along DNA molecules coated partly with Rad51 using concurrent fluorescence microscopy and optical tweezers**. *Biophys J* **91**:L78-80 (2006).

van Mameren J, Peterman EJ, Wuite GJ: **See me, feel me: methods to concurrently visualize and manipulate single DNA molecules and associated proteins**. *Nucleic Acids Res* **36**:4381-4389 (2008).

van Mameren J, Peterman EJ, Wuite GJ: **See me, feel me: methods to concurrently visualize and manipulate single DNA molecules and associated proteins**. *Nucleic Acids Res* **36**:4381-4389 (2008).

Vanzi F, Vladimirov S, Knudsen CR, Goldman YE, Cooperman BS: **Protein synthesis by single ribosomes**. *Rna* **9**:1174-1179 (2003).

W. Gilbert, B. Müller-Hill, **Isolation of *lac* repressor-operator interaction: III Kinetics studies**, *Journal of Molecular Biology*, **53**:401-417 (1966)

W. S. Reznikoff, R.B. Winter, and C.K. Hurley. **The location of the binding sites in *lac* operon**. *Proc. Natl. Acad. Sci. USA*, **71**:2314-2318 (1974)

Walter NG, Huang CY, Manzo AJ, Sobhy MA: **Do-it-yourself guide: how to use the modern single-molecule toolkit**. *Nat Methods* **5**:475-489 (2008).

Wang J., Fessi T, Schroeder KT, Ouellet J, Liu Y, Freeman AD, Lilley DM, **Single-molecule observation of the induction of k-turn RNA structure on binding L7Ae protein**. *Biophys. J.* **103**: 2541-8 (2012)

Wang MC, Uhlenbeck GE: **On the Theory of the Brownian Motion II**. *Rev. Mod. Phys.* **17**:323 – 342 (1945)

Wang MD, Yin H, Landick R, Gelles J, Block SM: **Stretching DNA with optical tweezers**. *Biophys J* **72**:1335-1346 (1997).

Wang MD, Yin H, Landick R, Gelles J, Block SM: **Stretching DNA with optical tweezers**. *Biophys J* **72**:1335-1346 (1997).

Watson JD, Crick FH: **Molecular structure of nucleic acids; a structure for deoxyribose nucleic acid**. *Nature* **171**:737-738 (1953).

Watson JD, Crick FH: **Molecular structure of nucleic acids; a structure for deoxyribose nucleic acid**. *Nature* **171**:737-738 (1953).

Wen JD, Lancaster L, Hodges C, Zeri AC, Yoshimura SH, Noller HF, Bustamante C, Tinoco I: **Following translation by single ribosomes one codon at a time**. *Nature* **452**:598-603 (2008).

Wiita, A.P. *et al.* **Probing the chemistry of thioredoxin catalysis with force**. *Nature* **450:** 124–127 (2007).

Woodside MT, Garcia-Garcia C, Block SM: **Folding and unfolding single RNA molecules under tension**. *Curr Opin Chem Biol* **12**:640-646 (2008).

Wuite GJ, Davenport RJ, Rappaport A, Bustamante C: **An integrated laser trap/flow control video microscope for the study of single biomolecules**. *Biophys J* **79**:1155-1167 (2000).

Wuite GJ, Davenport RJ, Rappaport A, Bustamante C: **An integrated laser trap/flow control video microscope for the study of single biomolecules**. *Biophys J* **79**:1155-1167 (2000).

Wuite GJ, Smith SB, Young M, Keller D, Bustamante C: **Single-molecule studies of the effect of template tension on T7 DNA polymerase activity**. *Nature* **404**:103-106 (2000).

Xiao F, Zhang H, Guo P: **Novel mechanism of hexamer ring assembly in protein/RNA interactions revealed by single molecule imaging**. *Nucleic Acids Res* **36**:6620-6632 (2008).

Y.M. Wang, R.H. Austin, E.C. Cox, **Single molecule measurements of repressor protein 1D diffusion on DNA** *Physical Review Letters*, **97**:048302 (2006)

Yildiz A, Forkey JN, McKinney SA, Ha T, Goldman YE, Selvin PR: **Myosin V walks hand-over-hand: single fluorophore imaging with 1.5-nm localization**. *Science* **300**:2061-2065 (2003).

Yildiz A, Selvin PR: **Fluorescence imaging with one nanometer accuracy: application to molecular motors**. *Acc Chem Res* **38**:574-582 (2005).

Yin H, Wang MD, Svoboda K, Landick R, Block SM, Gelles J: **Transcription against an applied force**. *Science* **270**:1653-1657 (1995).

Zlatanova J, van Holde K: **Single-molecule biology: what is it and how does it work?** *Mol Cell* **24**:317-329 (2006).

Acknowledgements:

I thank first of all Professor Francesco Pavone who is the mentor of this thesis and all the people working in his group (picture); a particular acknowledgement to the Single-Molecule subgroup: Carina, Marco, Francesco, Lucia, Martino, Matteo.

From top to bottom and from left to right: Francesco S. Pavone, Marco Capitanio, Francesco Vanzi, Martino Calamai, Leonardo Sacconi, Riccardo Cicchi, Claudia Crocini, Lucia Gardini, Carina Monico, Blaine Bisel, Irene Costantini, Ivana Pini, Lorenzo Tombaresi, Letizia Allegra, Jacopo Lotti, Ludovico Silvestri, Dimitris Kapsokalyvas, Matteo Prayer Galletti, Marcel van't Hoff, Daniela Selisca.